Mon. Not. R. Astron. Soc. **000**, 1–48 (2015) Printed 29 April 2015 (MN LATEX style file v2.2)

High-Velocity Features of Calcium and Silicon in the Spectra of Type Ia Supernovae

Jeffrey M. Silverman,[1,2,3] József Vinkó,[1,4] G. H. Marion,[1,5]
J. Craig Wheeler,[1] Barnabás Barna,[4] Tamás Szalai,[4]
Brian W. Mulligan,[1] Alexei V. Filippenko[6]
[1] *Department of Astronomy, University of Texas at Austin, Austin, TX 78712, USA*
[2] *NSF Astronomy and Astrophysics Postdoctoral Fellow*
[3] *email: jsilverman@astro.as.utexas.edu*
[4] *Department of Optics and Quantum Electronics, University of Szeged, Dóm tér 9, 6720 Szeged, Hungary*
[5] *Harvard-Smithsonian Center for Astrophysics, Cambridge, MA 02138, USA*
[6] *Department of Astronomy, University of California, Berkeley, CA 94720-3411, USA*

Accepted . Received ; in original form

ABSTRACT

"High-velocity features" (HVFs) are spectral features in Type Ia supernovae (SNe Ia) that have minima indicating significantly higher (by greater than about 6000 km s^{-1}) velocities than typical "photospheric-velocity features" (PVFs). The PVFs are absorption features with minima indicating typical photospheric (i.e., bulk ejecta) velocities (usually ∼9000–15,000 km s^{-1} near B-band maximum brightness). In this work we undertake the most in-depth study of HVFs ever performed. The dataset used herein consists of 445 low-resolution optical and near-infrared (NIR) spectra (at epochs up to 5 d past maximum brightness) of 210 low-redshift SNe Ia that follow the "Phillips relation." A series of Gaussian functions is fit to the data in order to characterise possible HVFs of Ca II H&K, Si II λ6355, and the Ca II NIR triplet. The temporal evolution of the velocities and strengths of the PVFs and HVFs of these three spectral features is investigated, as are possible correlations with other SN Ia observables. We find that while HVFs of Ca II are regularly observed (except in underluminous SNe Ia, where they are never found), HVFs of Si II λ6355 are significantly rarer, and they tend to exist at the earliest epochs and mostly in objects with large photospheric velocities. It is also shown that stronger HVFs of Si II λ6355 are found in objects that lack C II absorption at early times and that have red ultraviolet/optical colours near maximum brightness. These results lead to a self-consistent connection between the presence and strength of HVFs of Si II λ6355 and many other mutually correlated SN Ia observables, including photospheric velocity.

Key words: methods: data analysis – techniques: spectroscopic – supernovae: general

1 INTRODUCTION

Observations of Type Ia supernovae (SNe Ia) led to the discovery of the accelerating expansion of the Universe (Riess et al. 1998; Perlmutter et al. 1999) and have been extremely useful as a way to accurately measure cosmological parameters (e.g., Suzuki et al. 2012; Betoule et al. 2014; Rest et al. 2014). The cosmological utility of SNe Ia as precise distance indicators relies on the fact that their luminosity can be standardised. Phillips (1993) was the first to convincingly show that the light-curve decline rate of most SNe Ia is well correlated with luminosity at peak brightness, a connection now known as the "Phillips relation."

SNe Ia arise from the thermonuclear explosion of C/O white dwarfs (WDs; e.g., Hoyle & Fowler 1960; Colgate & McKee 1969; Nomoto et al. 1984; Nugent et al. 2011; Bloom et al. 2012), but beyond that basic statement, we still lack a detailed understanding of the progenitor systems and explosion mechanisms of SNe Ia (see Howell 2011 and Maoz et al. 2014 for further information). In general, the two leading progenitor scenarios are the single-degenerate (SD) channel, when the WD accretes matter from a nondegenerate companion star (e.g., Whelan & Iben 1973), and the double-degenerate (DD) channel, which is the result of the merger of two WDs (e.g., Iben & Tutukov 1984; Webbink 1984).

Detailed spectroscopic studies of large collections of low-redshift SNe Ia have been undertaken in the past (e.g.,

Barbon et al. 1990; Branch & van den Bergh 1993; Nugent et al. 1995; Hatano et al. 2000; Folatelli 2004; Benetti et al. 2005; Bongard et al. 2006; Hachinger et al. 2006; Bronder et al. 2008; Foley et al. 2008; Branch et al. 2009; Wang et al. 2009a; Walker et al. 2011; Nordin et al. 2011; Blondin et al. 2011; Konishi et al. 2011; Foley & Kasen 2011; Silverman et al. 2012), and have focused mainly on "photospheric-velocity features" (PVFs), which are absorption features with minima indicating typical photospheric (i.e., bulk ejecta) velocities (usually ∼9000–15,000 km s^{-1} near B-band maximum brightness). These features are formed at the outer edge of the optically–thick portion of the ejecta; thus, most absorption features in the spectra of SNe Ia should be PVFs. However, some recent work has focused on carefully identifying and characterising so-called "high-velocity features" (HVFs), which are spectral features that have minima indicating significantly higher velocities than typical photospheric velocities (i.e., 6000–13,000 km s^{-1} larger than PVFs, e.g., Mazzali et al. 2005; Maguire et al. 2012; Folatelli et al. 2013; Childress et al. 2014; Maguire et al. 2014).

In addition to these extensive samples, many studies of individual SNe Ia have presented evidence for HVFs (e.g., Hatano et al. 1999; Li et al. 2001; Gerardy et al. 2004; Thomas et al. 2004; Wang et al. 2009b; Foley et al. 2012b; Parrent et al. 2012; Silverman et al. 2012b; Childress et al. 2013; Marion et al. 2013; Maund et al. 2013; Pereira et al. 2013; Silverman et al. 2013) and have shown that they appear strongest in early-time spectra and weaken with time (as the PVFs strengthen). Previous work has also shown that HVFs are most often seen in the Ca II H&K (hereafter CaHK), Si II λ6355, and Ca II NIR triplet (hereafter CaIR3) features, though they are sometimes also present in other features as well (e.g., Parrent et al. 2012; Marion et al. 2013). Furthermore, the line-forming regions of the PVFs and HVFs appear to be physically distinct and substantially asymmetric, based in part on numerous spectropolarimetric observations (e.g., Leonard et al. 2005; Wang et al. 2003, 2006; Chornock & Filippenko 2008; Patat et al. 2009; Maund et al. 2013).

It has been suggested that the velocity of the CaHK feature is correlated with light-curve width (e.g., Maguire et al. 2012) and that HVFs are responsible for this relationship. However, Foley (2013) claims that Si II λ3858 usually dominates the CaHK profile and is actually the cause of the observed correlation. Recently, Childress et al. (2014) examined HVFs of CaIR3 in 58 low-redshift SNe Ia with spectra within 5 d of B-band maximum brightness and found that the existence and strength of HVFs is (positively) correlated with light-curve width and uncorrelated with SN colour. They also find that the existence and strength of the CaIR3 HVFs are anticorrelated with Si II λ6355 (photospheric) velocity. These results are confirmed by Maguire et al. (2014), who studied a different dataset, consisting of 258 low-redshift SNe Ia with spectra earlier than 5 d after maximum brightness. This study finds that ∼80 per cent (60–70 per cent) of SNe Ia at epochs earlier than 5 d before (after) maximum show evidence for HVFs of CaIR3, and that these features have velocities that are ∼7000 km s^{-1} faster than the PVFs seen in the same spectra.

Despite the recent interest in HVFs, an explanation of the physical origin of these features and how they might be related to SN Ia progenitors and their environments is still lacking. Interaction with circumstellar material (CSM) is one of the leading proposed causes of HVFs, which could arise from the SN ejecta sweeping up (or otherwise interacting with) a clumpy CSM, or a torus or shell of CSM (e.g., Kasen et al. 2003; Wang et al. 2003; Gerardy et al. 2004; Mazzali et al. 2005; Tanaka et al. 2006; Patat et al. 2009). Alternatively, HVFs could arise naturally from the SN Ia explosion mechanism itself, such as from helium detonations in WD envelopes (e.g., Shen & Moore 2014). No matter what the origin of HVFs, it seems likely that an abundance or density enhancement at high velocity (i.e., large radius in homologously expanding SN Ia ejecta) must be present (e.g., Mazzali et al. 2005; Tanaka et al. 2008), though perhaps ionisation effects play a role as well (Blondin et al. 2013).

In this work, we explore a large dataset of low-redshift ($z < 0.1$), low-resolution, optical and NIR SN Ia spectra observed earlier than 5 d before maximum brightness (described in Section 2), a subset of which was studied by Childress et al. (2014). In these data we carefully search for and measure the profiles of HVFs and PVFs of CaHK, Si II λ6355, and CaIR3 (discussed in detail in Section 3). The temporal evolution of these features, and how their velocities and strengths correlate with each other and other observables, are described in Section 4. We summarise our conclusions in Section 5.

2 DATASET

The majority of the SN Ia spectra used in this study come from the Berkeley SN Ia Program (BSNIP) and have been published in BSNIP I (Silverman et al. 2012a). Most of these data were obtained with the Shane 3 m telescope at Lick Observatory using the Kast double spectrograph (Miller & Stone 1993). The typical wavelength coverage of 3300–10,400 Å (with resolutions of ∼11 and ∼6 Å on the red and blue sides, respectively) allows us to observe the CaHK and CaIR3 features simultaneously. All objects have $z < 0.1$ with a median redshift of 0.02.

We require that each SN Ia have a well-determined date of maximum brightness so that we can assign an age to each spectrum. In this work, we only investigate spectra obtained earlier than 5 d after maximum brightness. Note that this is a superset of what was studied by Childress et al. (2014), who only used BSNIP spectra *within* 5 d of maximum. We removed objects which do not follow the "Phillips relation" *a priori*, including the extremely peculiar SN 2000cx (e.g., Li et al. 2001), SNe Iax (e.g., Li et al. 2003; Jha et al. 2006; Foley et al. 2013), and super-Chandrasekhar-mass objects (e.g., Howell et al. 2006; Scalzo et al. 2010; Silverman et al. 2011). A handful of the remaining spectra had signal-to-noise ratios (S/N) that were too low to reliably measure any spectral features or did not cover the wavelengths any of the three features under investigation (CaHK, Si II λ6355, and CaIR3). After all of these cuts, 226 spectra of 169 SNe Ia remained.

To this sample, we added low-resolution optical spectra obtained using the Marcario Low-Resolution Spectrograph (LRS; Hill et al. 1998) on the 9.2 m Hobby-Eberly Telescope (HET) at McDonald Observatory and the Robert Stobie Spectrograph (RSS; Nordsieck et al. 2001) on the 11.1 m by

9.8 m Southern African Large Telescope (SALT), and low-resolution NIR spectra obtained using SpeX (Rayner et al. 2003) on the NASA Infrared Telescope Facility (IRTF). Applying the same cuts as for the BSNIP sample, this yielded 128 spectra of 48 SNe Ia that covered at least the CaIR3 feature. Most of these data are unpublished and will appear in upcoming works (e.g., Marion et al., in preparation), although a handful of these spectra have appeared in previous publications (e.g., Quimby et al. 2006; Marion et al. 2009; Parrent et al. 2011). There are 11 SNe Ia with spectra in both this sample and BSNIP.

We also include in the current study 91 published spectra of 5 extremely well-observed SNe Ia: SNe 2009ig (Marion et al. 2013), 2011by[1] (Silverman et al. 2013), 2011fe (Vinkó et al. 2012; Parrent et al. 2012), 2012cg (Silverman et al. 2012b; Marion et al. 2012), and 2012fr (Childress et al. 2013; Zhang et al. 2014). This yields a total of 445 spectra of 210 SNe Ia that we analyse herein. Table A1 lists the names and phases of the spectra for each object. Note that all results discussed in Section 4 are consistent with what is found when using just the BSNIP sample alone. Thus, adding the other spectra into the current study does not bias any of our findings, yet it adds statistical weight and significance to the results.

To better characterise the objects in our sample, we attempt to classify each SN Ia using a variety of classification schemes. We consider an object "spectroscopically normal" if it is classified as "Ia-norm" by the SuperNova IDentification code (SNID; Blondin & Tonry 2007) as implemented in BSNIP I (Silverman et al. 2012a). Other "SNID Types" used in this work include "Ia-91bg" (e.g., Filippenko et al. 1992b; Leibundgut et al. 1993), which represent typically underluminous SNe Ia, and "Ia-91T" (e.g., Filippenko et al. 1992a; Phillips et al. 1992) and "Ia-99aa" (e.g., Li et al. 2001; Strolger et al. 2002; Garavini et al. 2004), which together represent typically overluminous SNe Ia.

Using the expansion velocity of the Si II λ6355 feature, Wang et al. (2009a) classified spectroscopically "normal" SNe Ia within 5 d of maximum brightness as either "normal velocity" (N) or "high velocity" (HV), with a velocity cutoff of 11,800 km s^{-1} at maximum brightness. While a sharp distinction between the two "Wang Types" may not exist (e.g., Silverman et al. 2012), we nonetheless utilise this classification scheme for illustrative purposes. Note that an individual SN Ia can be classified as N or HV, and each of its spectra may have PVFs, HVFs, or both. In other words, the Wang Type is used to classify a SN Ia, while the presence or absence of PVFs and HVFs is determined for each spectrum.

Another spectral classification scheme often used in SN Ia research was first introduced by Branch et al. (2006). Using the pseudo-equivalent widths (pEWs) of Si II λ6355 and Si II λ5750 in spectra near maximum brightness, they divide their spectral sample into four different groups: core normal (CN), broad line (BL), cool (CL), and shallow silicon (SS). This classification scheme is not used in the current work because it is effectively equivalent to a combination of SNID Types and Wang Types (CN = N, BL = HV, CL = Ia-91bg, SS = Ia-91T/99aa).

Benetti et al. (2005) used the rate of decrease of the Si II λ6355 expansion velocity before and near maximum brightness to define the velocity gradient, $\dot{v}$. Adopting these values, they separated their SN Ia sample into three subclasses, or "Benetti Types." High velocity gradient (HVG) and low velocity gradient (LVG) objects are normal-luminosity or overluminous SNe Ia with $\dot{v} \geqslant 70$ km s^{-1} d^{-1} and $\dot{v} < 70$ km s^{-1} d^{-1}, respectively. The third subclass (FAINT) have moderately large velocity gradients, but are underluminous ($\Delta m_{15}(B) \gtrsim 1.6$ mag). All three of the aforementioned classifications are listed for each object in Table A1.

Photometric information was obtained from published sources, when available. This includes the date of B-band maximum for each object, as well as light-curve width (characterised by $\Delta m_{15}(B)$) and $(B-V)_0$ colour (the observed $B-V$ colour of the SN at B-band maximum brightness). For the BSNIP data, this information came from Jha et al. (2006), Hicken et al. (2009), and Ganeshalingam et al. (2010). Photometric information for the HET, SALT, and IRTF data were obtained from a variety of sources (Quimby et al. 2006; Ganeshalingam et al. 2010; Stritzinger et al. 2011; Maguire et al. 2012; Hicken et al. 2012; Silverman et al. 2013). As for the five well-studied objects, their spectroscopic and photometric references are listed above. About two-thirds of the objects in this study have published $\Delta m_{15}(B)$ and $(B-V)_0$ values, and these are also presented in Table A1.

3 MEASUREMENT PROCEDURE

The measurement procedure used in this study is implemented in `IDL` and based in part on the one utilised extensively in BSNIP II (Silverman et al. 2012). It is briefly described by Silverman et al. (2013), but the description of our procedure herein is more in-depth. Each spectrum is first deredshifted (adopting the redshift listed in NED) and corrected for Milky Way (MW) reddening using values from Schlegel et al. (1998). Each of the three features measured (CaHK, Si II λ6355, and CaIR3) is then investigated individually.

For each feature, a local minimum in the spectrum is found, and the first local, relatively broad maxima are recorded to the left and right of this minimum. Note that the local maximum to the right of the minimum often corresponds to the peak of the P-Cygni profile. A concave downward quadratic function is fit to these local maxima, and the peaks of these parabolas are considered the endpoints of the spectral feature. These endpoints were visually inspected for every feature measured, and in about one-third of cases one or both of the endpoints were clearly incorrect, either still within the feature profile or very far from it. In these cases, the endpoints were chosen manually.

The two endpoints for each feature are then connected with a straight line, and this becomes the pseudo-continuum (black, dotted lines in Fig. 1). The continuum flux at each pixel is then subtracted from the observed flux, yielding the background-subtracted spectrum used in the procedure described below. This step is sometimes referred to as flattening the spectra and was used previously in BSNIP II (Sil-

[1] Note that there are also spectra of SN 2011by in the aforementioned HET/SALT/IRTF sample.

verman et al. 2012). One might instead *divide* the observed flux at each pixel by the continuum flux, though our tests indicate that this alternative approach does not significantly change the derived fit parameters; the values differ only at the few-percent level.

For each feature, the local minimum is found (when fitting only one velocity component, either PVF *or* HVF) or two separate local minima are found (when fitting two velocity components simultaneously, i.e., a PVF *and* HVF). These minima are then used as initial estimates in a non-linear least-squares fitting routine that fits the entire profile between the two endpoints with either one or two velocity components. Each component consists of one (for Si II λ6355), two (for CaHK, left column of Figure 1), or three (for CaIR3, right column of Figure 1) Gaussian functions and contains three free parameters. The relative separations of the Ca II lines come from their rest wavelengths, while their relative strengths come from their gf-weights[2]. We are thus operating in the optically thin limit, an assumption which has been shown in previous work using similar spectral feature fitting methods to not strongly affect the results (Childress et al. 2014; Maguire et al. 2014; Pan et al. 2015).

For CaIR3 and Si II λ6355, two fits were attempted for each profile: a one-component fit (PVF *or* HVF) and a two-component fit (both HVF *and* PVF). For CaHK, however, the possible presence of Si II λ3858 (e.g., Foley 2013) complicates matters. Thus, we attempt four fits for each CaHK profile: a one-component fit (PVF *or* HVF), a two-component fit (both HVF *and* PVF), a different two-component fit (PVF *or* HVF, but with a single component of Si II λ3858 included), and a three-component fit (both HVF *and* PVF, but with a single component of Si II λ3858 included). Each fit is then visually inspected, and in extreme cases where the fits do not match the data well, the initial estimates of local minima are changed and the fit is redone. As mentioned above, some spectra, mostly ones with low S/N, did not yield any acceptable fit.

While the *relative* separations and strengths of the spectral features are fixed as mentioned above, we do not impose any other constraints on the fit parameters. This differs from what was done by Maguire et al. (2014), who required that the CaIR3 PVF velocities be within 25 per cent of the Si II λ6355 velocity and that the CaIR3 HVF velocities be at least 2000 km s^{-1} faster than the Si II λ6355 velocity.

To decide which combination of fit components best represents the data, a variety of methods were used. All fits of a given spectral profile were visually inspected and the best fit was chosen via "χ-by-eye." This choice was then compared to the reduced-χ^2 value and the Bayesian information criterion (BIC) value for each fit. In the vast majority of cases, all three methods agreed unanimously. In the few cases where there was serious disagreement, we erred on the side of trusting fits with fewer parameters.

Once a best fit was chosen for each profile, the Gaussian fit parameters were used to calculate a velocity using the relativistic Doppler equation and a pEW (e.g., Garavini et al. 2007; Silverman et al. 2012) for each component of the fit. These values (and their uncertainties) for CaHK, Si II λ6355, and CaIR3 are listed in Tables A2, A3, A4, respectively. The formal uncertainty of the Gaussian fits indicates that the typical velocity error is $\sim$60 km s^{-1}. The minima of the spectral fits, however, are only accurate to a few Å, which implies a velocity uncertainty more like $\sim$200–400 km s^{-1}. This measurement uncertainty increases for weaker features. A few examples of Ca II "best fits" are displayed in Figure 1.

3.1 Ambiguous CaHK Fits

As mentioned above, the CaHK feature overlaps with the Si II λ3858 feature, which can affect the observed spectral profile (e.g., Foley 2013). This was seen in our data, as many spectra were fit equally well (in a reduced-χ^2 sense) by both a HVF and a PVF of CaHK, and Si II λ3858 and a PVF of CaHK. To break this degeneracy, we exploited the fact that the majority of the spectra studied herein include both the CaHK and CaIR3 features in the same observation. We assumed that if a spectrum showed a HVF of CaIR3 (based on the method outlined above), then it should also have a HVF of CaHK (and vice versa). In the two ambiguous cases where the spectra did not cover the CaIR3 feature, we found that the inferred Si II λ3858 velocity was significantly larger than the Si II λ6355 velocity in the same observations, and thus we identify those profiles as containing HVFs of CaHK (instead of Si II λ3858).

To test our assumption that a HVF of CaIR3 implies a HVF of CaHK, we temporarily changed all of our Si II λ3858 identifications to HVFs of CaHK. This led to large differences in the velocities of the HVFs of CaHK and the HVFs of CaIR3 in the same spectrum ($\sim$5000 km s^{-1}, as opposed to the more typical value of $\sim$500 km s^{-1}; see below). It also led to relatively small differences between the velocities of the HVFs and PVFs of CaHK in the same spectrum ($\sim$5500 km s^{-1}, as opposed to the average of $\sim$9000 km s^{-1}; again, see below). Therefore, it seems that our identifications of Si II λ3858 are correct. Furthermore, we also compare the velocity of Si II λ3858 (when we detect it) with that of Si II λ6355 in the same spectra and find the typical difference to be $\sim$600 km s^{-1}, consistent with previous work on velocities of various Si II spectral features (e.g., Silverman et al. 2012).

The opposite test to the one described above was also performed. Namely, we temporarily changed all of our HVFs of CaHK to Si II λ3858. After doing this, the average Si II λ3858 velocity was found to be $\sim$15,000 km s^{-1}, and on average about 2600 km s^{-1} faster than the Si II λ6355 velocity in the same observation. Thus, these inferred Si II λ3858 velocities are too high to be real and so our HVF CaHK identifications appear to be correct.

Another way to visualise this is shown in Figure 2. There we plot the velocity of Si II λ6355 versus the velocity of CaHK. The open points are PVFs of CaHK while the filled points are HVFs of CaHK, as determined using our method described above. The dotted line is the one-to-one line and shows that PVFs of CaHK are slightly faster than Si II λ6355 at low Si II velocities and comparable at higher Si II velocities. The dashed line is the cutoff between HVFs and PVFs used by Foley (2013); the classifications from his study mostly match those in this work. Finally, the solid line represents Si II λ3858 at the same velocity as Si II λ6355, if our HVFs of CaHK were actually misidentified Si II. Thus, if a solid point fell directly on this line, the velocity of our

[2] `http://www.nist.gov/pml/data/asd.cfm`.

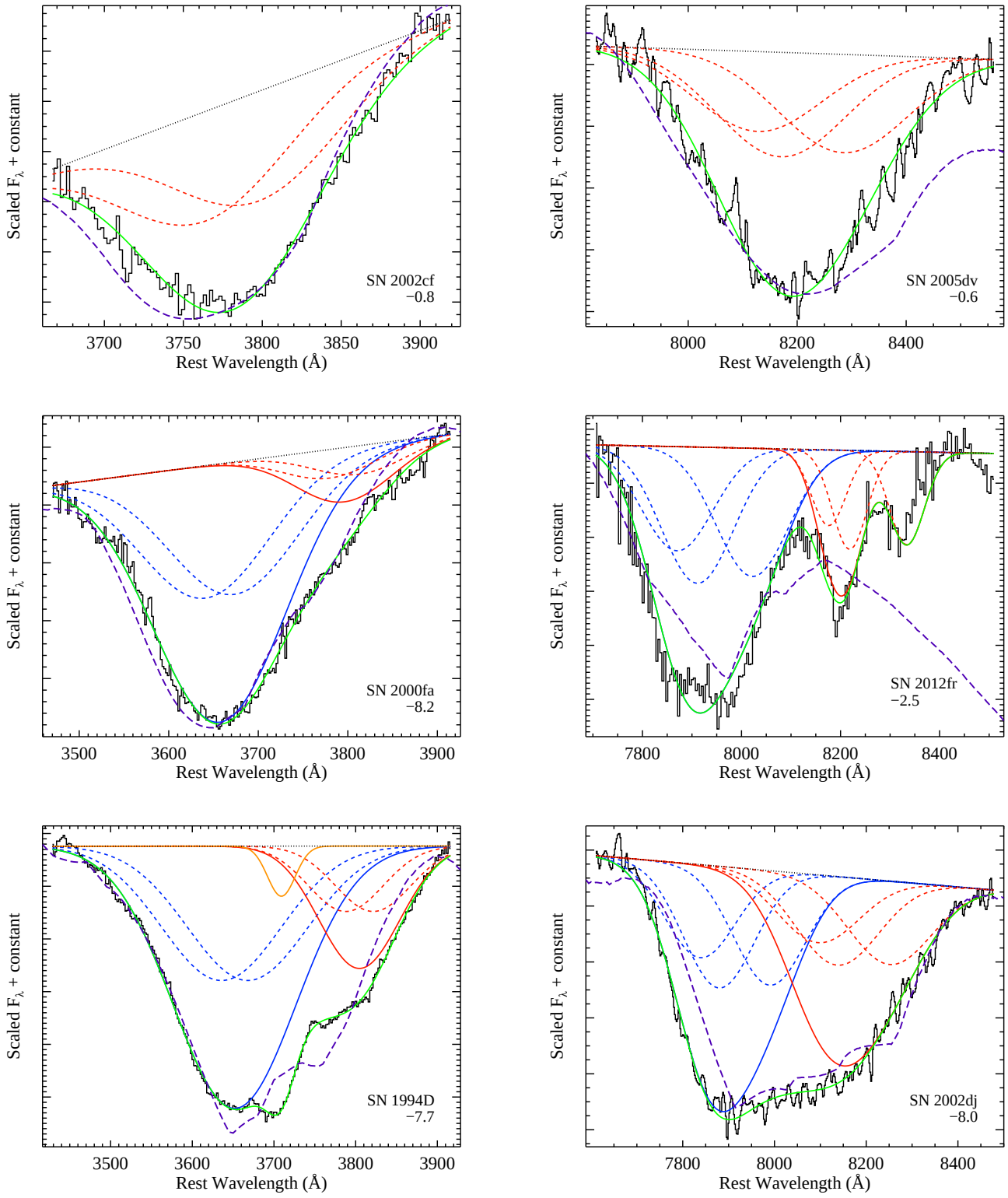

Figure 1. Fits to CaHK (*left column*) and CaIR3 (*right column*) showing PVFs (*red*) and HVFs (*blue*, where required). Individual Gaussian components are *short-dashed* and their sum is *solid*. Also shown are the sum of the total fit (*green*), the data (*black, solid*), the linear continuum (*black, dotted*), and a `SYNAPPS` (Thomas et al. 2011) fit (*purple, long-dashed*). Si II λ3858 is also required in the *bottom-left* fit (*orange, solid*). Each spectrum is labeled with its object name and age relative to *B*-band maximum brightness.

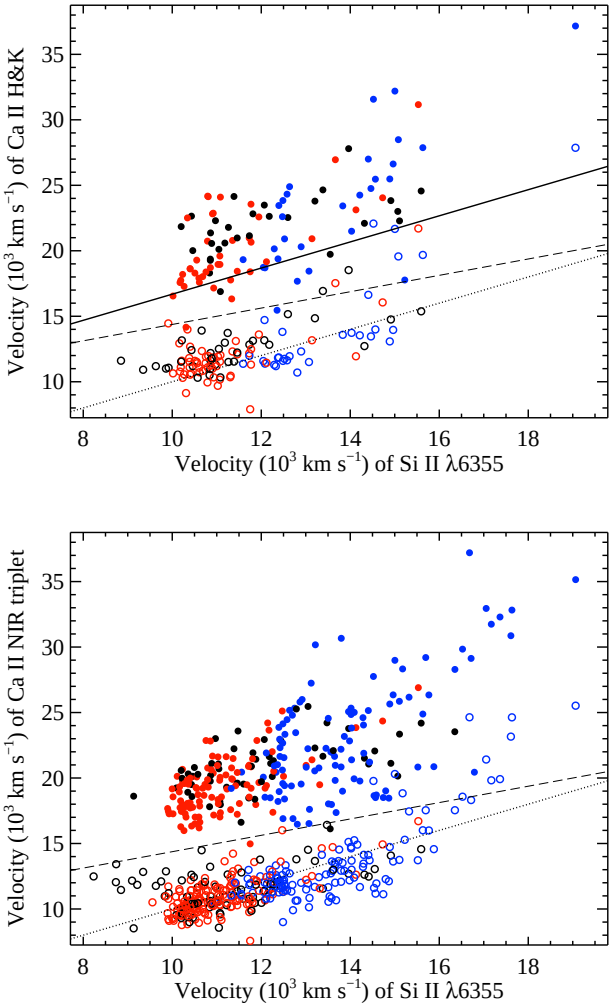

Figure 2. The velocity of CaHK (*top*) and CaIR3 (*bottom*) versus the velocity of Si II λ6355. Open points are PVFs of Ca II and filled points are HVFs of Ca II. Blue points are HV objects, red points are N objects, and black points are objects without a Wang Type. The dotted line is the one-to-one line; the dashed line is the cutoff between HVFs and PVFs used by Foley (2013). The solid line in the top panel represents Si II λ3858 at the same velocity as Si II λ6355, if our HVFs of CaHK were actually misidentified Si II. Since most of the filled points in the top panel lie above the solid line, it is unlikely that they are actually Si II λ3858, and thus they are probably HVFs of CaHK, as our assumption implies.

measured HVF of CaHK would match that of Si II λ6355 if it were actually Si II λ3858.

The fact that most of the filled points lie above this line implies that our identification of HVFs of CaHK is correct and that if those features were actually Si II λ3858, then their velocities would be significantly higher than that of Si II λ6355 in the same spectra (as discussed above). Finally, we note that our inferred velocities of the HVFs of CaHK and CaIR3 are highly correlated, as are the velocities of the PVFs of CaHK and CaIR3 as well as the velocities of Si II λ3858 and Si II λ6355. This once again supports our spectral identifications.

3.2 Ambiguous Si II λ6355 Fits

When applying the aforementioned fitting algorithm to the Si II λ6355 feature, we discovered that a single Gaussian (plus linear background) fits most spectral profiles quite well. However, as has been seen previously (e.g., Silverman et al. 2012), the stronger Si II λ6355 profiles appear non-Gaussian and look more Lorentzian in shape (though these are mostly at greater than 3 d past maximum brightness, well after HVFs of Si II λ6355 usually disappear; e.g., Marion et al. 2013). In addition, two Gaussian profiles (i.e., both a HVF and a PVF) fit nearly every observation very well, both via visual inspection as well as in a reduced-χ^2 sense. Thus, to decide whether one or two components were present in a given profile, other factors must be considered.

Some of the HVF+PVF fits to Si II λ6355 had the difference in velocity between the two components less than 4500 km s^{-1}. This is significantly smaller than the smallest difference between Ca II HVFs and PVFs (i.e., $\sim$6000 km s^{-1}; see Section 4.3) and our fitting algorithm is not capable of reliably distinguishing between two components that are so close to each other in velocity space (see Section 3.3.1). Thus, we are unable to say with confidence that two components are present and in these cases we prefer the one-component fit. Other HVF+PVF fits to Si II λ6355 indicated a velocity of the PVF of $\lesssim$ 9000 km s^{-1}, which is never seen at these epochs in the "relatively normal" SNe Ia used herein (e.g., Silverman et al. 2012). Therefore, we regard these fits as unreliable as well, and we instead use the one-component fit for these data.

After removing the unphysical two-component fits mentioned above, we find that there are nearly no reliable two-component fits where the measured HVF velocity is less than 16,500 km s^{-1}. Thus, our analysis indicates that HVFs of Si II λ6355 always remain above $\sim$16,500 km s^{-1}, consistent with previous work (e.g., Marion et al. 2013). Hence, we make the assumption that for a two-component (i.e., HVF+PVF) fit of Si II λ6355 to be preferred over a one-component fit, the inferred HVF velocity must be larger than 16,500 km s^{-1}.

Under this assumption, our measured PVF velocities of Si II λ6355 are consistent with previous measurements of the same data (Silverman et al. 2012; Childress et al. 2014). Figure 3 shows this by plotting the Si II λ6355 velocities for the 201 spectra in the current study (on the abscissa) that were also analysed in BSNIP II (Silverman et al. 2012, on the ordinate). Filled points represent spectra for which only one velocity component is detected in the current work. Pairs of open points connected with a horizontal line represent spectra for which both a PVF and a HVF velocity are measured in this work, with the left endpoint representing the PVF and the right endpoint representing the HVF. The "$\times$" along each line segment represents the pEW-weighted mean of the Si II λ6355 PVF and HVF velocities for that spectrum. The dotted line is the one-to-one line.

For velocities less than about 16,000 km s^{-1}, only the PVF velocity was measured in BSNIP II, whether or not a HVF was actually present in the Si II λ6355 profile. There are 11 spectra in which we detect two components herein that fall into this category, and all of them have relatively weak HVFs (which were simply missed by the fitting algorithm used in BSNIP II). For Si II λ6355 velocities that are

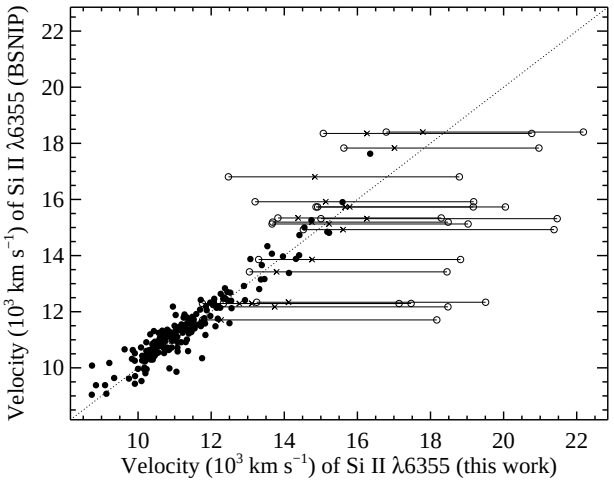

Figure 3. Si II λ6355 velocities for the 201 spectra in the current study (on the abscissa) that were also analysed in BSNIP II (Silverman et al. 2012, on the ordinate). Filled points are spectra with one velocity component. Open points connected with a horizontal line are spectra with two velocity components; the left endpoint is the PVF, the right endpoint is the HVF, and the "×" is the pEW-weighted mean of the Si II λ6355 PVF and HVF velocities for that spectrum. The dotted line is the one-to-one line.

greater than ∼16,000 km s^{-1}, BSNIP II typically measured the pEW-weighted mean of the Si II λ6355 PVF and HVF velocities. The 8 spectra which have both a HVF and PVF component that are in this category were mostly observed at early times when the PVF velocity was high and the pEW of the HVF was large. This likely caused the two components to be severely blended and thus the pEW-weighted mean of the two velocities was measured in BSNIP II. Finally, when considering only spectra with one component, the BSNIP II velocities and those measured in the current work are consistent.

3.3 Checks of the Fitting Procedure

3.3.1 Synthetic Data

To test the limits of our fitting algorithm, we constructed synthetic spectral profiles with a variety of Gaussian input parameters. The first test varied only the separation in velocity/wavelength space between the two components (i.e., HVFs and PVFs). We started with representative values of PVF and HVF velocities and widths from our fit to one of our relatively high-S/N spectra (SN 2002dj, $t = -8$ d). The velocity of the PVF was held constant at its value from the fit to the actual data (∼14,600 km s^{-1}), while the velocity of the HVF component was varied. Random noise was also added to the Gaussian functions to more closely resemble real data.

The HVF velocities tested ranged from the original value from the fit to the data (∼24,200 km s^{-1}) down to ∼17,700 km s^{-1}, in steps of 500 km s^{-1}. This allowed us to create 13 synthetic spectra with velocity differences between the HVF and PVF of 9600–3100 km s^{-1}. We then applied our spectral fitting algorithm as outlined above to these synthetic data. For all spectra with velocity separations greater than or equal to 4500 km s^{-1}, our fitting procedure preferred a two-component profile, while spectra with separations in velocity below this value were better fit by a one-component CaIR3 profile. Thus, it seems that our fitting algorithm is able to "resolve" distinct PVF and HVF components when they are separated by greater than about 4500 km s^{-1}. As we will show below, the smallest velocity difference between HVFs and PVFs seen in our data is ∼5000 km s^{-1}. Therefore, it seems unlikely that nature produces HVFs and PVFs with velocity separations of less than about 5000 km s^{-1}; otherwise, our algorithm would probably have detected them.

A similar test was performed by varying the depth of the HVF, while holding the depth of the PVF constant (along with the width and velocity of both components). The difference in velocity between the HVF and PVF used in this test was ∼9000 km s^{-1}, which is typical for our dataset (see below). The depth of the HVF was varied such that we tested depth ratios (HVF depth divided by PVF depth) of 1–0.05, in steps of 0.05. Two-component fits to the CaIR3 profile (i.e., HVF+PVF) were preferred in spectra where the ratio of depths was greater than 0.1. Thus, if there is a HVF whose depth is less than about 10 per cent that of the PVF, or vice versa, we will likely be unable to detect it using our fitting algorithm. The smallest finite ratio between the strengths of HVFs and PVFs of Ca II that we measure in our data is about 0.12 (see below). Therefore, nature *may* produce HVFs that are so weak compared to their PVFs (or vice versa) that our algorithm cannot detect them.

3.3.2 `SYNAPPS` *Fits*

As another check to our spectral measurement technique, we use the spectrum-synthesis code `SYNAPPS` (Thomas et al. 2011). `SYNAPPS` (and its modeling kernel `SYN++`) is derived from `SYNOW` (Fisher et al. 1997), which can compute spectra of SNe in the photospheric phase using the Sobolev approximation (Sobolev 1960; Castor 1970; Jeffery 1989). By varying many parameters automatically and simultaneously, `SYNAPPS` can find an optimum fit to an input spectrum via χ^2-minimisation. `SYNAPPS` assumes that spectral lines are formed via resonance scattering above a sharp photosphere. The location of this photosphere (in velocity space) is defined by the $v_{\rm ph}$ parameter, and the ejecta are assumed to be in homologous expansion at a photospheric temperature defined by the $T_{\rm phot}$ parameter.

For each input ion, the minimum and maximum velocity of the line-forming region are defined by the $v_{\rm min}$ and $v_{\rm max}$ parameters, respectively. In cases where $v_{\rm min} \gtrsim v_{\rm ph}$, the line-forming region is considered "detached" from the photosphere; by definition, this is the case for all HVFs. Each input ion also requires a value for the optical depth of a "reference line," $\tau_{\rm ref}$ (usually the strongest optical line), an e-folding velocity width of the optical-depth profile above the photosphere, v_e, and an excitation temperature, $T_{\rm exc}$.

`SYNAPPS` was used to fit 11 spectra that were chosen semirandomly to represent various CaHK and CaIR3 profile shapes (i.e., differing relative strengths of HVFs, PVFs, and Si II λ3858). Each fit used ions that are typically found in SNe Ia (i.e., O I, Ca II, Mg II, Si II, S II, and Fe II); some fits also included Si III, Fe III, or Ti II. `SYNAPPS` was also allowed to include a "detached" version of Ca II, representing the

HVFs. Some of these fits can be seen in Figure 1 as the purple, long-dashed curves.

In general, the SYNAPPS fits match well with our Gaussian fits to the data in that the spectral shapes agree, and when our fitting algorithm detects a HVF, it is also required in the SYNAPPS fit (and vice versa). Note that the SYNAPPS fits were not intended to perfectly match the entire spectral range covered by the data; they were used mainly to identify and disentangle the HVF and PVF components of the CaHK and CaIR3 features. The sum of the Gaussian fits used herein tend to reproduce the details of the profile better than the SYNAPPS fits, as the latter appear to be "smoothed out" and are unable to match the smaller-scale features in the data.

Given the uncertainties of the measured velocities using our fitting algorithm and the degeneracy in the SYNAPPS fits between input velocity and $\tau_{\rm ref}$, the velocities derived using the two methods are consistent within $\sim$2σ (i.e., $\sim$ 1200 km s^{-1}). The largest disagreement in the velocities comes when the PVFs are weak. In these cases, there are large uncertainties in the SYNAPPS parameters, and one can change the value of $\tau_{\rm ref}$ a small amount to force the velocity of the PVFs to match what is measured using our fitting algorithm.

As for the measured strengths of the features as characterised by their pEWs, the SYNAPPS fits and the measurements from our fitting algorithm are roughly consistent, but not as close to each other as the velocities of the features. This is possibly caused by the uncertainty associated with the $\tau_{\rm ref}$ parameter in the SYNAPPS fits. Furthermore, SYNAPPS indicates that the Si II λ3858 feature is always present in the observations, but is only noticeably strong in spectra where our fitting algorithm required it to be included in the Gaussian fits. In conclusion, while both SYNAPPS and our spectral feature fitting algorithm have their distinct pros and cons, their general agreement (especially regarding the existence of HVFs) is encouraging.

3.4 Comparisons to Previous Measurements

Marion et al. (2013) present a detailed study of the well-observed Type Ia SN 2009ig, specifically focusing on HVFs of various ions in the pre- and near-maximum-brightness spectra. This study is one of the very few that seriously investigates HVFs of Si II λ6355 (as we also do in this work). To compare and contrast with SN 2009ig, they also discuss HVFs in a handful of other objects. To derive the velocities, Marion et al. (2013) fit Gaussians to the cores of the features without removing the continuum. They inspect the positions of the derived minima visually and then calculate the velocity and uncertainty of HVFs and PVFs in CaHK, Si II λ6355, and CaIR3.

The dataset used herein includes 16 of their spectra of SN 2009ig, as well as 16 spectra of 9 other SNe Ia studied by Marion et al. (2013). For the 7 (27) spectra present in both samples that include the CaHK (CaIR3) feature, we find that both the HVF and PVF velocities are consistent at the 2–3σ level, with a nearly constant offset of $\sim$1400 km s^{-1} ($\sim$900 km s^{-1}) between the two studies. Similar results are found for the Si II λ6355 feature, where the average offset in the HVF velocity is $\sim$1100 km s^{-1} (for 8 spectra) and in the PVF velocity is $\sim$400 km s^{-1} (for 14 spectra). We detect about half the number of HVFs of Si II λ6355 as Marion et al. (2013), likely owing to the different fitting algorithms employed in the two studies. Finally, we note that the offsets are such that the HVF velocities measured herein tend to be higher than those of Marion et al. (2013), while the PVF velocities tend to be lower, thus leading to the current study finding larger velocity differences between the two components.

Childress et al. (2014), as mentioned above, studied HVFs of CaIR3 in a relatively large sample of SNe Ia spectra near maximum brightness, which represents a subset of the sample used herein. They used two Gaussians to fit each CaIR3 profile and assumed equal strength in each of the triplet components. Childress et al. (2014) also forced a minimum velocity difference between the HVFs and the PVFs in a given spectrum of 2000 km s^{-1}, and required that the velocity and width of the PVFs be within 10 per cent of those of the Si II λ6355 feature in the same spectrum. As described in Section 3, our fitting algorithm does not impose such strict limits on the fit parameters.

The measured Si II λ6355 PVF (CaIR3 HVF and PVF) velocities of the 56 spectra that are in both datasets are consistent at the 1–2σ level, with typical offsets of $\sim$300 km s^{-1} ($\sim$500 km s^{-1}). These offsets are such that the velocities measured herein tend to be larger than those reported by Childress et al. (2014). They also measure pEWs for the Si II λ6355 PVFs and the CaIR3 PVFs and HVFs. These values are consistent with what we measure at the 2–3σ level (offsets of $\sim$9 Å), and once again our values tend to be larger than those of Childress et al. (2014). These relatively minor differences are likely caused by the assumption of optically thin (this work, see above) versus optically thick (Childress et al. 2014) spectral features.

4 RESULTS & ANALYSIS

4.1 The Existence of HVFs in CaHK and CaIR3

Using the aforementioned algorithm, we calculate the pEW and expansion velocities of HVFs and PVFs for the CaHK and CaIR3 features; these are listed in Tables A2 and A4, respectively. For CaHK, we fit a total of 126 spectra of 84 SNe Ia; 5 of these spectra have HVFs only, 12 have PVFs only, 79 have both HVFs and PVFs present, 15 have PVFs and a Si II λ3858 feature, and 15 have both HVFs and PVFs, in addition to Si II λ3858. On the other hand, we fit the CaIR3 feature in a total of 382 spectra of 192 SNe Ia; 16 of these spectra have HVFs only, 105 have PVFs only, and 261 have both HVFs and PVFs present.

There are eight SNe Ia in the sample that exhibit only HVFs in their earliest spectra; most of these observations are earlier than 7 d before maximum brightness. We have multiple spectra of three of these objects, and all three eventually develop PVFs. Childress et al. (2013) found evidence for HVFs, but not PVFs, in their earliest spectra of SN 2012fr, consistent with what is found herein using the same observations. On the other hand, Marion et al. (2013) detected HVFs, but *not* PVFs, in early-time spectra of SN 2009ig, while we *do* detect PVFs (as well as HVFs) in the same data. Note that Maguire et al. (2014) found no spectra with only HVFs in their sample.

SN Ia spectra tend to evolve from having only HVFs (in ∼4 per cent of cases), to having both HVFs and PVFs (in the majority of spectra, i.e., ∼ 65–75 per cent), to having only PVFs (in ∼ 20–30 per cent of the observations). This generic picture of spectra changing with time (HVFs→HVFs+PVFs→PVFs) is consistent with what has been seen in previous work (e.g., Childress et al. 2013; Marion et al. 2013). As mentioned above, spectra with only HVFs are seen almost exclusively at very early times. Spectra with only PVFs are seen as early as ∼12 d before maximum brightness and as late as 5 d past maximum (which are the oldest spectra included in the current study). Data that show both HVFs and PVFs simultaneously are observed at all epochs studied herein ($-16 < t < 5$ d), implying that there is evidence of some SNe Ia showing HVFs at epochs as late as 5 d past maximum brightness, though most HVFs are gone by about 5 d *before* maximum.

When considering the entire dataset studied herein, we find that ∼67 per cent of all objects show HVFs in at least one spectrum. This is almost exactly the same percentage that was found by Maguire et al. (2014). When looking at only early-time observations ($t \lesssim -4$ d), ∼91 per cent of the objects show evidence of HVFs, which is consistent with, but slightly higher than, what was found previously (83 per cent, Maguire et al. 2014).

Of the SNe Ia for which we fit the CaHK or CaIR3 features, ∼28 per cent of them are HV objects, consistent with the overall SN Ia population (e.g., Wang et al. 2009a; Silverman et al. 2012). Of the SNe Ia with a known Wang Type, 77 per cent (71 per cent) of HV objects show HVFs of CaHK (CaIR3), while 70 per cent (62 per cent) of N objects shows HVFs of CaHK (CaIR3). Similarly, (SNID Type) Ia-norm objects contain HVFs of CaHK 78 per cent of the time and HVFs of CaIR3 70 per cent of the time, and all 10 Ia-91T/99aa objects in our dataset show HVFs of Ca II. Given the number of SNe Ia in each category, these percentages are all mutually consistent. On the other hand, only 1 out of 17 Ia-91bg objects show HVFs of Ca II. This significant dearth of HVFs in underluminous SNe Ia (i.e., Ia-91bg objects) has been noticed in previous work as well (Maguire et al. 2012; Childress et al. 2014; Maguire et al. 2014).

The entire BSNIP dataset averages ∼2 spectra per object (Silverman et al. 2012a), and since these data make up the bulk of the sample used herein, there are not many objects for which we have multiple spectra. Thus, we are only able to determine a Benetti Type for a handful of the objects studied in this work. For those SNe Ia with a Benetti Type, 62 per cent (72 per cent) of HVG objects show HVFs of CaHK (CaIR3), while 85 per cent (82 per cent) of LVG objects shows HVFs of CaHK (CaIR3). Only 1 of 8 SNe Ia with a Benetti Type of FAINT (i.e., underluminous objects) contained HVFs. These numbers are consistent with what was found above using Wang and SNID Types, given the association of HV/N/Ia-91bg objects with HVG/LVG/FAINT objects (e.g., Silverman et al. 2012).

A possible bias leading to the above result is that we do not have any spectra of Ia-91bg (or FAINT) objects at epochs earlier than 3 days before maximum brightness. Thus, perhaps, Ia-91bg/FAINT objects have HVFs, but they disappear earlier than in other SN Ia subtypes. We reject this idea in part because at $t = -3$ d, about half of all SNe Ia show HVFs, and this is also the same epoch when HVFs and PVFs tend to be about equal in strength (see Section 4.2). Conversely, 6 of the 9 objects that show only PVFs at $t < -3$ d are spectroscopically somewhat similar to SN 1991bg or have relatively narrow light curves and thus appear to be border cases between Ia-norm and Ia-91bg. The remaining 3 objects in this category all have their earliest spectra at $t \approx -6$ d, so HVFs could have been present at earlier times, but have faded by the time our spectra were obtained.

We further investigate whether the apparent lack of HVFs in Ia-91bg/FAINT objects is an observational bias by determining the typical epoch at which HVFs "disappear." This was done by taking each object with more than 1 spectrum in our dataset and fitting a line to the strength of the HVF relative to the PVF (see Section 4.2) versus time in order to find the epoch at which the relative strength of the HVF drops below our detection threshold of 0.1 (see Section 3.3.1); we refer to this as the "epoch of disappearance." This epoch is then compared to the light-curve width (i.e., $\Delta m_{15}(B)$) in order to search for any relationship between peak luminosity and the epoch of disappearance.

In the current sample, there were 26 SNe Ia with known $\Delta m_{15}(B)$ values and for which we were able to determine an epoch of disappearance. The latter for these objects is about $t = -1$ d to $t = +0.5$ d. When comparing the epoch of disappearance to $\Delta m_{15}(B)$, we find a large amount of scatter. The epoch of disappearance may decrease with increasing $\Delta m_{15}(B)$, but the slope of the linear fit is consistent with 0. Using our best linear fit to the data, we find the epoch of disappearance to be about −1.0 d for $\Delta m_{15}(B)$ values of 1.4–1.6 mag (e.g., Ganeshalingam et al. 2010, typical for Ia-91bg/underluminous objects).

There are no objects classified as Ia-91bg in this work with spectra obtained earlier than 3 d before maximum brightness. However, according to the above analysis, Ia-91bg spectra obtained earlier than ∼1 d before maximum *should* show HVFs. Thus, Ia-91bg objects (equivalently, Benetti FAINT objects or SNe Ia with narrow light curves) seem to *never* show HVFs, while all other SN Ia subtypes studied herein (HV, N, Ia-norm, Ia-91T/99aa, LVG, and HVG objects) *always* show HVFs (in spectra obtained earlier than ∼6 d before maximum). Owing to there being relatively few Ia-91bg objects in our sample, however, there is a small possibility that they may have HVFs at epochs earlier than about 3 d before maximum, but these features would have to disappear even earlier than one would expect based on the rest of our dataset.

4.2 Ca II pEWs

The pEWs of CaHK and CaIR3 for both HVFs and PVFs are listed in Tables A2 and A4, respectively. The temporal evolution of these pEWs is displayed in Figure 4. Open symbols represent PVFs while filled symbols represent HVFs. Blue points are high-velocity (HV) objects, red points are normal-velocity (N) objects, and black points are objects for which we could not determine a Wang Type. Squares are Ia-norm objects, stars are Ia-91bg objects, triangles are Ia-91T/99aa objects, and circles are objects which do not have a SNID Type.

At all epochs there is large scatter in the pEWs of HVFs and PVFs for both Ca II features. For $t \gtrsim -9$ d,

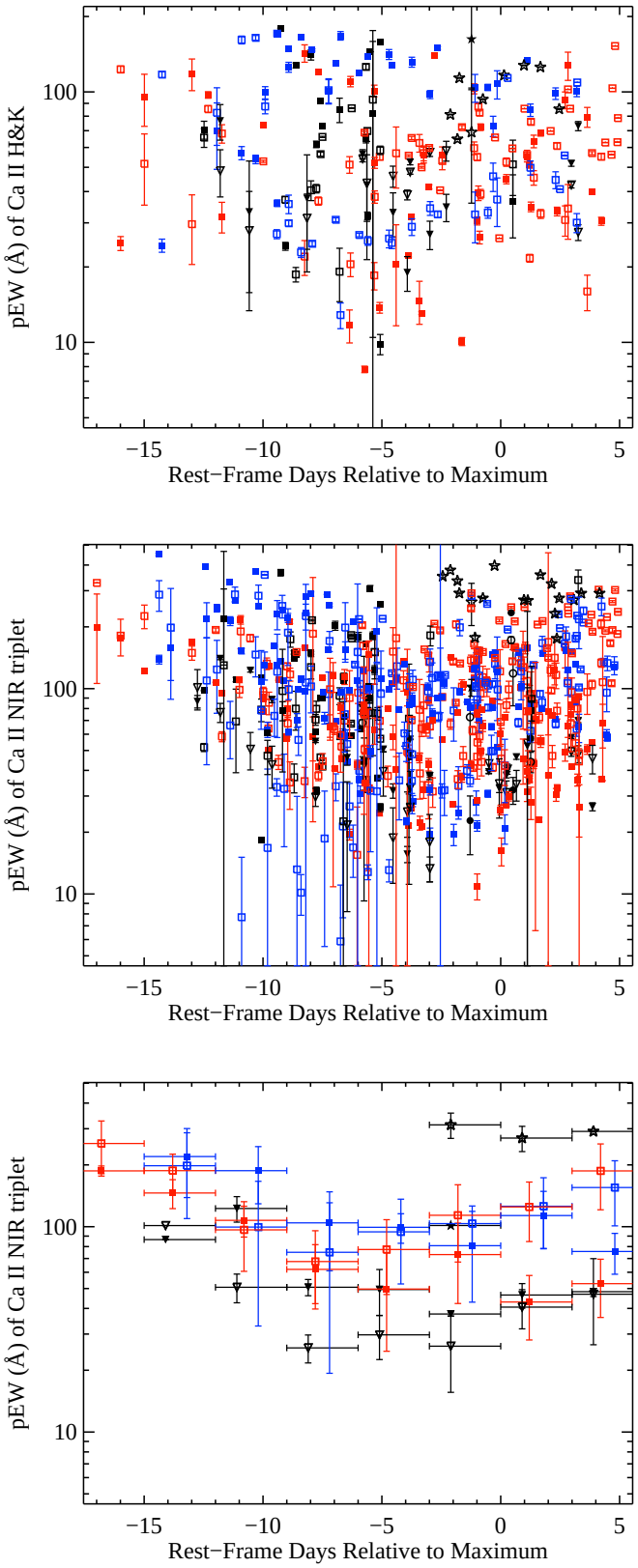

Figure 4. The CaHK (*top*) and CaIR3 (*middle* and *bottom*) pEWs versus time. The bottom panel shows the median pEW in time bins of 3 d for objects that are classified as Ia-91bg, Ia-91T/99aa, HV, or N (shifted slightly from bin centre for clarity). The horizontal error bars represent the width of each bin while the vertical error bars are the median absolute deviation in each bin. Open symbols are PVFs; filled symbols are HVFs. Blue points are HV objects, red points are N objects, and black points are objects without a Wang Type. Squares are Ia-norm, stars are Ia-91bg, triangles are Ia-91T/99aa, and circles are objects without a SNID Type. There is large scatter in the pEWs of HVFs and PVFs for both Ca II features at all epochs, though the pEWs of HVFs (PVFs) tend to decrease (increase) with time.

the pEWs of the HVFs tend to decrease with time while those of the PVFs tend to increase with time, as expected. One specific counterexample to this is SN 2009ig, which has stronger PVFs than HVFs at the very earliest times, but quickly evolves to have the HVFs dominate the profile (until $t \approx -6$ d; see also Marion et al. 2013). The typical epoch at which the strengths of the HVFs and PVFs of the Ca II features are equal is about 4 d before maximum brightness. That being said, individual SNe Ia achieve equal HVF and PVF strength at a range of epochs ($-8 < t < 2$ d), which matches what has been found previously (Marion et al. 2013).

HV objects tend to have strong HVFs at the earliest times, but they decrease in strength relatively quickly, leading to somewhat weak HVFs in HV objects near maximum brightness. The latter part of this result has been seen previously (Childress et al. 2014; Maguire et al. 2014), but at a much stronger level than what is found in the current study. We attribute this difference not only to the epochs studied (the previous works only used spectra within 5 d of maximum brightness), but also to the fact that these prior studies contained too few HV objects (∼13 per cent of their sample, versus 28 per cent herein; Childress et al. 2014; Maguire et al. 2014). This difference is discussed in more detail in Section 4.4.

While Ia-91bg objects never show HVFs, they do exhibit some of the largest pEWs of PVFs. On the other hand, Ia-91T/99aa objects always show HVFs, but the pEWs of their PVFs and HVFs are some of the lowest values seen in Figure 4. These results have been found previously and are relatively unsurprising since strong (weak) absorption features are a defining characteristic of Ia-91bg (Ia-91T/99aa) objects (Silverman et al. 2012; Folatelli et al. 2013; Childress et al. 2014).

To investigate the *relative* strength of HVFs to PVFs, Childress et al. (2014) defined $R_{\rm HVF}$ as the ratio of pEW of the HVF of CaIR3 to the pEW of the PVF of CaIR3. In this work, we define $R_{\rm CaHK}$ and $R_{\rm CaIR3}$ as the ratios of pEWs of the HVFs to the PVFs of CaHK and CaIR3, respectively. Note that spectra with only PVFs have a ratio of identically zero, while spectra with only HVFs have an undefined ratio. The values of $R_{\rm CaHK}$ and $R_{\rm CaIR3}$ are listed in Tables A2 and A4, respectively.

The ratios found herein span a range of 0–20, though most are less than 4. This is much larger than what was measured by Childress et al. (2014), who do not find ratios larger than ∼2. The difference is likely caused by the smaller epoch range studied in Childress et al. (2014); they only use spectra within 5 d of maximum. When considering only spectra from these epochs in the current work, we find that most of the ratios are less than 2.5, with only 4 spectra falling above this value. Thus, our $R_{\rm CaIR3}$ values are consistent with those in Childress et al. (2014). While one might expect $R_{\rm CaHK}$ to be correlated with $R_{\rm CaIR3}$, we find that this is not true. One explanation is that the CaHK and CaIR3 absorption strengths depend on temperature in different ways and the material that is responsible for the HVFs is likely at a different temperature than the photospheric material (e.g., Childress et al. 2014). In addition, the values of $R_{\rm CaHK}$ might be skewed slightly by the presence of weak Si II λ3858 absorption, though we find that this is likely a relatively small contamination (see Section 4.5 for more).

4.3 Ca II Velocities

The expansion velocities of HVFs and PVFs for the CaHK and CaIR3 features are listed in Tables A2 and A4, respectively. Figure 5 shows the temporal evolution of the CaHK (top) and CaIR3 (bottom) velocities. Colours and shapes of data points are the same as in Figure 4; measurement uncertainties are comparable to the size of the data points. The black dashed line represents the best-fitting natural exponential function to all of the PVF velocities, while the blue and red dashed lines use only HV and N objects, respectively. Similarly, the black dotted line is the best-fitting natural exponential function to all of the HVF velocities, and the blue and red dotted lines use only HV and N objects, respectively.

For any given object, all of the measured velocities tend to decrease with time, as expected and as seen in previous work (e.g., Silverman et al. 2012). Furthermore, in a given spectrum, the difference in velocity between the CaHK and CaIR3 features (for both PVFs and HVFs) is typically ∼500 km s^{-1}. The exponential fits in Figure 5 show that in general, for both Ca II features, the HVFs (dotted lines) and PVFs (dashed lines) of HV objects start out with higher velocities than the N objects, and their velocities decrease more quickly with time. Consequently, the HV and N objects have similar HVF and PVF velocities near maximum brightness. This may not be surprising (i.e., that HV objects have higher velocities), but we note that the Wang Type classification is based on the near-maximum-brightness velocity of Si II λ6355, and not the Ca II features.

Furthermore, we find that Ia-norm and Ia-91bg objects have consistent PVF velocities (recall that only a single Ia-91bg object shows a HVF), while Ia-91T/99aa objects have significantly lower HVF and PVF velocities. The Ia-91T/99aa objects also show a much slower decrease in their velocities with time, so once again the velocities become consistent with the rest of the sample by maximum brightness. As for the Benetti Types, HVG objects tend to start with higher velocities and decrease their velocities more quickly, as compared to LVG objects, consistent with the behaviour of the Wang HV and N objects above.

These results are somewhat different than what was seen in the early-time Ca II velocities reported in BSNIP II (Silverman et al. 2012), but the studies are consistent for data closer to maximum brightness. This is likely due to strong HVFs of Ca II in early-time spectra being blended with PVFs and biasing the measurements in BSNIP II. The velocities presented herein more accurately reflect the actual spectral profiles and expansion velocities present in the data since we carefully take into account the (possible) presence of HVFs in each observation.

In order to show how the velocities of a few individual objects evolve with time, in Figure 6 we plot a subset of the data displayed in the bottom panel of Figure 5. Figure 6 shows only CaIR3 velocities of objects for which we have more than seven spectra.[3] All of the PVF (HVF) ve-

[3] SN 2009ig is the only object in our dataset with more than

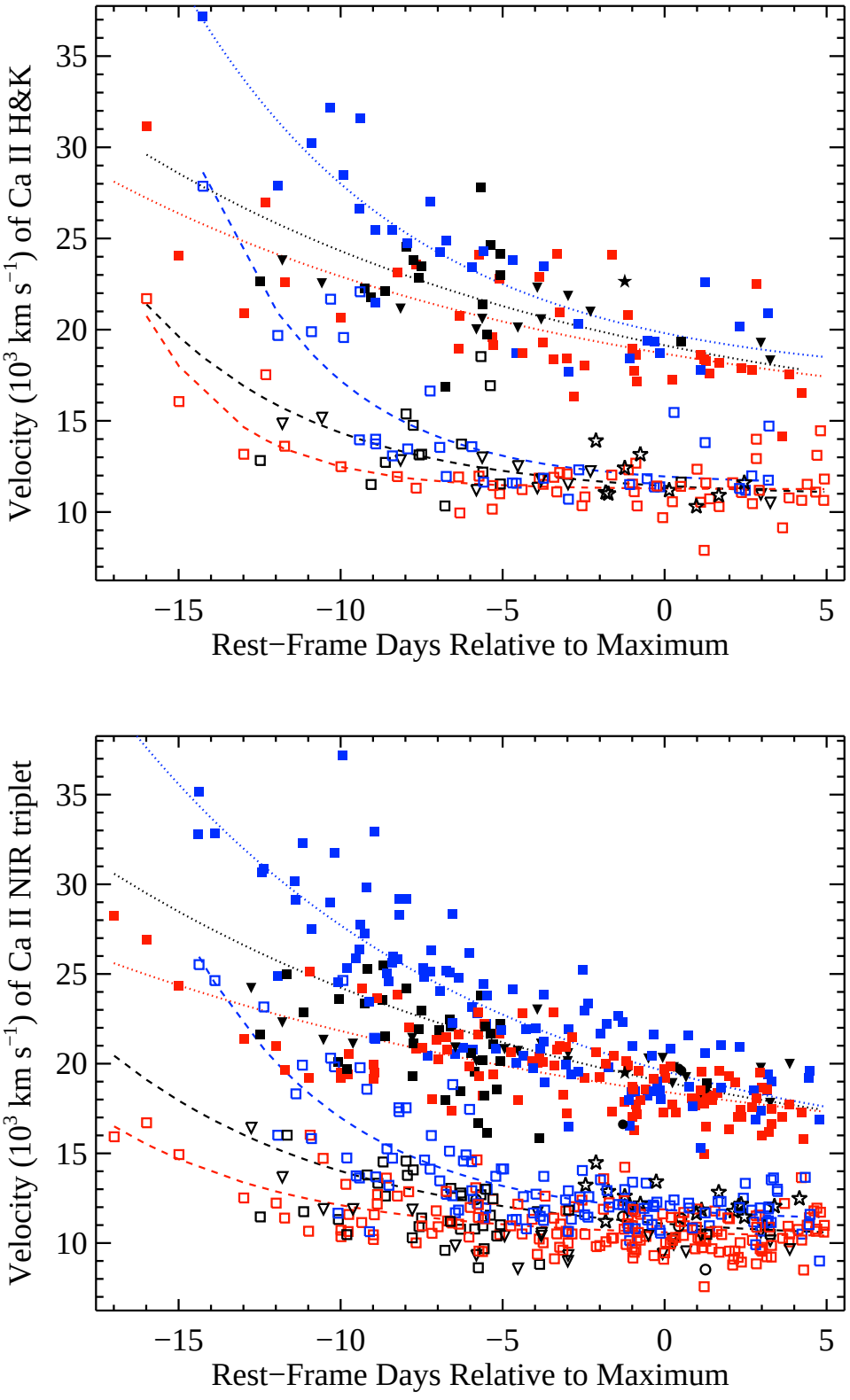

Figure 5. The CaHK (*top*) and CaIR3 (*bottom*) velocities versus time. Colours and shapes of data points are the same as in Figure 4. Measurement uncertainties are comparable to the size of the data points. The black, blue, and red dashed lines are natural exponential function fits to PVF velocities of all objects, HV objects only, and N objects only, respectively. The black, blue, and red dotted lines are natural exponential function fits to HVF velocities of all objects, HV objects only, and N objects only, respectively. Note the gap between the HVF and PVF points, especially for $t \gtrsim -5$ d; this minimum difference between HVF and PVF velocities appears to be real and not merely a measurement artifact.

locities of a given object are connected with a dashed (solid) line. This sample of eight objects includes the five extremely well-observed SNe Ia mentioned above (SNe 2009ig, 2011by, 2011fe, 2012cg—the lone Ia-91T/99aa object in the Figure, and 2012fr), in addition to SNe 2006X, 2010kg, and 2011ao. The above conclusions for the entire sample appear to also hold for this subset. Namely, HV objects tend to have faster HVFs and PVFs and their velocities decrease more quickly with time than N objects.

In both panels of Figure 5 and in Figure 6, there is a noticeable gap between the HVF and PVF points, especially for $t \gtrsim -5$ d. We further investigate this gap by calculating the difference in velocity between the HVFs and PVFs in a given spectrum for all observations where both components are observed. The temporal evolution of this separation for CaHK (CaIR3) is shown in top (bottom) panel of Figure 7.

Both Ca II features, in all subtypes, show a large range of values for the velocity separation at all epochs, but the difference tends to decrease with time. In fact, a linear fit to the data indicates a decrease at the 4σ level (7σ level) for CaHK (CaIR3) from ∼11,000 km s^{-1} to ∼8000 km s^{-1}. The typical velocity separation for both Ca II features is ∼9000 km s^{-1}, slightly higher than the 7000 km s^{-1} value found by Maguire et al. (2014), and all of the SN Ia subtypes studied herein have consistent typical velocity differences. No velocity differences are detected in the present study less than 5000 km s^{-1}, consistent with Marion et al. (2013). In fact, the vast majority of the velocity differences are greater than 6000 km s^{-1}, significantly larger than the minimum separation that our fitting algorithm is able to "resolve" (see Section 3.3.1). Thus, the gaps between the HVFs and PVFs in Figures 5 and 6 appear to be real.

While Figure 7 plots the velocity difference between HVFs and PVFs in a given spectrum, we also investigated the velocity separations for a given object at all epochs. To do this, each object's maximum PVF velocity, usually from the earliest spectrum of the object in question, was compared to its minimum HVF velocity (usually from the latest spectrum of the object in question). The vast majority of objects, ∼96 per cent, have all of their HVF velocities larger than all of their PVF velocities (i.e., the minimum HVF velocity is larger than the maximum PVF velocity).

In contrast, there are five objects with a measured PVF velocity that is larger than the lowest HVF velocity. Four of these objects (SNe 2002bo, 2006X, 2009ig, and 2010kg) show some of the fastest photospheric velocities ever observed in SNe Ia (e.g., Benetti et al. 2004; Wang et al. 2008; Marion et al. 2013; Silverman et al., in preparation, respectively) and are thus all classified as HV objects. There are many other HV objects in the current sample, however, that do not show a PVF velocity larger than their lowest HVF velocity. Perhaps this is caused by the fact that we do not have sufficiently early spectra for these other HV objects to show such a fast PVF. The fifth object in this category is SN 2011fe, which was spectroscopically observed at extremely early epochs (e.g., Parrent et al. 2012). It is interesting to note that all five of these objects also show evidence for a HVF of Si II λ6355 in their earliest epochs. Although, once again, a handful of other objects show HVFs of Si II λ6355 but do not have any PVF velocities that are larger than their lowest HVF velocity (see Section 4.6).

seven spectra where we are able to fit CaHK. Thus, we did not make a plot corresponding to Figure 6 for CaHK.

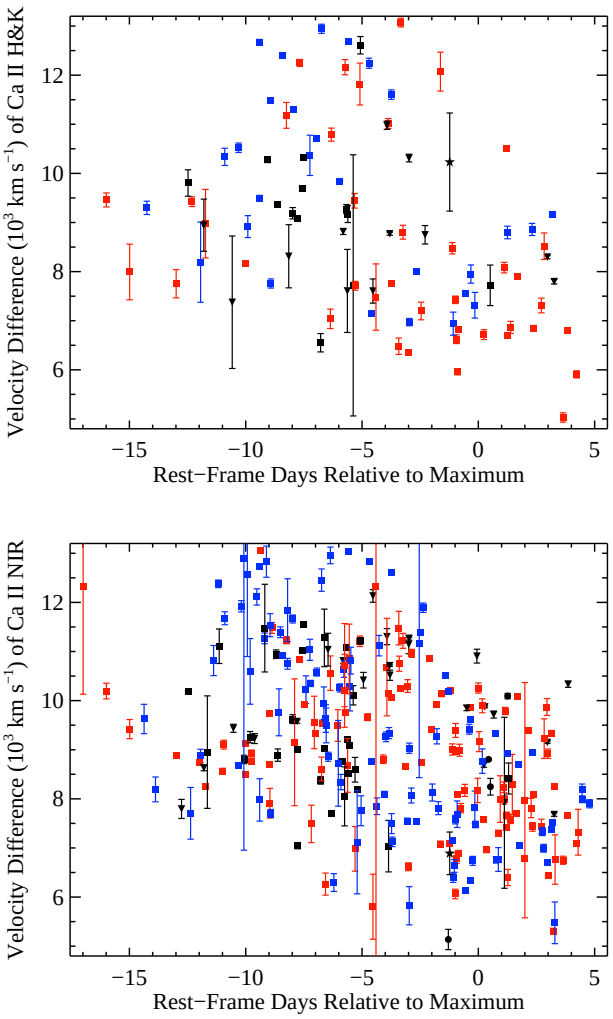

Figure 7. The temporal evolution of the difference in velocity between HVFs and PVFs of CaHK (*top*) and CaIR3 (*bottom*). Colours and shapes of data points are the same as in Figure 4. Note that three of these objects have early-time PVFs with higher velocities than their later-time HVFs.

4.4 HVFs of Ca II Compared to Other Observables

In order to connect our analysis of HVFs to possible SN Ia progenitors and environments, we compare the absolute strengths (pEWs), relative strengths ($R_{\rm CaHK}$ and $R_{\rm CaIR3}$), and velocities measured herein to other observables. Using the photometric information discussed at the end of Section 2, we find no correlation between $(B-V)_0$ and the pEWs of the HVFs or the PVFs of CaHK and CaIR3 at any epoch. The latter was also seen by Childress et al. (2014) for their low-reddening ($-0.15 < (B-V)_0 < 0.15$ mag), near maximum-brightness (within 5 d of maximum) sample. There is also no significant correlation between $(B-V)_0$

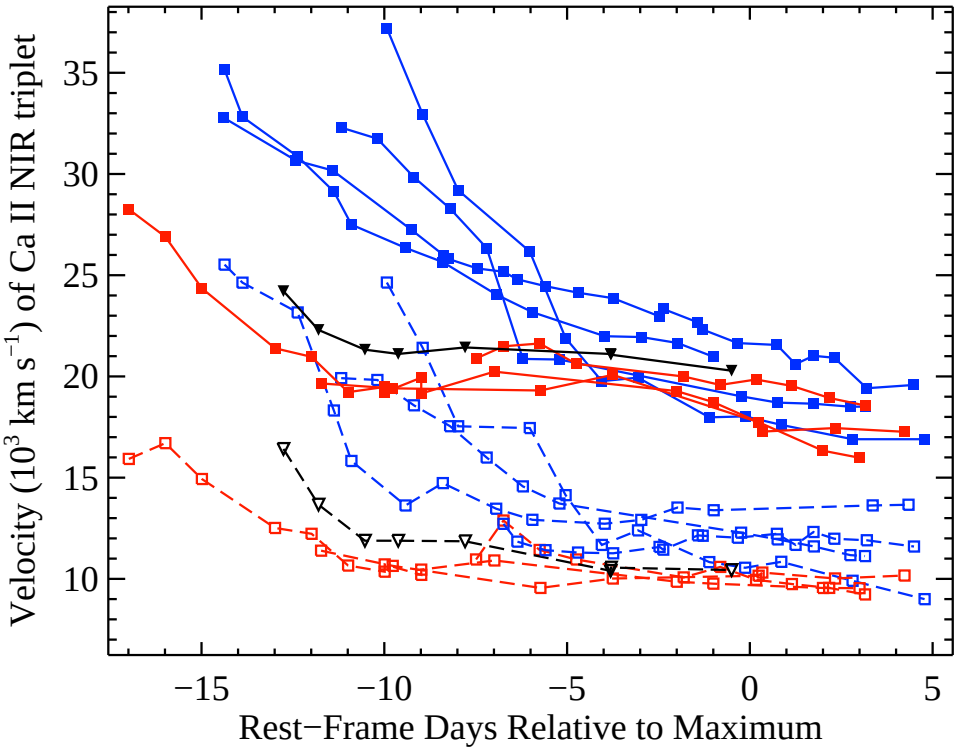

Figure 6. The CaIR3 velocities versus time for the eight SNe Ia for which we have more than seven spectra (see main text for the list of objects). All PVF (HVF) velocities of a given object are connected with a dashed (solid) line. Colours and shapes of data points are the same as in Figure 4. Measurement uncertainties are comparable to the size of the data points.

and $R_{\rm CaHK}$ or $R_{\rm CaIR3}$ at any epoch, again consistent with Childress et al. (2014).

The so-called "Phillips relation" correlates the light-curve decline rate of SNe Ia with their luminosity at peak brightness (Phillips 1993). Faster-declining SNe Ia tend to be underluminous and are also often spectroscopically Ia-91bg objects. In contrast, slow-declining objects are usually overluminous and are of the Ia-91T/99aa subtype. Figure 8 compares $R_{\rm CaHK}$ (top) and $R_{\rm CaIR3}$ (bottom) to the light-curve decline rate, characterised by the $\Delta m_{15}(B)$ parameter. For objects with multiple spectra, the median R value for a given object is plotted in the figure.[4] The dashed vertical line at $\Delta m_{15}(B) = 1.6$ mag represents a typical cutoff between normal-declining and fast-declining objects (e.g., Ganeshalingam et al. 2010). The dotted vertical line at $\Delta m_{15}(B) = 1.4$ mag is a more conservative fast-declining cutoff. The horizontal dashed line at $R = 1$ represents where the pEWs of the HVFs and the PVFs are equal.

Both $R_{\rm CaHK}$ and $R_{\rm CaIR3}$ possibly show an overall decrease with $\Delta m_{15}(B)$, though the range of observed R values definitely decreases at higher values of $\Delta m_{15}(B)$. The overluminous and normal luminosity objects ($\Delta m_{15}(B) <$ 1.6 mag) exhibit a wide range of R values, from identically 0 (i.e., no HVFs) to ∼7. On the other hand, the underluminous SNe Ia ($\Delta m_{15}(B) > 1.6$ mag) almost all have R values that are 0, and the very few that are nonzero are all less than 1. A Kolmogorov-Smirnov (KS) test indicates that $R_{\rm CaHK}$ and $R_{\rm CaIR3}$ values for normal and slow-declining objects are statistically different than those of the fast-declining objects ($p = 0.007$ and $p = 10^{-5}$ for CaHK and CaIR3, respectively).

These results still hold true even if the "fast-declining cutoff" is more conservative ($\Delta m_{15}(B) = 1.4$ mag), with KS tests indicating significant differences in $R_{\rm CaHK}$ and $R_{\rm CaIR3}$ values above and below this cutoff ($p = 10^{-5}$ and $p = 5 \times 10^{-8}$, respectively). This is consistent with what was seen in Section 4.1 when SNID Type was used instead of light-curve decline rate (i.e., Ia-91bg objects often show fast-declining light curves). Furthermore, the results presented here match those of Maguire et al. (2012), Childress et al. (2014), and Maguire et al. (2014).

Figure 9 displays the PVF velocity of Si II λ6355 versus $R_{\rm CaIR3}$ for spectra obtained earlier than 5 d before maximum brightness (top) and later than 5 d before maximum (bottom); a similar plot using $R_{\rm CaHK}$ is not shown but is qualitatively similar, though with fewer data points. Once again, the median values of both $R_{\rm CaIR3}$ and Si II λ6355 velocity for a given object are used for SNe Ia with multiple spectra in each epoch range. The dashed vertical line at 11,800 km s^{-1} in each panel represents the cutoff between N and HV objects while the horizontal dashed line at $R = 1$

[4] Here, and elsewhere, when using the median R value, we note that the results are unchanged when we instead use the mean R value or the R value from the earliest, latest, or closest-to-maximum brightness spectrum in our sample.

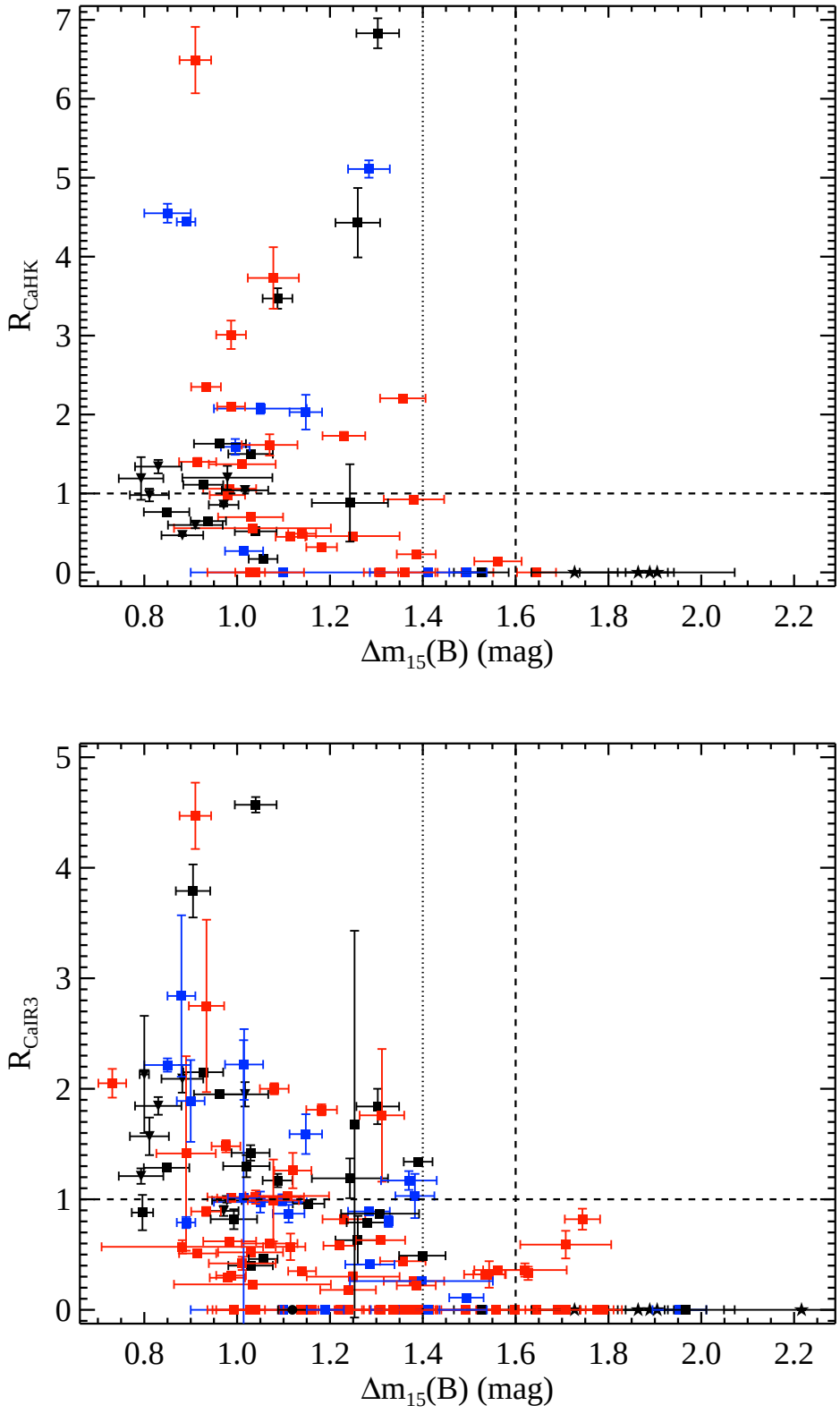

Figure 8. $R_{\rm CaHK}$ (*top*) and $R_{\rm CaIR3}$ (*bottom*) versus light-curve decline rate ($\Delta m_{15}(B)$). The median R value of a given object is used for objects with multiple spectra. The dashed vertical line is a typical cutoff between normal- and fast-declining objects; the dotted vertical line is a more conservative cutoff. The horizontal dashed line is where the pEWs of the HVFs and PVFs are equal. Colours and shapes of data points are the same as in Figure 4.

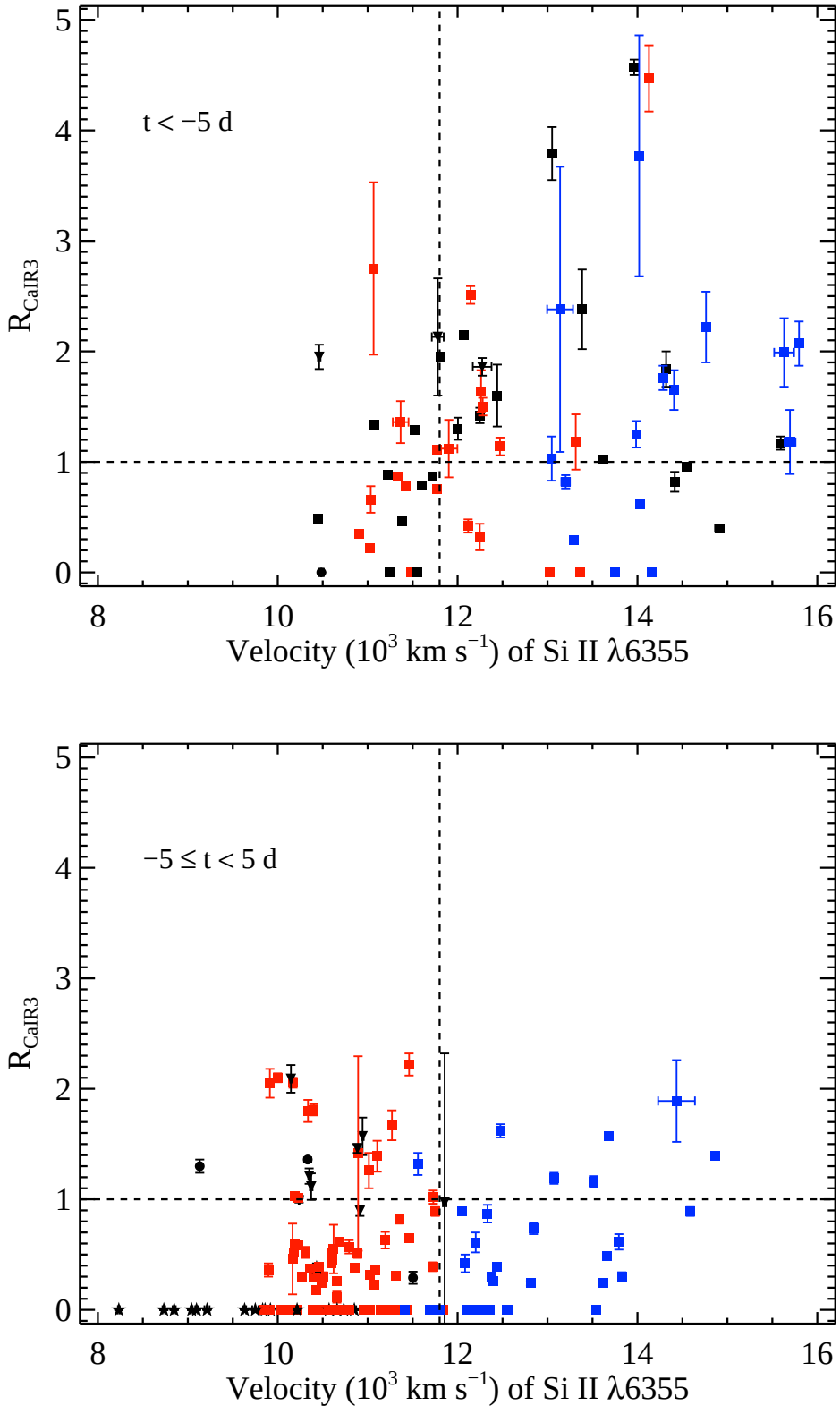

Figure 9. $R_{\rm CaIR3}$ versus Si II λ6355 (PVF) velocity for spectra obtained earlier than 5 d before maximum brightness (*top*) and later than 5 d before maximum (*bottom*). The median R value and velocity of a given SN Ia are used for objects with multiple spectra in each epoch range. The dashed vertical line in each panel are the cutoffs between N and HV objects. The horizontal dashed line in each panel are where the pEWs of the HVFs and PVFs are equal. Colours and shapes of data points are the same as in Figure 4.

represents where the pEWs of the HVFs and the PVFs are equal.

Aside from the Ia-91bg objects (i.e., the stars in Figure 9), which we have shown almost never contain HVFs, there is a large range of $R_{\rm CaIR3}$ values at all Si II λ6355 velocities in both age ranges. Thus, we find no correlation between these two parameters and no significant difference in $R_{\rm CaIR3}$ (or $R_{\rm CaHK}$) values for N versus HV objects. This is inconsistent with Childress et al. (2014) and Maguire et al. (2014), both of which find that HV objects do not show HVFs. On the contrary, we find many HV objects with relatively strong HVFs at all epochs, represented by blue points in the upper-right quadrants of the panels in Figure 9. Compare this to the bottom panel of Figure 5 in Childress et al. (2014) and the left panel of Figure 6 in Maguire et al. (2014), both of which lack objects in the upper-right quadrant.

Our results are unchanged even if we restrict our sample only to spectra within 5 d of maximum brightness (top panel of Figure 9), in order to match the epochs studied in the two aforementioned works. Thus, this discrepancy is likely caused by the fact that Childress et al. (2014) and Maguire et al. (2014) have too few HV objects in their datasets. As mentioned in Section 4.1, $\sim$28 per cent of the objects studied herein are HV objects, which matches the overall SN Ia population (e.g., Wang et al. 2009a; Silverman et al. 2012). On the other hand, only $\sim$13 per cent of the objects studied by Childress et al. (2014) and Maguire et al. (2014) were HV. This difference in sample demographics likely led to the inconsistency discussed above.

Many other SN Ia observables were compared to $R_{\rm CaHK}$ and $R_{\rm CaIR3}$, but almost none showed any significant correlation. For completeness, we list here the parameters investigated. Some normal SNe Ia are found to exhibit C II absorption features in their early-time spectra (e.g., Parrent et al. 2011; Thomas et al. 2011; Folatelli et al. 2012; Silverman & Filippenko 2012). This C is likely unburned fuel from the progenitor WD. No difference in $R_{\rm CaHK}$ ($R_{\rm CaIR3}$) is found for objects with or without C II absorption features when investigating 107 (252) spectra, consistent with what was found by Maguire et al. (2014).

Narrow Na I D absorption features have been found to be preferentially blueshifted (relative to the host galaxy's rest frame) in SNe Ia (e.g., Sternberg et al. 2011; Foley et al. 2012a; Maguire et al. 2013). When using 40 spectra that have the shift of these features measured, we find no difference in R values of objects with blueshifted versus redshifted Na I D lines. The rise time of a SN Ia light curve is usually calculated by extrapolating early-time photometry backward in time to a flux of zero. Using rise times of 74 objects published by Ganeshalingam et al. (2011), we find no correlation with $R_{\rm CaHK}$ or $R_{\rm CaIR3}$.

Concentrating now on late-time spectra of SNe Ia, we compare the R values calculated herein to nebular velocities — that is, the average of the [Fe II] λ7155 and [Ni II] λ7378 velocities (Maeda et al. 2010). The nebular velocity has been found to correlate with the velocity gradient near maximum brightness, as well as the near-maximum ejecta velocity (i.e., PVF velocity) (e.g., Maeda et al. 2010; Silverman et al. 2013), neither of which were seen to correlate with the strengths of HVFs in the current work. Thus, it is unsurprising that the nebular velocity is unrelated to $R_{\rm CaHK}$ and $R_{\rm CaIR3}$ for 22 and 47 spectra, respectively.

On the other hand, the full-width at half-maximum intensity (FWHM) of the [Fe III] λ4701 feature, which is detected in many SN Ia nebular spectra, is somewhat correlated with $R_{\rm CaHK}$ and $R_{\rm CaIR3}$ (Pearson r value of $\sim$0.6). This is consistent with previous work which found the FWHM of this feature to be anticorrelated with $\Delta m_{15}(B)$ (e.g., Silverman et al. 2013), and we have shown above that $R_{\rm CaHK}$ and $R_{\rm CaIR3}$ are also anticorrelated with $\Delta m_{15}(B)$.

For 242 spectra, we compared $R_{\rm CaHK}$ and $R_{\rm CaIR3}$ to host-galaxy type, as listed in NED. SNe Ia in E/S0 hosts are found to have significantly lower R values than those found in Sa/Sb/Sc/Sd/Irr hosts. We note that this result was also seen by Pan et al. (2015). There is a well-established connection between early-type hosts and underluminous SNe Ia, and late-type hosts and normal/overluminous SNe Ia (e.g., Hamuy et al. 1995; Sullivan et al. 2006; Pan et al. 2014), so this finding is completely consistent with the aforementioned result that underluminous, Ia-91bg objects show relatively weak (or nonexistent) HVFs.

We searched for correlations between the SN Ia observables mentioned above and the velocities of the Ca II HVFs and PVFs, but found no significant results. Our analysis indicates that Ca II velocities (both the HVFs and PVFs) are uncorrelated with $(B-V)_0$, $\Delta m_{15}(B)$, the presence or absence of C II absorption, the relative Doppler shift of narrow Na I D absorption, light-curve rise time, nebular velocity, FWHM of [Fe III] λ4701, and host-galaxy type.

4.5 Si II λ3858

The Si II λ3858 absorption feature has been discussed in multiple sections above, but here we summarise our results regarding it. Foley (2013) claim that Si II λ3858 usually dominates the CaHK profile, but the findings of both Childress et al. (2014) and Maguire et al. (2014) are inconsistent with this conclusion. We agree with the latter two works, as outlined below. As discussed in Section 3.1, the only extra assumption we made in order to determine whether Si II λ3858 was present in a given spectrum was as follows: if a spectrum showed a HVF of CaIR3, then it should also have a HVF of CaHK, and vice versa. This broke the degeneracy between Si II λ3858 (PVF) absorption and CaHK HVF absorption.

We tested this assumption by supposing Si II λ3858 was never present. This led to velocity differences between HVFs of CaHK and CaIR3 of $\sim$5000 km s^{-1} (instead of the more typical value of $\sim$500 km s^{-1}) and velocity differences between CaHK HVFs and PVFs of $\sim$5500 km s^{-1} (as opposed to the median value of $\sim$9000 km s^{-1}). The assumption was further investigated by assuming that Si II λ3858 was *always* present (instead of HVFs of CaHK). This again yielded inconsistent results, namely the Si II λ3858 velocities were $\sim$2600 km s^{-1} faster than the Si II λ6355 velocities in a given spectrum (compared to the more typical value of $\sim$600 km s^{-1}, e.g., Silverman et al. 2012). Note that this was previously shown graphically in Figure 2. Thus, our assumption seems to be valid.

Si II λ3858 is detected in the CaHK profile in $\sim$ 24 per cent (30/126) of the spectra fit, and half of these also show evidence for a HVF of CaHK. These spectra represent $\sim$27 per cent (23/84) of the SNe Ia in the current dataset. When Si II λ3858 is detected, its pEW is $\sim$70 Å

smaller than that of Si II λ6355 in the same spectrum, which represents a factor of $\sim$6 (see Section 4.7). This difference in strength is larger than expected given typical SN Ia photospheric temperatures and the gf-weights of the two Si II lines.[5] While weak absorption from Si II λ3858 may actually be present in a higher percentage of the data, our fitting algorithm is unable to detect such a feature. Furthermore, no evidence of a HVF of Si II λ3858 is detected in any of the observations.

Figure 10 shows the temporal evolution of the velocity of the Si II λ3858 absorption feature (using the same epoch range as previous temporal evolution figures in this work, and adopting the same data-point colours and shapes as in Figure 4). The Si II λ3858 feature is detected mostly at epochs later than 8 d before maximum brightness (there is one detection at $t \approx -12$ d) and, as expected, the velocities tend to decrease with time. The detection of Si II λ3858, as well as the strength (i.e., pEW) and velocity of the feature when detected, are uncorrelated with any of the aforementioned SN Ia classification schemes (i.e., SNID Type, Wang Type, and Benetti Type), as well as any of the other SN Ia observables mentioned in Section 4.4 (except, of course, the Si II λ6355 PVF velocity). Another possible exception is that Si II λ3858 might be detected more frequently in N objects, as opposed to other subtypes, though the relatively small total number of detections makes this result rather weak.

4.6 The Existence of HVFs in Si II λ6355

Using the algorithm described in Section 3, the pEWs and expansion velocities were calculated for both HVFs and PVFs of Si II λ6355; the values are listed in Table A3. HVFs of Si II λ6355 have rarely been carefully studied previously, with Marion et al. (2013) representing one of the most detailed works on the subject. In the present study, Si II λ6355 was fit in a total of 422 spectra of 208 SNe Ia; 2 of these spectra have only HVFs, 326 have only PVFs, and 94 have both HVFs and PVFs detected. SN 2012fr is the only object in our sample with spectra showing only HVFs of Si II λ6355, and this is found for only the two earliest spectra (14.4 and 14.0 d before maximum brightness). As mentioned in Section 4.1, this is consistent with an in-depth study of this object which found HVFs of CaIR3 and Si II λ6355 but no PVFs in these spectra (Childress et al. 2013).

Like the Ca II features, SNe Ia tend to evolve from having only Si II λ6355 HVFs, though this is seen only in one object and at very early times, to having both HVFs and PVFs, to having only PVFs, which is what is seen in the majority of the spectra, $\sim$77 per cent. Spectra with only Si II λ6355 PVFs are detected as early as 15 d before maximum and as late as 5 d past maximum (i.e., the oldest spectra in the current study), while spectra with both HVFs and PVFs are observed at all epochs studied ($-16 < t < 5$ d).

Unlike the Ca II features, however, HVFs of Si II λ6355 are somewhat rare in SN Ia spectra. Only $\sim$16 per cent of all SNe Ia studied herein show evidence for Si II λ6355 HVFs in at least one spectrum (compared to $\sim$67 per cent for HVFs of CaHK and CaIR3). In early-time observations ($t \lesssim -5$ d), $\sim$32 per cent of objects have detectable HVFs of Si II λ6355, much lower than the $\sim$91 per cent of objects that exhibit HVFs of Ca II at these early epochs.

All spectra obtained earlier than 11 d before maximum brightness contain HVFs of Si II λ6355, while they are seen in 21 spectra of 7 SNe Ia for $t > -5$ d. This latter result is inconsistent with Childress et al. (2014), who find no HVFs of Si II λ6355 at these epochs. The difference is likely caused by the larger dataset used herein, as well as by differences in the spectral fitting algorithms used. The low detection rate of HVFs of Si II λ6355 could be explained by an inherent rarity of HVFs of Si II λ6355, the possibility that they disappear at very early times, or some combination of both.

As when fitting the Ca II features, we find that $\sim$ 29 per cent of the objects for which we fit the Si II λ6355 feature are HV objects, again consistent with the overall SN Ia population (e.g., Wang et al. 2009a; Silverman et al. 2012). Furthermore, only 8 objects had their Wang Type changed when using the PVF velocity calculated in this work as compared to previous work (e.g., Silverman et al. 2012), and all of these SNe Ia had velocities that were near the cutoff between HV and N objects. For the SNe Ia with a Wang Type, 33 per cent of HV objects contain HVFs of Si II λ6355, while only 6 per cent of N objects show HVFs of Si II λ6355. This dramatic difference has never been convincingly seen before, although it was previously suggested by Tanaka et al. (2008), and is significantly different than the HVFs of Ca II which are found in similar percentages of HV and N objects. This result may be surprising since one might expect PVFs with higher velocities to be blended more severely with any possible HVF, and thus one might be biased *against* finding distinct HVFs of Si II λ6355 in HV objects.

Much like Ca II, however, HVFs of Si II λ6355 are found in similar numbers of Ia-norm and Ia-91T/99aa objects (14 per cent and 19 per cent, respectively) while no HVFs are seen in Ia-91bg objects. As mentioned previously, the BSNIP dataset (which represents the bulk of the sample studied herein) is not well suited to velocity-gradient measurements or Benetti Type classifications. That being said, we report our results here for completeness, though note the relatively low numbers of objects involved. We find no HVFs of Si II λ6355 in FAINT objects, consistent with Ia-91bg objects having no HVFs. On the other hand, 29 per cent of LVG objects and 27 per cent of HVG objects show evidence for HVFs of Si II λ6355. This is somewhat different than the aforementioned predominance of Si II λ6355 HVFs in HV objects and the relative lack of them in N objects. However, given the relatively small number of SNe Ia for which we can measure a reliable Benetti Type, these percentages are formally consistent with the results found when using Wang Types.

4.7 Si II λ6355 pEWs

The pEWs of Si II λ6355 are listed in Table A3 and their temporal evolution is displayed in Figure 11. Like the Ca II features, there is significant scatter in the pEWs of the HVFs and PVFs of Si II λ6355. In addition, the HVF pEWs tend to decrease with time while the PVF pEWs typically increase with time. As discussed above, HVFs of Si II λ6355 disappear at much earlier epochs than either Ca II feature. The strengths (i.e., pEWs) of HVFs and PVFs are seen to be equal for CaHK and CaIR3 for $-8 < t < 2$ d, while this

[5] `http://www.nist.gov/pml/data/asd.cfm`.

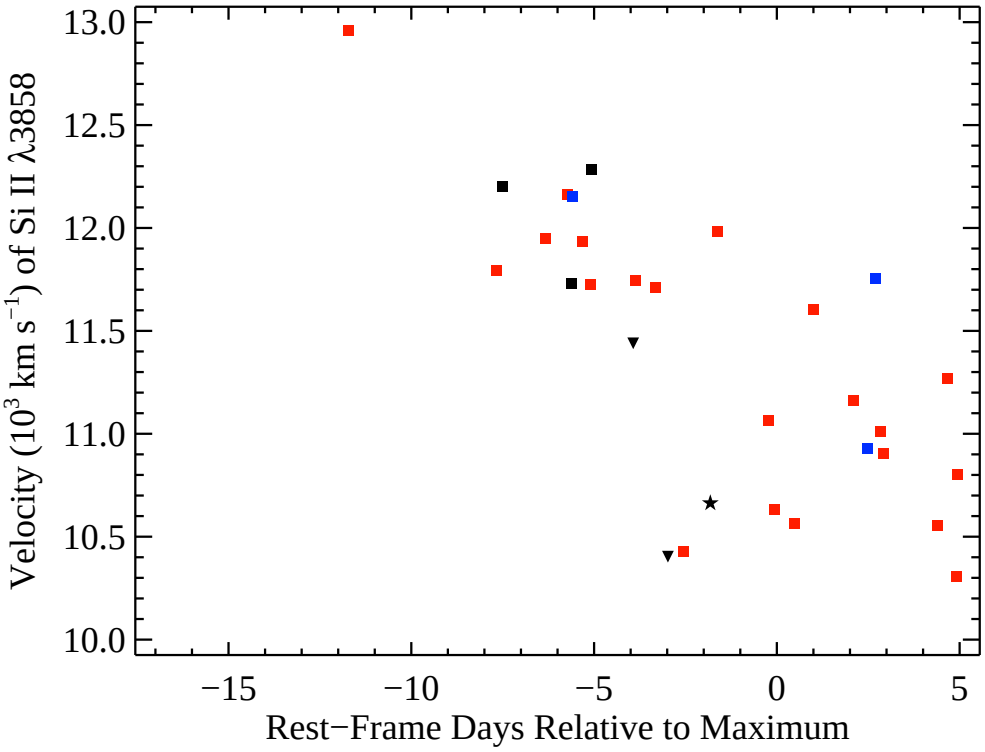

Figure 10. The Si II λ3858 velocity versus time. Colours and shapes of data points are the same as in Figure 4. Measurement uncertainties are comparable to the size of the data points.

is achieved for Si II λ6355 $\sim$11 d before maximum brightness. In fact, there are only 5 spectra in which the pEW of the Si II λ6355 HVF is larger than that of the Si II λ6355 PVF, and all of these were obtained at $t < -11$ d. In spite of this, moderately strong HVFs of Si II λ6355 are observed in a handful of objects through $t \approx -6$ d and in some objects through $t \approx 5$ d, and these are almost exclusively HV objects.

As mentioned in Section 4.6, HV objects tend to show HVFs of Si II λ6355 significantly more often than N objects, and, according to Figure 11, on average they exhibit stronger HVFs than N objects when detected in both subtypes at the same epoch. Similar to the Ca II pEWs, though not quite as extreme, Ia-91bg objects have relatively large pEWs of Si II λ6355 PVFs but no HVFs, and Ia-91T/99aa objects have relatively low pEWs of both Si II λ6355 PVFs and HVFs.

Analogous to the Ca II features, we define $R_{\rm Si}$ as the ratio of pEWs of the HVFs to the PVFs of Si II λ6355.[6] Once again, spectra with only PVFs are defined to have a ratio of zero, while spectra with only HVFs have an undefined ratio; the values of $R_{\rm Si}$ are listed in Table A3. For nearly all spectra studied herein, $R_{\rm Si} < 1$. There are five spectra whose ratio is larger than unity, and they represent the earliest spectral observations of SNe 2012cg and 2012fr (Silverman et al. 2012b; Childress et al. 2013, respectively). Note that SN 2012fr was also the sole object in this work found to have spectra showing HVFs of Si II λ6355 *without* PVFs.

[6] Note that $R_{\rm Si}$ defined here is unrelated to the so-called "Si II ratio," $\Re$(Si II), which was defined by Nugent et al. (1995) as the ratio of the depth of the Si II λ5972 feature to the depth of the Si II λ6355 feature.

4.8 Si II λ6355 Velocities

The measured PVF and HVF velocities of the Si II λ6355 feature are listed in Table A3, and Figure 12 shows the temporal evolution of these velocities. As in Figure 5, the black dashed line is the best-fitting natural exponential function to all Si II λ6355 PVF velocities, while the blue and red dashed lines use only HV and N objects, respectively. The black dotted line is the best-fitting natural exponential function to all Si II λ6355 HVF velocities, and the blue and red dotted lines use only HV and N objects, respectively.

Like the Ca II features, the measured velocities (both PVFs and HVFs) of a given object tend to decrease with time. The exponential fits in Figure 12 show that, again as seen in the Ca II features, the HVFs (dotted lines) and PVFs (dashed lines) of HV objects start out with higher velocities than the N objects and likely decrease their velocity more quickly with time. For Si II λ6355, however, the HVF and PVF velocities of the HV objects are almost always larger than those of the N objects at a given epoch. This is by construction, at least for the PVF velocities, since the PVF Si II λ6355 velocity is how a Wang Type is assigned to a given object.

Ia-91bg objects are found to have the lowest Si II λ6355 velocities, with Ia-91T/99aa objects having slightly larger

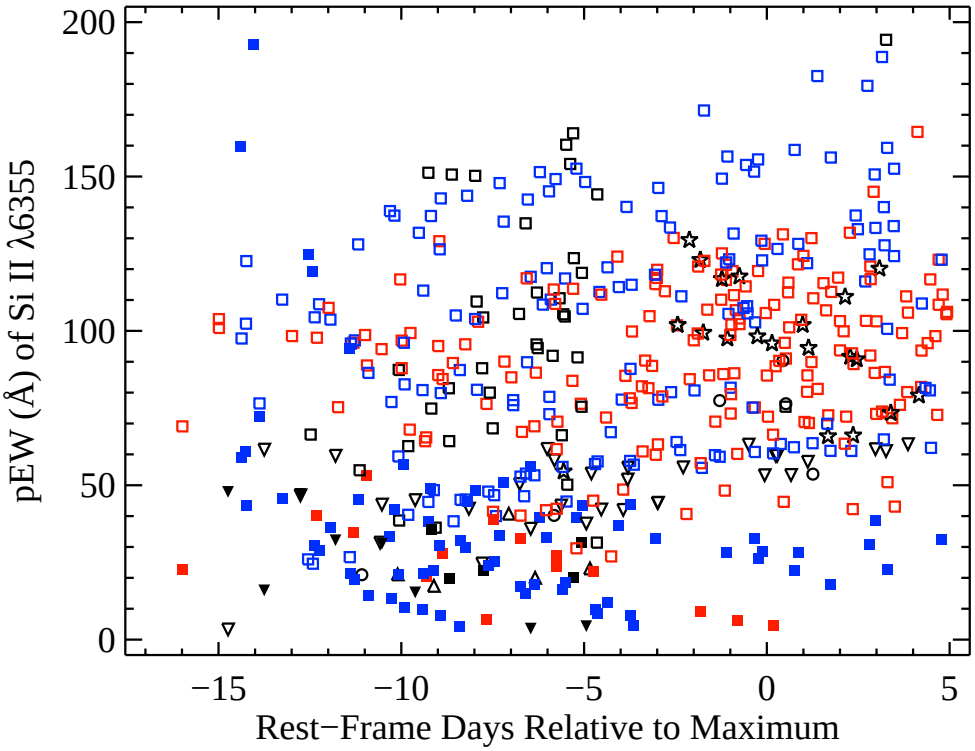

Figure 11. The Si II λ6355 pEWs versus time. Colours and shapes of data points are the same as in Figure 4. Measurement uncertainties are comparable to the size of the data points.

velocities. N objects have slightly larger velocities than that and, of course, HV objects exhibit the highest velocities. This is consistent with previous Si II λ6355 velocity studies (e.g., Silverman et al. 2012).

Only Si II λ6355 velocities of objects for which we have more than seven spectra are shown in Figure 13 (thus, this is a subset of what is displayed in Figure 12). As in Figure 6, the PVF (HVF) velocities of a given object are connected with a dashed (solid) line. The nine objects plotted in Figure 13 include the five extremely well-observed SNe Ia mentioned above (SNe 2009ig, 2011by, 2011fe, 2012cg — the lone Ia-91T/99aa object in the Figure — and 2012fr), in addition to SNe 1994D, 2006X, 2010kg, and 2011ao. The aforementioned conclusions once again hold for this subset: HV objects have faster HVFs and PVFs at all epochs, and they likely decrease more quickly with time than N objects.

As with the Ca II features, the Si II λ6355 feature shows a distinct gap between HVF and PVF velocities. This gap is most noticeable for $t \gtrsim -6$ d. Once again, the difference in velocity between the HVFs and PVFs in a given spectrum is calculated. While this difference tends to decrease with time, there is a very large amount of scatter at all epochs, similar to the CaIR3 feature. The typical velocity separation for Si II λ6355 is $\sim$6000 km s^{-1}, slightly less than what was found for the Ca II features (i.e., $\sim$9000 km s^{-1}). No velocity differences are found less than 4200 km s^{-1}, and most are greater than 5000 km s^{-1}. These values are somewhat larger than the minimum separation resolvable by our fitting algorithm (see Section 3.3.1), so as was the case for CaIR3, the gap between the Si II λ6355 HVFs and PVFs is likely real.

As was done for the Ca II features, the velocity separations for a given object at all epochs were investigated for Si II λ6355. Again, each object's maximum PVF velocity, usually from the earliest spectrum of the object in question, was compared to its minimum HVF velocity, usually from the latest spectrum of the object in question. All objects studied herein have all of their HVF velocities larger than all of their PVF velocities (i.e., the minimum HVF velocity is larger than the maximum PVF velocity).

4.9 HVFs of Si II λ6355 Compared to Other Observables

As with the Ca II features, we compare the $R_{\rm Si}$ values of the Si II λ6355 feature to other SN Ia observables. The SN colour is being characterised in this work using the observed $B-V$ colour at B-band maximum brightness, with only a correction for MW reddening (Schlegel et al. 1998) having been applied. Thus, there are many objects in the sample that have large (i.e., red) values of $(B-V)_0$ caused by reddening from their host galaxy. When ignoring highly reddened objects ($(B-V)_0 > 0.4$ mag; e.g., Foley et al. 2011), the mean $R_{\rm Si}$ value is more than twice as large for objects with $(B-V)_0 > 0$ mag as compared to objects with $(B-V)_0 < 0$ mag ($\sim$0.037 and $\sim$0.016 mag, respectively). Both of these values are quite close to $R_{\rm Si} = 0$, since there are relatively few objects that show HVFs of Si II λ6355;

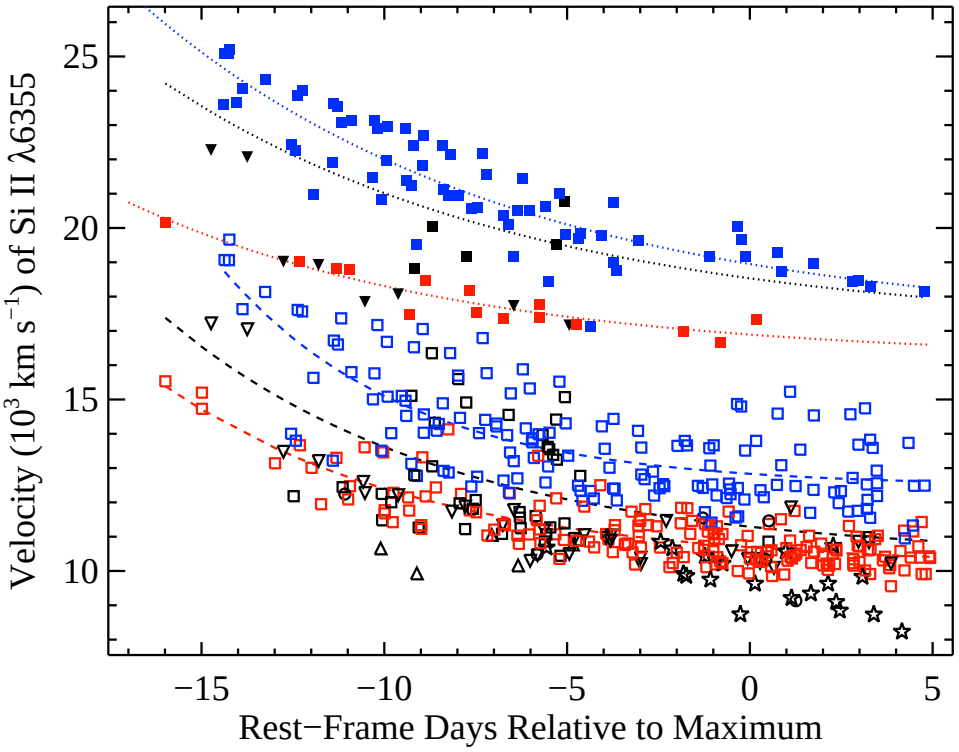

Figure 12. The Si II λ6355 velocities versus time. Colours and shapes of data points are the same as in Figure 4. Measurement uncertainties are comparable to the size of the data points. Like Figure 5, the black, blue, and red dashed lines are natural exponential function fits to PVF velocities of all objects, HV objects only, and N objects only, respectively. The black, blue, and red dotted lines are natural exponential function fits to HVF velocities of all objects, HV objects only, and N objects only, respectively.

thus, this result is of somewhat low significance. If correct, however, it indicates that $R_{\rm Si}$ is larger for intrinsically redder SNe Ia, which are also found to show larger Si II λ6355 velocities (e.g., Foley et al. 2011; Milne et al. 2014).

Like the Ca II features, no HVFs of Si II λ6355 are found in fast-declining SNe Ia, while normal- and slow-declining objects show a range of $R_{\rm Si}$ values (from identically 0 to $\sim$0.5). In fact, no object with $\Delta m_{15}(B) > 1.45$ mag show HVFs of Si II λ6355, and the difference in $R_{\rm Si}$ values above and below this cutoff is statistically significant. These findings are consistent with the results discussed in Section 4.6 where SNID Type was used instead of light-curve decline rate.

As also seen in Section 4.6, the majority of the Si II λ6355 HVFs are found in HV objects. Another way to present this result is shown in Figure 14, which displays the (PVF) velocity of Si II λ6355 versus $R_{\rm Si}$. The median values (of both $R_{\rm Si}$ and Si II λ6355 velocity) are used for objects with multiple spectra. The dashed line at 11,800 km s^{-1} represents the cutoff between N and HV objects.

The typical value of $R_{\rm Si}$ that we measure increases with Si II λ6355 velocity, although there are only a handful of objects with $R_{\rm Si} \neq 0$. Of these SNe Ia that show HVFs of Si II λ6355, three are N objects, while two are Ia-91T/99aa and five are unclassified objects. On the other hand, 13 are HV objects, while HV objects make up less than 30 per cent of the current dataset. Also note that the five unclassified objects with HVFs of Si II λ6355 are all found to have velocities greater than 11,800 km s^{-1}, and are thus *likely* HV objects. About half of the highest-velocity objects (i.e., Si II λ6355 velocity greater than 14,000 km s^{-1}) show HVFs of Si II λ6355; compare this to the entire dataset, in which only $\sim$16 per cent of objects show HVFs of Si II λ6355.

As mentioned in Section 4.4, C II absorption features are sometimes found in early-time optical spectra of SNe Ia, likely coming from unburned progenitor WD material (e.g., Parrent et al. 2011; Thomas et al. 2011; Folatelli et al. 2012; Silverman & Filippenko 2012). For 288 spectra, we find a statistically significant difference in values of $R_{\rm Si}$ for objects with versus without C II absorption features. The mean $R_{\rm Si}$ value for SNe Ia with detected C II is $\sim$0.011, while the mean $R_{\rm Si}$ value for those without C II is nearly twice as large ($\sim$0.019). This implies that objects lacking C II absorption features also show stronger HVFs. Consistent with this finding, and previous results in the current work, HV objects have also been shown to lack C II absorption (e.g., Silverman & Filippenko 2012).

Other SN Ia observables were also compared to $R_{\rm Si}$, but none of them showed any significant correlation. As was done for the Ca II feature, we list the observables investigated for completeness. No difference in $R_{\rm Si}$ values is found for objects with blueshifted versus redshifted narrow Na I D absorption lines when using 47 spectra. Similarly, no correlation is found between $R_{\rm Si}$ and the light-curve rise times of 43 of the objects published by Ganeshalingam et al. (2011), the nebular velocity (of 17 objects), or the FWHM of the [Fe III]

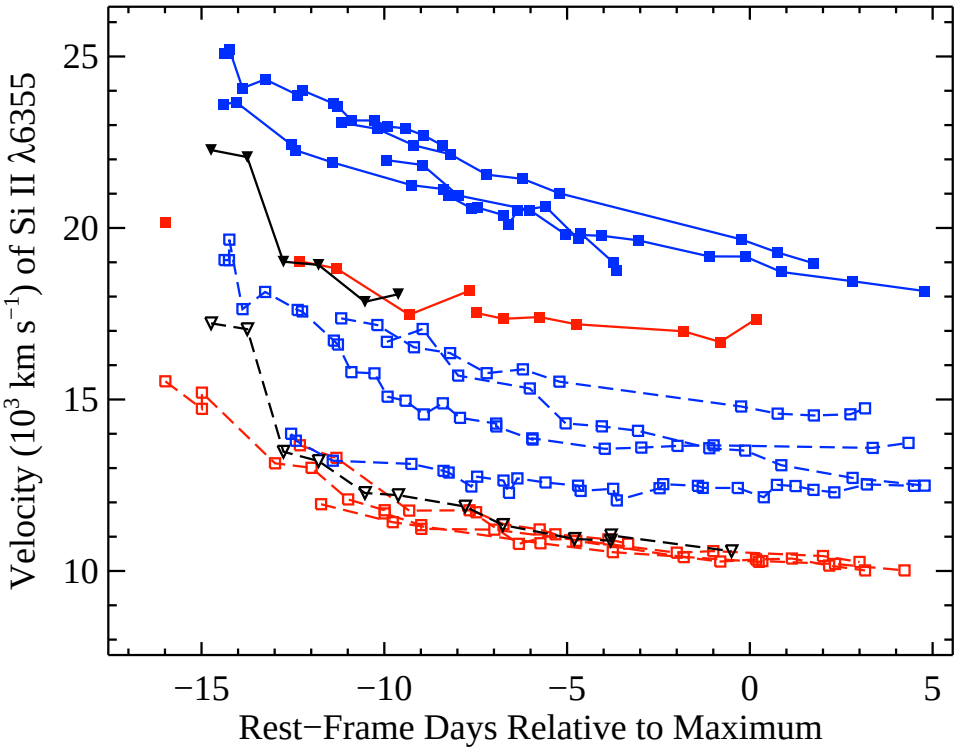

Figure 13. The Si II λ6355 velocities versus time for the nine SNe Ia for which we have more than seven spectra (see main text for the list of objects). All PVF (HVF) velocities of a given object are connected with a dashed (solid) line. Colours and shapes of data points are the same as in Figure 4. Measurement uncertainties are comparable to the size of the data points.

λ4701 feature (of 17 objects). Finally, the host-galaxy type (as reported in NED) is related to the value of $R_{\rm Si}$ for 287 spectra in the same way as $R_{\rm CaHK}$ and $R_{\rm CaIR3}$; objects in E/S0 hosts tend to have lower R values than those found in other galaxy types.

In summary, Si II λ6355 HVFs are never found in slow-declining (i.e., Ia-91bg/FAINT) objects, as is the case with HVFs of CaHK and CaIR3. Unlike the HVFs of Ca II, however, HVFs of Si II λ6355 are relatively rare overall, yet there are significantly more HV objects with Si II λ6355 HVFs as compared to any other SN Ia subtype. Furthermore, we find that objects showing strong HVFs of Si II λ6355 also tend to have redder optical colours at maximum brightness and lack C II absorption in their early-time spectra. This connection between photospheric velocity, ultraviolet (UV)/optical colour near maximum, and C II absorption have all been recognised in previous works mentioned above, but the addition of the association between HV objects and relatively strong HVFs of Si II λ6355 is new and unique to the current work. We also note the possibility that HV objects preferentially occur in the inner regions of their host galaxies (Wang et al. 2013; Pan et al. 2015).

As discussed above and in Wang et al. (2009a), the Wang Type classifications, and thus the correlations in the previous paragraph, only apply to "typical" SNe Ia. These objects make up ∼70 per cent of the SN Ia population (Li et al. 2011), are spectroscopically "normal" (e.g., according to SNID), and usually have $\Delta m_{15}(B) = 1.1 \pm 0.3$ mag (e.g., Ganeshalingam et al. 2010). For such objects, there seems to be an observational dichotomy, or, more likely, a continuous distribution of multiple observables that are mutually correlated. Table 1 presents this dichotomy, or rather, the extremes of this continuous distribution. In essence, we find that a "typical" SN Ia with a relatively large near-maximum photospheric velocity, which would lead to classification as a HV object, will likely lack early-time C II absorption, tend to have relatively red UV/optical colours near maximum brightness, will show relatively strong HVFs of Si II λ6355, and may be found in the inner regions of its host galaxy.

5 CONCLUSIONS

We have conducted the most detailed study of HVFs performed to date, using a sample of 445 low-resolution optical and NIR spectra at epochs up to 5 d past maximum brightness of 210 low-redshift SNe Ia that follow the "Phillips relation." By fitting a series of Gaussian functions, we are able to determine whether a given spectrum shows evidence for HVFs of CaHK, Si II λ6355, or CaIR3, as well as measure the velocities and pEWs of the PVFs and HVFs of these three spectral features. Our measured values are consistent with previous studies of HVFs (e.g., Marion et al. 2013; Childress et al. 2014), and our detection, or lack thereof, of HVFs also matches spectral fits produced via `SYNAPPS`.

In general, SNe Ia are found to have HVFs with no corresponding PVFs at the earliest epochs and these features

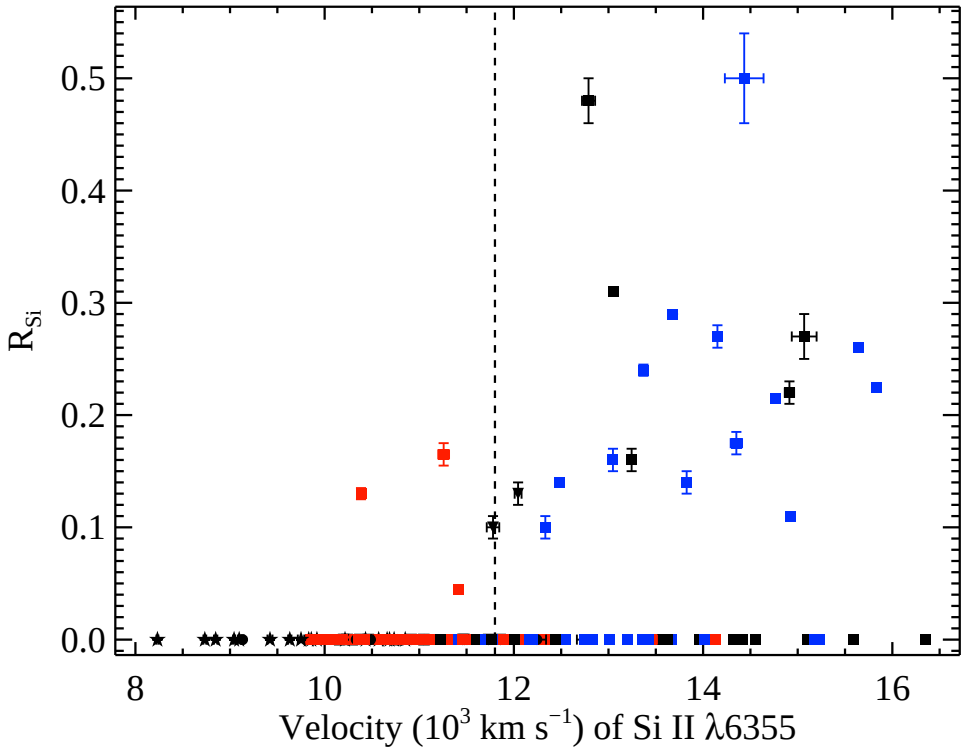

Figure 14. R_{Si} versus Si II λ6355 (PVF) velocity. The median R value and velocity are used for objects with multiple spectra. The dashed line is the cutoff between N and HV objects. Colours and shapes of data points are the same as in Figure 4.

Table 1. Correlated Observables of "Typical"[a] SNe Ia

Observable	HV objects	N objects	Example Reference(s)
Si II λ6355 (PVF) velocity near maximum	$>11{,}800$ km s^{-1}	$<11{,}800$ km s^{-1}	Wang et al. (2009a)
Early-time C II absorption features	No	Yes	Silverman & Filippenko (2012)
UV/optical colours near maximum	Red	Blue	Foley et al. (2011); Milne et al. (2014)
HVFs of Si II λ6355	Strong	Weak/None	**This Work**
Location within host galaxy	Inner ∼70 per cent?	Everywhere?	Wang et al. (2013); Pan et al. (2015)

[a] "Typical" SNe Ia are objects that are spectroscopically "normal" (e.g., according to SNID) and usually have $\Delta m_{15}(B) = 1.1 \pm 0.3$ mag (e.g., Ganeshalingam et al. 2010); thus, they can be assigned a Wang Type.

weaken and slow down with time. PVFs appear later and grow stronger with time, while also slowing down. HVFs and PVFs of CaHK, Si II λ6355, and CaIR3 are found (in at least some objects) at nearly all epochs studied herein. SNe Ia with faster PVFs tend to have faster HVFs.

About two-thirds of all objects in the current sample show HVFs of Ca II. For objects with spectra obtained earlier than ∼4 d before maximum brightness, ∼91 per cent show HVFs, and the remaining ∼9 per cent all seem to be underluminous/Ia-91bg/FAINT objects. This connection between the relative strength of Ca II HVFs and luminosity has also been seen in previous work (Maguire et al. 2012; Childress et al. 2014; Maguire et al. 2014). Our analysis further indicates that Si II λ3858 is detectable in the CaHK profile of ∼24 per cent of spectra, implying that it does not usually dominate the spectral profile in this wavelength range.

We also investigate HVFs of Si II λ6355, a relatively unexplored area of research, but see Marion et al. (2013) for one of the best previous studies of Si II λ6355 HVFs. As with the Ca II features, no HVFs of Si II λ6355 are found in underluminous/Ia-91bg/FAINT objects. On the other hand, Si II λ6355 HVFs are much rarer than their Ca II counterparts, and are detected in only ∼16 per cent of the objects in the current sample. Even at early times ($t < -5$ d), HVFs of Si II λ6355 are seen in only ∼32 per cent of SNe Ia.

Despite their rarity, Si II λ6355 HVFs are observed about one-third of the time in HV objects, compared to only 5–10 per cent of the time in all other SN Ia subtypes. We also find that stronger HVFs of Si II λ6355 are associated with a lack of C II absorption at early times and relatively red

UV/optical colours near maximum brightness. These new-found connections, in conjunction with previous work, led to Table 1, which presents a list of correlated parameters that likely constitute a continuous distribution of SN Ia observables.

Future SN Ia models should utilise the empirical relations and observational constraints set forth in this and previous work regarding HVFs. For example, if HVFs arise purely from an opacity effect, then a stronger line (i.e., one with a larger pEW) would form at a larger radius in the SN photosphere. Assuming homologous expansion, this would correspond to a larger observed velocity for the HVFs of a stronger line.

Using the measurements of HVFs of Si II λ6355 and CaIR3 discussed above, 94 per cent of all spectra have $R_{\rm Si} < R_{\rm CaIR3}$, while the remaining ∼6 per cent are consistent with equality. Thus, all HVFs of CaIR3 are consistent with being stronger, relative to their PVFs, than those of Si II λ6355. In ∼80 per cent of observations, HVFs of CaIR3 have larger velocities than HVFs of Si II λ6355, with ∼5 per cent consistent with equality. The remaining ∼15 per cent of spectra, where Si II λ6355 HVFs are significantly faster than CaIR3 HVFs, include SNe Ia with some of the fastest Si II λ6355 velocities ever observed (e.g., SNe 2006X and 2010kg; Wang et al. 2008; Silverman et al., in preparation, respectively). Thus, CaIR3 is stronger and also faster than Si II λ6355, except in these extremely high-velocity objects, and so the HVFs of Si II λ6355 and CaIR3 *could* be caused primarily by opacity effects in most SNe Ia.

While opacity may play a role, an abundance or density enhancement or an ionisation change at high velocity (i.e., large radius) is likely required to produce detectable HVFs. Gerardy et al. (2004) showed that a model in which SN ejecta collide with a circumstellar shell can yield observed velocities of the CaIR3 HVF feature. Mulligan & Wheeler (2015, in preparation) show that the evolution in time of the PVF and HVF profiles, and the nearly constant velocity gap between the two sets of features, can be reproduced by a model of the interaction between SN Ia ejecta and a circumstellar shell of small mass contained within a few tenths of a solar radius near the exploding WD. Figure 15 shows the evolution of the CaIR3 PVF and HVF velocities as open and filled circles, respectively, for a shell with mass 0.005 $M_\odot$. Also shown in the figure (as open and filled squares, respectively) are the PVF and HVF velocities measured herein for SN 2011fe.

The model PVF velocities match quite well the measured values from the current work at early times and near maximum brightness, though in between these times they are slightly higher than the data indicate. The model HVF velocities match fairly well at most epochs, but are sometimes slightly slower than the measured values. Prior to about 13 d before maximum brightness the photosphere is at the contact discontinuity, below the shell, and thus only the HVF is seen in the model. At later times, the photosphere moves deeper into the ejecta, allowing the PVF to be observed, but the CSM shell still has enough optical depth to yield HVFs. The evolution of the features in the model is caused by the receding velocity of the photosphere and the free expansion of the higher-velocity shell material that leads to weaker absorption in the HVFs (Mulligan & Wheeler 2015, in preparation).

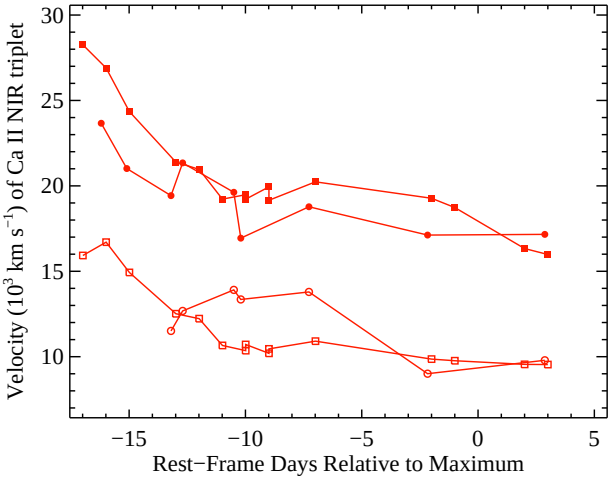

Figure 15. The measured CaIR3 velocities of SN 2011fe from the current work (squares) and model CaIR3 velocities from Mulligan & Wheeler (2015, in preparation; circles). Open points are PVFs and filled points are HVFs.

The current work now stands as an observational benchmark against which theoretical models of SNe Ia can be compared. Any successful model of a normal or overluminous SN Ia that follows the "Phillips relation" must naturally produce HVFs of Ca II since they are found so ubiquitously and at a range of pre- and near-maximum-brightness epochs. On the other hand, models of underluminous/Ia-91bg objects should never produce Ca II HVFs. Furthermore, based on spectropolarimetric observations, the HVFs of Ca II should also show polarisation, distinct from any polarisation present in the PVFs (e.g., Leonard et al. 2005; Wang et al. 2003, 2006; Chornock & Filippenko 2008; Patat et al. 2009; Maund et al. 2013). Similarly, HVFs of Si II λ6355 should be occasionally produced in N and overluminous/Ia-91T/99aa objects, never produced in underluminous/Ia-91bg objects, and preferentially more often (but still somewhat rarely) produced in HV objects. It is now clear that the detection and characterisation of HVFs is yet one more piece of the SN Ia puzzle.

ACKNOWLEDGMENTS

We thank the referee, M. J. Childress, for useful comments and stimulating discussion that helped improve this paper, R. J. Foley, K. Maguire, A. A. Miller, and L. Wang for useful discussions, and the staffs at the Lick, Keck, and McDonald Observatories for their assistance with the observations. The HET is a joint project of the University of Texas at Austin, the Pennsylvania State University, Stanford University, Ludwig-Maximilians-Universität München, and Georg-August-Universität Göttingen. The HET is named in honor of its principal benefactors, William P. Hobby and Robert E. Eberly. The Marcario Low Resolution Spectrograph is named for Mike Marcario of High Lonesome Optics who fabricated several optics for the instrument but died before its completion. The LRS is a joint project of the HET partnership and the Instituto de Astronomía de la Universidad

Nacional Autónoma de México. Some of the data presented herein were obtained at the W. M. Keck Observatory, which is operated as a scientific partnership among the California Institute of Technology, the University of California, and NASA; the observatory was made possible by the generous financial support of the W. M. Keck Foundation. The authors wish to recognise and acknowledge the very significant cultural role and reverence that the summit of Mauna Kea has always had within the indigenous Hawaiian community; we are most fortunate to have the opportunity to conduct observations from this mountain. This research has made use of the NASA/IPAC Extragalactic Database (NED) which is operated by the Jet Propulsion Laboratory, California Institute of Technology, under contract with NASA. J.M.S. is supported by an NSF Astronomy and Astrophysics Postdoctoral Fellowship under award AST-1302771. J.V. and T.S. are supported by Hungarian OTKA Grants NN 107637 and PD 112325, respectively. J.C.W.'s supernova group at UT Austin is supported by NSF Grant AST 11-09801. A.V.F. is grateful for support from the Christopher R. Redlich Fund, the TABASGO Foundation, and NSF grant AST-1211916. Some work on this paper was done in the hospitable climate of the Aspen Center for Physics that is supported by NSF Grant PHY-1066293.

REFERENCES

Barbon R., Benetti S., Rosino L., Cappellaro E., Turatto M., 1990, A&A, 237, 79
Benetti S., et al., 2004, MNRAS, 348, 261
Benetti S., et al., 2005, ApJ, 623, 1011
Betoule M., et al., 2014, A&A, 568, A22
Blondin S., Dessart L., Hillier D. J., Khokhlov A. M., 2013, MNRAS, 429, 2127
Blondin S., Mandel K. S., Kirshner R. P., 2011, A&A, 526, A81
Blondin S., Tonry J. L., 2007, ApJ, 666, 1024
Bloom J. S., et al., 2012, ApJ, 744, L17
Bongard S., Baron E., Smadja G., Branch D., Hauschildt P. H., 2006, ApJ, 647, 513
Branch D., Dang L. C., Baron E., 2009, PASP, 121, 238
Branch D., et al., 2006, PASP, 118, 560
Branch D., van den Bergh S., 1993, AJ, 105, 2231
Bronder T. J., et al., 2008, A&A, 477, 717
Castor J. I., 1970, MNRAS, 149, 111
Childress M. J., et al., 2013, ApJ, 770, 29
Childress M. J., Filippenko A. V., Ganeshalingam M., Schmidt B. P., 2014, MNRAS, 437, 338
Chornock R., Filippenko A. V., 2008, AJ, 136, 2227
Colgate S. A., McKee C., 1969, ApJ, 157, 623
Filippenko A. V., et al., 1992a, ApJ, 384, L15
Filippenko A. V., et al., 1992b, AJ, 104, 1543
Fisher A., Branch D., Nugent P., Baron E., 1997, ApJ, 481, L89
Folatelli G., 2004, New Astronomy Reviews, 48, 623
Folatelli G., et al., 2012, ApJ, 745, 74
Folatelli G., et al., 2013, ApJ, 773, 53
Foley R. J., 2013, MNRAS, 435, 273
Foley R. J., et al., 2012a, ApJ, 752, 101
Foley R. J., et al., 2012b, ApJ, 744, 38
Foley R. J., et al., 2013, ApJ, 767, 57
Foley R. J., Filippenko A. V., Jha S. W., 2008, ApJ, 686, 117
Foley R. J., Kasen D., 2011, ApJ, 729, 55
Foley R. J., Sanders N. E., Kirshner R. P., 2011, ApJ, 742, 89
Ganeshalingam M., et al., 2010, ApJS, 190, 418
Ganeshalingam M., Li W., Filippenko A. V., 2011, MNRAS, 416, 2607
Garavini G., et al., 2004, AJ, 128, 387
Garavini G., et al., 2007, A&A, 470, 411
Gerardy C. L., et al., 2004, ApJ, 607, 391
Hachinger S., Mazzali P. A., Benetti S., 2006, MNRAS, 370, 299
Hamuy M., Phillips M. M., Maza J., Suntzeff N. B., Schommer R. A., Aviles R., 1995, AJ, 109, 1
Hatano K., Branch D., Fisher A., Baron E., Filippenko A. V., 1999, ApJ, 525, 881
Hatano K., Branch D., Lentz E. J., Baron E., Filippenko A. V., Garnavich P. M., 2000, ApJ, 543, L49
Hicken M., et al., 2009, ApJ, 700, 331
Hicken M., et al., 2012, ApJS, 200, 12
Hill G. J., et al., 1998, in D'Odorico S., ed., Society of Photo-Optical Instrumentation Engineers (SPIE) Conference Series Vol. 3355 of Society of Photo-Optical Instrumentation Engineers (SPIE) Conference Series, Hobby-Eberly Telescope low-resolution spectrograph: mechanical design. pp 433–443
Howell D. A., 2011, Nature Communications, 2, 350
Howell D. A., et al., 2006, Nature, 443, 308
Hoyle F., Fowler W. A., 1960, ApJ, 132, 565
Iben Jr. I., Tutukov A. V., 1984, ApJS, 54, 335
Jeffery D. J., 1989, ApJS, 71, 951
Jha S., Branch D., Chornock R., Foley R. J., Li W., Swift B. J., Casebeer D., Filippenko A. V., 2006, AJ, 132, 189
Jha S., et al., 2006, AJ, 131, 527
Kasen D., et al., 2003, ApJ, 593, 788
Konishi K., et al., 2011, AJ, submitted (arXiv:1103.2497)
Leibundgut B., et al., 1993, AJ, 105, 301
Leonard D. C., Li W., Filippenko A. V., Foley R. J., Chornock R., 2005, ApJ, 632, 450
Li W., et al., 2001, PASP, 113, 1178
Li W., et al., 2003, PASP, 115, 453
Li W., et al., 2011, MNRAS, 412, 1441
Li W., Filippenko A. V., Treffers R. R., Riess A. G., Hu J., Qiu Y., 2001, ApJ, 546, 734
Maeda K., et al., 2010, Nature, 466, 82
Maguire K., et al., 2012, MNRAS, 426, 2359
Maguire K., et al., 2013, MNRAS, 436, 222
Maguire K., et al., 2014, MNRAS, 444, 3258
Maoz D., Mannucci F., Nelemans G., 2014, ARA&A, 52, 107
Marion G. H., et al., 2012, The Astronomer's Telegram, 4215, 1
Marion G. H., et al., 2013, ApJ, 777, 40
Marion G. H., Höflich P., Gerardy C. L., Vacca W. D., Wheeler J. C., Robinson E. L., 2009, AJ, 138, 727
Maund J. R., et al., 2013, MNRAS, 433, L20
Mazzali P. A., et al., 2005, ApJ, 623, L37
Miller J. S., Stone R. P. S., 1993, Lick Obs. Tech. Rep. 66. Santa Cruz: Lick Obs.
Milne P. A., Foley R. J., Brown P. J., Narayan G., 2014, ApJ, submitted (arXiv:1408.1706)

Nomoto K., Thielemann F.-K., Yokoi K., 1984, ApJ, 286, 644
Nordin J., et al., 2011, A&A, 526, A119
Nordsieck K. H., Burgh E. B., Kobulnicky H. A., Williams T. B., O'Donoghue D., Percival J. W., Smith M. P., 2001, in American Astronomical Society Meeting Abstracts Vol. 33 of Bulletin of the American Astronomical Society, The Prime Focus Imaging Spectrograph for the Southern African Large Telescope. p. 102.04
Nugent P., Phillips M., Baron E., Branch D., Hauschildt P., 1995, ApJ, 455, L147
Nugent P. E., et al., 2011, Nature, 480, 344
Pan Y.-C., et al., 2014, MNRAS, 438, 1391
Pan Y.-C., Sullivan M., Maguire K., Gal-Yam A., Hook I. M., Howell D. A., Nugent P. E., Mazzali P. A., 2015, MNRAS, 446, 354
Parrent J. T., et al., 2012, ApJ, 752, L26
Parrent J. T., Thomas R. C., Fesen R. A., Marion G. H., Challis P., Garnavich P. M., Milisavljevic D., Vinkò J., Wheeler J. C., 2011, ApJ, 732, 30
Patat F., Baade D., Höflich P., Maund J. R., Wang L., Wheeler J. C., 2009, A&A, 508, 229
Pereira R., et al., 2013, A&A, 554, A27
Perlmutter S., et al., 1999, ApJ, 517, 565
Phillips M. M., 1993, ApJ, 413, L105
Phillips M. M., Wells L. A., Suntzeff N. B., Hamuy M., Leibundgut B., Kirshner R. P., Foltz C. B., 1992, AJ, 103, 1632
Quimby R., Höflich P., Kannappan S. J., Rykoff E., Rujopakarn W., Akerlof C. W., Gerardy C. L., Wheeler J. C., 2006, ApJ, 636, 400
Rayner J. T., et al., 2003, PASP, 115, 362
Rest A., et al., 2014, ApJ, 795, 44
Riess A. G., et al., 1998, AJ, 116, 1009
Scalzo R. A., et al., 2010, ApJ, 713, 1073
Schlegel D. J., Finkbeiner D. P., Davis M., 1998, ApJ, 500, 525
Shen K. J., Moore K., 2014, ApJ, 797, 46
Silverman J. M., et al., 2012a, MNRAS, 425, 1789
Silverman J. M., et al., 2012b, ApJ, 756, L7
Silverman J. M., et al., 2013, MNRAS, 436, 1225
Silverman J. M., Filippenko A. V., 2012, MNRAS, 425, 1917
Silverman J. M., Ganeshalingam M., Filippenko A. V., 2013, MNRAS, 430, 1030
Silverman J. M., Ganeshalingam M., Li W., Filippenko A. V., Miller A. A., Poznanski D., 2011, MNRAS, 410, 585
Silverman J. M., Kong J. J., Filippenko A. V., 2012, MNRAS, 425, 1819
Sobolev V. V., 1960, Moving envelopes of stars. Cambridge: Harvard University Press
Sternberg A., et al., 2011, Science, 333, 856
Stritzinger M. D., et al., 2011, AJ, 142, 156
Strolger L., et al., 2002, AJ, 124, 2905
Sullivan M., et al., 2006, ApJ, 648, 868
Suzuki N., et al., 2012, ApJ, 746, 85
Tanaka M., et al., 2008, ApJ, 677, 448
Tanaka M., Mazzali P. A., Maeda K., Nomoto K., 2006, ApJ, 645, 470
Thomas R. C., Branch D., Baron E., Nomoto K., Li W., Filippenko A. V., 2004, ApJ, 601, 1019
Thomas R. C., et al., 2011, ApJ, 743, 27
Thomas R. C., Nugent P. E., Meza J. C., 2011, PASP, 123, 237
Vinkó J., et al., 2012, A&A, 546, A12
Walker E. S., et al., 2011, MNRAS, 410, 1262
Wang L., Baade D., Höflich P., Wheeler J. C., Kawabata K., Khokhlov A., Nomoto K., Patat F., 2006, ApJ, 653, 490
Wang L., et al., 2003, ApJ, 591, 1110
Wang X., et al., 2008, ApJ, 675, 626
Wang X., et al., 2009a, ApJ, 699, L139
Wang X., et al., 2009b, ApJ, 697, 380
Wang X., Wang L., Filippenko A. V., Zhang T., Zhao X., 2013, Science, 340, 170
Webbink R. F., 1984, ApJ, 277, 355
Whelan J., Iben Jr. I., 1973, ApJ, 186, 1007
Zhang J.-J., Wang X.-F., Bai J.-M., Zhang T.-M., Wang B., Liu Z.-W., Zhao X.-L., Chen J.-C., 2014, AJ, 148, 1

APPENDIX A: TABLES OF OBJECTS AND SPECTRAL MEASUREMENTS

Table A1 lists each SN Ia that we analyse herein and the (rest-frame) phases of their spectra. Also presented are published $\Delta m_{15}(B)$ and $(B-V)_0$ values, as well as spectral classifications based on various classification schemes.

Table A1: Summary of SNe Ia

SN Name	Phase(s) (d)[a]	$\Delta m_{15}(B)$ (mag)[b]	$(B-V)_0$ (mag)[c]	SNID (Sub)Type[d]	Benetti Type[e]	Wang Type[f]
SN 1989M	2.5,3.5	1.10 (20)	···	Ia-norm	HVG	HV
SN 1991T	−10.1,−9.1	0.92 (03)	0.090 (036)	Ia-91T	···	···
SN 1991bg	0.1,1.1	1.89 (05)	0.714 (044)	Ia-91bg	FAINT	···
SN 1994D	−12.3,−11.3,−9.3,−7.7,−6.3,−5.3,−3.9,−3.3	1.36 (05)	−0.053 (035)	Ia-norm	LVG	N
SN 1994S	1.1	0.98 (04)	−0.090 (038)	Ia-norm	···	N
SN 1995D	3.8	1.03 (07)	−0.121 (033)	Ia-norm	···	N
SN 1995E	−2.5	0.98 (06)	0.668 (040)	Ia-norm	···	N
SN 1995ac	−6.3	0.93 (04)	−0.124 (036)	Ia-91T	···	···
SN 1997Y	1.3	1.25 (10)	−0.030 (000)	Ia-norm	···	N
SN 1997br	−4.8	1.08 (17)	0.160 (130)	Ia-91T	···	···
SN 1997do	−5.7	1.04 (05)	−0.019 (036)	Ia-norm	···	···
SN 1998dk	−7.2,−0.5	1.05 (10)	0.190 (000)	Ia-norm	···	HV
SN 1998dm	−12.5,−5.6	0.85 (05)	0.303 (034)	Ia-norm	···	···
SN 1998ef	−8.6	1.30 (05)	−0.072 (037)	Ia-norm	···	···
SN 1998es	0.3	0.98 (03)	0.056 (042)	Ia-99aa	···	···
SN 1999aa	−10.6,0.2	0.79 (05)	−0.093 (033)	Ia-99aa	···	···
SN 1999ac	−3.7,−0.9	1.18 (03)	−0.038 (033)	Ia-norm	HVG	N
SN 1999cp	4.9	1.03 (03)	−0.047 (031)	Ia-norm	LVG	N
SN 1999da	−2.1	1.90 (17)	0.522 (037)	Ia-91bg	FAINT	···
SN 1999dk	−6.6	1.15 (03)	0.003 (037)	Ia-norm	···	···
SN 1999dq	−3.9,3.0	0.97 (03)	0.050 (034)	Ia-99aa	HVG	···
SN 1999gd	−1.1	1.16 (06)	0.410 (000)	Ia-norm	···	N
SN 1999gh	4.1	1.69 (05)	0.190 (000)	Ia-norm	FAINT	N
SN 2000cp	2.9	···	···	Ia-norm	···	N
SN 2000cw	4.8	1.31 (04)	−0.072 (031)	Ia-norm	···	N
SN 2000dg	−5.1,4.7	···	···	Ia-norm	···	N
SN 2000dk	1.0	1.64 (04)	−0.051 (032)	Ia-norm	FAINT	N
SN 2000dm	−1.6	1.56 (05)	−0.111 (037)	Ia-norm	HVG	N
SN 2000dn	−5.6,−0.9	1.12 (03)	−0.092 (036)	Ia-norm	LVG	N
SN 2000dx	−9.3	···	···	Ia-norm	···	···
SN 2000fa	−8.3	0.91 (03)	0.007 (037)	Ia-norm	···	N
SN 2001az	−3.2	···	···	Ia-norm	···	N
SN 2001ba	−4.6	0.99 (04)	−0.160 (033)	Ia-norm	···	···
SN 2001bf	1.2	0.93 (03)	−0.058 (034)	Ia-norm	···	N
SN 2001br	3.5,3.5	1.35 (06)	0.067 (033)	Ia-norm	···	HV
SN 2001bp	0.5	···	···	Ia-norm	···	···
SN 2001cp	1.4	0.92 (04)	−0.035 (033)	Ia-norm	···	N
SN 2001da	−1.1	1.23 (05)	0.130 (032)	Ia-norm	HVG	N
SN 2001eh	−5.6,−4.5,3.3	0.81 (04)	−0.110 (033)	Ia-99aa	···	···
SN 2001ep	2.8	1.49 (06)	0.027 (043)	Ia-norm	HVG	N
SN 2001ex	−1.8	···	···	Ia-91bg	···	···
SN 2001fe	−1.0	1.03 (17)	−0.014 (047)	Ia-norm	···	N
SN 2002aw	2.1	···	···	Ia-norm	···	N
SN 2002bf	3.0	···	···	Ia-norm	···	HV
SN 2002bo	−11.9,−1.1	1.15 (04)	0.315 (052)	Ia-norm	HVG	HV

Continued on next page

Table A1 — Continued

SN Name	Phase(s) (d)[a]	$\Delta m_{15}(B)$ (mag)[b]	$(B-V)_0$ (mag)[c]	SNID (Sub)Type[d]	Benetti Type[e]	Wang Type[f]
SN 2002cd	1.1	0.96 (03)	0.576 (030)	Ia-norm	LVG	HV
SN 2002cf	−0.8	1.86 (06)	0.353 (047)	Ia-91bg	···	···
SN 2002ck	3.6	···	···	Ia-norm	···	N
SN 2002cr	−6.8,−5.8,−3.9	1.26 (05)	−0.102 (038)	Ia-norm	···	···
SN 2002cs	−7.8	1.03 (05)	−0.066 (034)	Ia-norm	···	···
SN 2002cu	−5.3	1.43 (04)	−0.016 (033)	Ia-norm	···	···
SN 2002de	−0.3	1.00 (03)	0.043 (031)	Ia-norm	HVG	HV
SN 2002dj	−8.0	1.09 (03)	0.053 (033)	Ia-norm	···	···
SN 2002dk	−1.2	···	···	Ia-91bg	···	···
SN 2002eb	1.7	0.99 (03)	−0.125 (031)	Ia-norm	···	N
SN 2002ef	4.7	1.04 (10)	0.309 (032)	Ia-norm	···	N
SN 2002er	−4.6	1.28 (05)	0.103 (034)	Ia-norm	···	HV
SN 2002eu	−0.1	···	···	Ia-norm	HVG	N
SN 2002fb	1.0	···	···	Ia-91bg	···	···
SN 2002ha	−0.9,4.9	1.38 (06)	−0.093 (048)	Ia-norm	LVG	N
SN 2002he	−5.9,−1.0,0.3,3.2	1.49 (04)	−0.050 (037)	Ia-norm	HVG	HV
SN 2002hu	−5.8	1.02 (05)	−0.121 (035)	Ia-99aa	···	···
SN 2002hw	−6.3	1.53 (06)	0.558 (061)	Ia-norm	···	···
SN 2003U	−2.6	···	···	Ia-norm	···	N
SN 2003W	−7.0,−6.0,−5.1	1.10 (03)	0.106 (036)	Ia-norm	···	···
SN 2003Y	−1.7	1.73 (09)	0.830 (047)	Ia-91bg	···	···
SN 2003cq	−0.2	···	···	Ia-norm	···	HV
SN 2003fa	−8.2	0.98 (10)	−0.087 (098)	Ia-99aa	···	···
SN 2003gn	−5.4,3.3	1.24 (08)	−0.011 (037)	Ia-norm	···	···
SN 2003gt	−5.1	1.06 (03)	−0.019 (032)	Ia-norm	···	···
SN 2003he	2.7	0.99 (03)	−0.010 (033)	Ia-norm	LVG	N
SN 2003hs	−5.5	···	···	Ia-norm	···	···
SN 2003iv	1.8	···	−0.100 (100)	Ia-norm	HVG	N
SN 2003kf	−7.5	0.93 (04)	−0.014 (039)	Ia-norm	···	···
SN 2004as	−4.4	1.11 (03)	0.021 (034)	Ia-norm	···	HV
SN 2004bl	4.6	···	···	Ia-norm	HVG	N
SN 2004br	3.5	0.68 (16)	−0.097 (046)	Ia-norm	···	N
SN 2004bv	−7.1	0.89 (04)	0.082 (033)	Ia-91T	···	···
SN 2004bw	−10.0,−7.1	1.31 (05)	−0.079 (034)	Ia-norm	···	N
SN 2004dt	−6.5,1.4	1.29 (05)	−0.080 (034)	Ia-norm	HVG	HV
SN 2004ef	−5.5	1.38 (04)	0.048 (033)	Ia-norm	···	HV
SN 2004eo	−5.6	1.39 (03)	−0.042 (031)	Ia-norm	···	···
SN 2004ey	−7.6	0.96 (06)	−0.110 (039)	Ia-norm	···	···
SN 2004fu	−2.7,2.4	···	···	Ia-norm	HVG	HV
SN 2004fz	−5.2	1.40 (05)	−0.127 (039)	Ia-norm	···	···
SN 2004gs	0.4	1.77 (04)	0.046 (032)	Ia-norm	···	N
SN 2004gu	−4.7	0.80 (04)	···	Ia-norm	···	···
SN 2005M	−1.4	0.83 (04)	−0.082 (032)	Ia-norm	HVG	N
SN 2005W	0.6	1.15 (06)	···	Ia-norm	···	N
SN 2005ag	0.5	0.86 (01)	···	Ia-norm	···	N
SN 2005am	4.5	1.71 (09)	−0.008 (062)	Ia-norm	FAINT	N

Continued on next page

Table A1 — Continued

SN Name	Phase(s) (d)[a]	$\Delta m_{15}(B)$ (mag)[b]	$(B-V)_0$ (mag)[c]	SNID (Sub)Type[d]	Benetti Type[e]	Wang Type[f]
SN 2005ao	−1.3,0.5	···	···	Ia	···	···
SN 2005bc	1.6	1.39 (05)	0.382 (033)	Ia-norm	LVG	N
SN 2005bl	−5.6	···	···	Ia-91bg	···	···
SN 2005cf	−10.9,−2.1,−1.2	1.08 (03)	−0.062 (031)	Ia-norm	HVG	N
SN 2005cg	−10.1,−9.1,−4.3,−0.4,4.5	···	···	Ia-norm	HVG	HV
SN 2005de	−0.8	1.22 (03)	0.010 (032)	Ia-norm	HVG	N
SN 2005dv	−0.6	···	···	Ia-norm	···	HV
SN 2005el	−6.7,1.2	1.31 (05)	−0.114 (035)	Ia-norm	LVG	N
SN 2005er	−0.3,1.7	···	···	Ia-91bg	HVG	···
SN 2005eq	−6.0,−3.0,0.7	0.88 (05)	−0.021 (034)	Ia-99aa	HVG	···
SN 2005eu	−10.1,−9.1,−5.5	0.94 (04)	−0.072 (040)	Ia-norm	···	···
SN 2005hj	−5.2,−4.3,0.5,2.4,3.3	···	···	Ia-norm	LVG	N
SN 2005iq	−5.9	1.28 (05)	−0.116 (050)	Ia-norm	···	···
SN 2005ki	1.6	1.53 (05)	−0.160 (048)	Ia-norm	LVG	N
SN 2005lz	0.6	1.60 (05)	−0.071 (059)	Ia-norm	···	N
SN 2005ms	−1.9	0.99 (04)	−0.071 (048)	Ia-norm	HVG	N
SN 2005na	0.0,1.0	1.24 (06)	−0.128 (042)	Ia-norm	HVG	N
SN 2006D	3.7	1.41 (08)	0.050 (039)	Ia-norm	···	N
SN 2006N	−1.9,−0.9	1.56 (04)	0.014 (042)	Ia-norm	HVG	N
SN 2006S	−3.9,3.0	0.89 (06)	0.046 (046)	Ia-norm	LVG	N
SN 2006X	−11.2,−10.2,−9.2,−8.2,−7.2,−6.2,−5.2,−0.2,0.8,1.8,2.8,3.2	1.10 (04)	1.260 (034)	Ia-norm	HVG	HV
SN 2006ax	−10.1	1.03 (04)	−0.105 (038)	Ia-norm	···	···
SN 2006bt	−5.3,−4.5,2.3	1.01 (07)	0.104 (034)	Ia-norm	HVG	N
SN 2006bu	4.2	···	···	Ia-norm	···	N
SN 2006bz	−2.4	2.22 (17)	0.575 (064)	Ia-91bg	···	···
SN 2006cj	3.4	···	···	Ia-norm	···	N
SN 2006cm	−1.2	1.14 (19)	1.055 (052)	Ia-norm	···	N
SN 2006cp	−5.3	0.99 (05)	0.063 (039)	Ia-norm	···	···
SN 2006cq	2.0	···	···	Ia-norm	···	N
SN 2006cs	2.3	···	···	Ia-91bg	···	···
SN 2006cz	1.1	···	···	Ia-99aa	···	···
SN 2006dm	−7.9	1.54 (03)	−0.022 (034)	Ia-norm	HVG	N
SN 2006ef	3.2	1.38 (05)	0.004 (034)	Ia-norm	···	HV
SN 2006ej	−3.7	1.40 (15)	−0.046 (062)	Ia-norm	HVG	HV
SN 2006em	4.2	···	···	Ia-91bg	···	···
SN 2006et	3.3	0.73 (03)	0.161 (064)	Ia-norm	LVG	N
SN 2006gt	3.1	···	···	Ia-91bg	···	···
SN 2006gj	4.7	1.39 (17)	0.340 (100)	Ia-norm	···	N
SN 2006gr	−8.7	0.81 (04)	0.059 (036)	Ia-norm	···	···
SN 2006ke	2.4	···	···	Ia-91bg	HVG	···
SN 2006kf	−9.0,−3.1	1.71 (10)	−0.081 (041)	Ia-norm	···	N
SN 2006lf	−6.3	1.31 (08)	−0.068 (052)	Ia-norm	···	···
SN 2006le	−8.7	0.90 (04)	−0.133 (034)	Ia-norm	···	···
SN 2006or	−2.8	···	···	Ia-norm	···	N
SN 2006os	−0.9	···	···	Ia-norm	···	N
SN 2006qo	−11.1	1.05 (10)	0.153 (042)	Ia	···	···

Continued on next page

Table A1 — Continued

SN Name	Phase(s) (d)[a]	$\Delta m_{15}(B)$ (mag)[b]	$(B-V)_0$ (mag)[c]	SNID (Sub)Type[d]	Benetti Type[e]	Wang Type[f]
SN 2006sr	−2.3,2.7	1.41 (13)	−0.017 (066)	Ia-norm	HVG	HV
SN 2007A	2.4	···	···	Ia-norm	LVG	N
SN 2007F	−9.4,3.2	0.98 (03)	−0.060 (033)	Ia-norm	···	N
SN 2007N	0.4	···	···	Ia	···	···
SN 2007O	−0.3	···	···	Ia-norm	···	N
SN 2007S	−6.0	0.93 (04)	0.400 (032)	Ia-norm	···	N
SN 2007af	−9.8,−1.3,0.2,2.8,3.8	1.22 (05)	−0.014 (036)	Ia-norm	HVG	N
SN 2007al	3.4	···	···	Ia-91bg	···	···
SN 2007ba	2.1	···	···	Ia-91bg	···	···
SN 2007bd	−5.8	···	−0.060 (040)	Ia-norm	···	N
SN 2007bc	0.6	1.37 (06)	−0.113 (036)	Ia-norm	···	N
SN 2007bm	−7.8	···	···	Ia-norm	···	···
SN 2007bz	1.7	···	···	Ia-norm	···	HV
SN 2007ca	−11.1	···	0.290 (050)	Ia-norm	···	···
SN 2007ci	−6.6,−1.7	1.74 (04)	0.003 (042)	Ia-norm	···	N
SN 2007co	−4.1,−0.6,0.9	1.04 (10)	−0.008 (032)	Ia-norm	LVG	N
SN 2007cq	−5.8	1.12 (03)	0.004 (032)	Ia	···	···
SN 2007fb	2.0	···	···	Ia-norm	LVG	N
SN 2007fr	−5.8,−1.3	1.79 (04)	−0.095 (045)	Ia-norm	···	N
SN 2007gi	−7.3,−0.4	···	···	Ia-norm	HVG	HV
SN 2007gk	−1.7	···	···	Ia-norm	HVG	HV
SN 2007hj	−1.2	1.95 (06)	0.090 (038)	Ia-norm	FAINT	HV
SN 2007le	−10.3,−9.4	1.01 (04)	0.280 (039)	Ia-norm	HVG	HV
SN 2007s1[g]	−1.2	1.24 (05)	−0.066 (033)	Ia-norm	···	N
SN 2007on	−3.0,−3.0	···	···	Ia-norm	···	N
SN 2007qe	−8.2,−6.5,−2.5	1.01 (03)	−0.021 (038)	Ia-norm	···	HV
SN 2008Z	−2.3	0.91 (06)	0.109 (059)	Ia-99aa	···	···
SN 2008ar	−8.9,−5.6,1.5,2.8,4.3	1.08 (05)	−0.101 (047)	Ia-norm	···	N
SN 2008bt	−1.1	···	···	Ia-91bg	···	···
SN 2008cl	4.2	···	···	Ia-norm	···	HV
SN 2008s1[h]	−6.4,−4.4,−3.4,0.5,4.4	1.39 (04)	−0.167 (037)	Ia-norm	···	N
SN 2008dx	2.5	···	···	Ia-91bg	FAINT	···
SN 2008ec	−9.8,−8.9,−6.0,−0.2,1.0	1.36 (06)	0.081 (034)	Ia-norm	LVG	N
SN 2008ei	3.3	···	···	Ia-norm	HVG	HV
SN 2008s5[i]	1.3	···	···	Ia	LVG	···
SN 2008hm	1.3	0.80 (02)	···	Ia-norm	···	···
SN 2008hs	−8.9,−7.9,−6.3	···	···	Ia-norm	···	···
SN 2008hv	−11.7,−9.2,−6.6	1.25 (01)	0.039 (009)	Ia-norm	···	···
SN 2009F	−3.0	1.97 (05)	0.635 (036)	Ia-norm	···	···
SN 2009ad	−3.4	0.88 (17)	−0.006 (136)	Ia-norm	···	N
SN 2009an	−5.8,−3.8,−2.9	1.33 (01)	0.124 (009)	Ia-norm	HVG	HV
SN 2009fx	−2.2	···	···	Ia-norm	···	N
SN 2009ig	−14.4,−14.3,−14.2,−13.9,−13.3,−12.4,−12.3,−11.4,−11.3, −10.9,−10.9,−10.9,−10.3,−9.9,−9.4,−8.9,−8.4,−7.9, −6.9,−6.9,−6.0,−6.0,−4.0,−3.0,−2.0,−1.0,3.4,4.3	0.89 (02)	0.059 (033)	Ia-norm	LVG	HV
SN 2009no	2.1	···	···	Ia-norm	···	N

Continued on next page

Table A1 — Continued

SN Name	Phase(s) (d)[a]	$\Delta m_{15}(B)$ (mag)[b]	$(B-V)_0$ (mag)[c]	SNID (Sub)Type[d]	Benetti Type[e]	Wang Type[f]
SN 2009nq	−3.1	1.11 (09)	0.106 (051)	Ia-norm	···	N
SN 2010Y	−7.2,−3.2	1.63 (01)	0.062 (019)	Ia-norm	···	N
PTF 10bjs	−9.8,−8.6,−7.4,−6.6,−5.5,−1.8,0.2	0.88 (03)	−0.090 (020)	Ia-norm	···	HV
SN 2010ai	−10.5,−8.6,−3.7,−0.8	1.34 (01)	0.048 (015)	Ia-norm	HVG	N
PTF 10fps	0.0,0.9,3.9	1.62 (09)	0.140 (040)	Ia-norm	FAINT	N
SN 2010dm	−6.5	0.80 (01)	0.190 (040)	Ia-99aa	···	···
PTF 10icb	−9.8	1.02 (05)	0.060 (020)	Ia-norm	···	···
SN 2010ex	1.1	···	···	Ia-norm	···	N
PTF 10qjl	−3.0	1.12 (04)	−0.100 (020)	Ia-norm	···	N
SN 2010ii	−6.1,−0.5	···	···	Ia-norm	···	HV
SN 2010it	−9.5,−8.5,−6.6,−2.6,−0.6,3.3	···	···	Ia-norm	HVG	HV
PTF 10ygu	−3.7	0.90 (03)	0.440 (030)	Ia-norm	···	HV
SN 2010iw	−4.9,−3.0,−0.1,3.9	···	···	Ia-99aa	HVG	···
SN 2010kg	−9.9,−9.0,−8.0,−6.0,−5.0,−4.1,−3.1,−1.1,−0.1,0.9,2.8,4.8	1.37 (06)	0.300 (085)	Ia-norm	HVG	HV
SN 2011ao	−7.5,−6.7,−5.8,−4.8,−1.8,−0.8,0.2,1.2,2.2,3.2	···	···	Ia-norm	HVG	N
SN 2011by	−11.7,−9.8,−5.7,−3.8,0.2,0.3,2.3,4.2	1.14 (03)	−0.061 (032)	Ia-norm	LVG	N
SN 2011dm	−5.5	···	···	Ia-norm	···	···
SN 2011ek	−6.0,−5.0,3.0	1.19 (04)	0.180 (040)	Ia-norm	···	HV
SN 2011fe	−17.0,−16.0,−15.0,−15.0,−13.0,−12.0,−11.0, −10.0,−10.0,−9.0,−9.0,−7.0,−2.0,−1.0,2.0,3.0	1.07 (06)	−0.067 (085)	Ia-norm	LVG	N
SN 2011gy	−1.1	···	···	Ia-norm	···	HV
SN 2011hb	−5.8,−2.9,3.0	···	···	Ia-norm	HVG	N
SN 2011ia	−3.0	···	···	Ia-norm	···	N
SN 2012I	−1.0	···	···	Ia-norm	···	N
SN 2012bh	0.0	···	···	Ia-norm	···	N
SN 2012cg	−14.7,−13.8,−12.8,−11.8,−10.5,−9.6,−7.8,−6.8,−4.8,−3.8,−3.8,−0.5	0.83 (05)	0.120 (050)	Ia-99aa	LVG	···
SN 2012da	−1.0	···	···	Ia-norm	···	N
SN 2012fr	−14.4,−14.1,−12.6,−12.4,−11.4,−9.3,−8.4,−8.2,−7.6,−7.5, −6.7,−6.6,−6.4,−5.6,−4.7,−4.6,−3.7,−3.6,−2.5,−2.4,−1.4, −1.3,−0.3,0.4,0.7,1.3,1.7,2.3,3.2,4.5	0.85 (05)	···	Ia-norm	LVG	HV
SN 2013cs	−8.9,−3.0	···	···	Ia-norm	···	HV
SN 2013di	−1.6	···	···	Ia-norm	···	N

[a]Phases are in rest-frame days.

[b]Uncertainties are in parentheses, in units of 0.01 mag.

[c]Uncertainties are in parentheses, in units of 0.001 mag.

[d]Spectral classification using the SuperNova IDentification code (SNID; Blondin & Tonry 2007) as implemented in BSNIP I (Silverman et al. 2012a).

[e]Classification based on the velocity gradient of the Si II λ6355 line (Benetti et al. 2005). "HVG" = high velocity gradient; "LVG" = low velocity gradient; "FAINT" = faint/underluminous.

[f]Classification based on the velocity of the Si II λ6355 line (Wang et al. 2009a). "HV" = high velocity; "N" = normal.

[g]Also known as SNF20071021-000.

[h]Also known as SNF20080514-002.

[i]Also known as SNF20080909-030.

Tables A2, A3, and A4 list measured values of the Ca II H&K (CaHK), Si II λ6355, and Ca II near-IR triplet (CaIR3) features, respectively. The velocity for each component is displayed, as well as the pseudo-equivalent width (pEW; e.g., Garavini et al. 2007; Silverman et al. 2012). Also shown for each feature is R, the ratio of the pEW of the HVF to the pEW of the PVF, as defined by Childress et al. (2014). Fits with no HVF have $R \equiv 0$ and fits with no PVF have undefined values of R.

Table A2: CaHK Fit Results

SN Name	Phase (d)[a]	HVF v (10^3 km s^{-1})	HVF pEW (Å)	PVF v (10^3 km s^{-1})	PVF pEW (Å)	$R^{b}_{\rm CaHK}$	Si II λ3858 v (10^3 km s^{-1})	Si IIλ3858 pEW (Å)
SN 1989M	2.5	···	···	11.19 (0.05)	81.8 (0.8)	0	10.93 (0.05)	92.3 (0.4)
SN 1991bg	0.1	···	···	11.19 (0.05)	233.1 (2.4)	0	···	···
SN 1994D	−12.3	26.95 (0.07)	97.3 (1.2)	17.53 (0.07)	85.4 (1.1)	1.14 (0.02)	···	···
SN 1994D	−7.7	23.56 (0.05)	120.0 (0.8)	11.31 (0.05)	36.7 (0.6)	3.27 (0.05)	11.79 (0.05)	5.2 (0.2)
SN 1994D	−6.3	20.74 (0.12)	110.0 (1.2)	9.95 (0.05)	20.5 (0.9)	5.36 (0.24)	11.95 (0.05)	5.4 (0.3)
SN 1994D	−5.3	19.60 (0.14)	101.0 (1.4)	10.16 (0.05)	18.5 (0.9)	5.46 (0.28)	11.94 (0.05)	8.0 (0.3)
SN 1994D	−3.9	22.87 (0.10)	22.2 (0.6)	11.86 (0.05)	55.6 (0.2)	0.40 (0.01)	11.75 (0.05)	15.9 (0.5)
SN 1994D	−3.3	24.17 (0.09)	13.1 (0.4)	11.10 (0.05)	50.0 (0.2)	0.26 (0.01)	11.71 (0.05)	30.3 (0.4)
SN 1994S	1.1	18.62 (0.09)	54.8 (1.1)	10.54 (0.06)	56.0 (1.0)	0.98 (0.03)	···	···
SN 1995D	3.8	17.57 (0.05)	39.8 (0.3)	10.77 (0.05)	57.0 (0.3)	0.70 (0.01)	···	···
SN 1995E	−2.5	18.03 (0.14)	56.1 (1.6)	10.83 (0.12)	53.0 (1.6)	1.06 (0.04)	···	···
SN 1997Y	1.3	18.30 (0.05)	34.8 (0.6)	11.60 (0.05)	75.9 (0.8)	0.46 (0.01)	···	···
SN 1997do	−5.7	27.80 (0.05)	64.9 (1.2)	18.52 (0.08)	125.8 (1.3)	0.52 (0.01)	···	···
SN 1998dk	−7.2	27.00 (0.29)	100.7 (4.6)	16.64 (0.29)	101.5 (4.5)	0.99 (0.06)	···	···
SN 1998dk	−0.5	19.38 (0.05)	104.2 (0.8)	11.82 (0.05)	33.0 (0.7)	3.16 (0.07)	···	···
SN 1998dm	−12.5	22.63 (0.21)	70.5 (2.5)	12.82 (0.17)	65.7 (2.3)	1.07 (0.05)	···	···
SN 1998dm	−5.6	21.36 (0.16)	32.0 (1.2)	12.19 (0.05)	69.8 (0.7)	0.46 (0.02)	11.73 (0.05)	6.8 (0.7)
SN 1998ef	−8.6	22.10 (0.05)	127.5 (0.7)	12.72 (0.05)	18.7 (0.5)	6.83 (0.19)	···	···
SN 1999aa	−10.6	22.54 (0.19)	33.2 (4.9)	15.16 (1.33)	27.9 (4.8)	1.19 (0.27)	···	···
SN 1999ac	−0.9	18.63 (0.05)	26.3 (0.8)	12.68 (0.05)	82.6 (0.9)	0.32 (0.01)	···	···
SN 1999cp	4.9	···	···	10.64 (0.05)	125.9 (1.0)	0	10.31 (0.05)	26.4 (0.4)
SN 1999da	−2.1	···	···	13.91 (0.05)	162.4 (1.5)	0	···	···
SN 1999dq	−3.9	22.30 (0.05)	19.0 (0.7)	11.32 (0.07)	38.8 (0.7)	0.49 (0.02)	11.44 (0.05)	9.7 (0.3)
SN 1999dq	3.0	19.27 (0.05)	51.8 (0.6)	10.97 (0.05)	42.5 (0.5)	1.22 (0.02)	···	···
SN 2000cp	2.9	···	···	11.19 (0.13)	171.4 (5.2)	0	10.90 (0.12)	58.6 (2.4)
SN 2000cw	4.8	···	···	14.45 (0.05)	304.9 (1.6)	0	···	···
SN 2000dg	−5.1	22.82 (0.43)	13.8 (1.4)	11.00 (0.05)	55.1 (0.7)	0.25 (0.03)	11.72 (0.05)	11.7 (0.7)
SN 2000dg	4.7	···	···	11.09 (0.05)	112.3 (1.8)	0	11.27 (0.05)	13.5 (0.5)
SN 2000dk	1.0	···	···	12.35 (0.05)	171.4 (1.9)	0	11.60 (0.05)	22.8 (0.7)
SN 2000dm	−1.6	24.10 (0.40)	10.1 (1.3)	12.03 (0.05)	72.3 (0.5)	0.14 (0.02)	11.98 (0.05)	19.8 (0.8)
SN 2000dn	−0.9	17.74 (0.06)	39.5 (1.4)	11.11 (0.07)	87.2 (1.3)	0.45 (0.02)	···	···
SN 2000dx	−9.3	22.28 (0.09)	179.6 (2.6)	···	···	···	···	···
SN 2000fa	−8.3	23.12 (0.09)	142.7 (1.6)	11.94 (0.25)	22.0 (1.4)	6.49 (0.42)	···	···
SN 2001az	−3.2	20.97 (0.10)	56.1 (1.3)	12.17 (0.10)	56.9 (1.6)	0.99 (0.04)	···	···
SN 2001bf	1.2	18.40 (0.05)	51.0 (0.4)	7.90 (0.05)	21.7 (0.3)	2.35 (0.04)	···	···
SN 2001bp	0.5	19.36 (0.32)	36.4 (4.7)	11.64 (0.26)	51.4 (5.1)	0.71 (0.12)	···	···
SN 2001cp	1.4	17.59 (0.10)	63.5 (1.5)	10.72 (0.07)	45.4 (1.2)	1.40 (0.05)	···	···
SN 2001da	−1.1	20.79 (0.07)	102.9 (1.5)	12.31 (0.09)	59.6 (1.4)	1.73 (0.05)	···	···
SN 2001eh	−5.6	20.59 (0.14)	42.4 (4.6)	12.98 (0.83)	43.3 (5.1)	0.98 (0.16)	···	···
SN 2001eh	−4.5	20.11 (0.06)	33.0 (1.5)	12.51 (0.24)	46.1 (1.8)	0.72 (0.04)	···	···
SN 2001eh	3.3	18.30 (0.05)	73.1 (0.8)	10.51 (0.05)	27.5 (0.8)	2.66 (0.08)	···	···
SN 2001ep	2.8	···	···	12.93 (0.05)	204.6 (2.1)	0	11.01 (0.05)	9.9 (0.7)
SN 2001ex	−1.8	···	···	11.07 (0.06)	129.6 (3.3)	0	10.66 (0.09)	15.9 (1.0)
SN 2001fe	−1.0	18.96 (0.06)	30.6 (0.6)	11.53 (0.05)	54.9 (0.7)	0.56 (0.01)	···	···
SN 2002aw	2.1	···	···	11.61 (0.11)	139.6 (4.3)	0	11.16 (0.12)	24.2 (1.7)
SN 2002bo	−11.9	27.87 (0.67)	69.7 (8.4)	19.68 (0.47)	82.5 (8.5)	0.85 (0.13)	···	···
SN 2002bo	−1.1	18.45 (0.20)	104.1 (3.4)	11.51 (0.13)	32.4 (3.0)	3.21 (0.31)	···	···

Continued on next page

Table A2 — Continued

SN Name	Phase (d)[a]	HVF v (10^3 km s^{-1})	HVF pEW (Å)	PVF v (10^3 km s^{-1})	PVF pEW (Å)	$R^{b}_{\rm CaHK}$	Si II λ3858 v (10^3 km s^{-1})	Si II λ3858 pEW (Å)
SN 2002cd	1.1	17.77 (0.05)	133.5 (1.0)	···	···	···	···	···
SN 2002cf	−0.8	···	···	13.16 (0.05)	186.9 (2.1)	0	···	···
SN 2002ck	3.6	14.16 (0.08)	79.5 (1.6)	9.13 (0.05)	16.0 (1.0)	4.98 (0.34)	···	···
SN 2002cr	−6.8	16.88 (0.16)	84.9 (2.0)	10.33 (0.10)	19.2 (1.8)	4.43 (0.44)	···	···
SN 2002cs	−7.8	23.83 (0.05)	61.8 (0.8)	14.76 (0.05)	41.1 (0.6)	1.50 (0.03)	···	···
SN 2002de	−0.3	19.32 (0.15)	73.1 (2.9)	11.37 (0.11)	46.0 (2.4)	1.59 (0.10)	···	···
SN 2002dj	−8.0	24.57 (0.09)	140.6 (1.7)	15.38 (0.08)	40.5 (1.5)	3.47 (0.13)	···	···
SN 2002dk	−1.2	22.65 (0.97)	162.5 (15.0)	12.41 (0.23)	69.0 (13.2)	2.35 (0.50)	···	···
SN 2002eb	1.7	18.20 (0.05)	68.4 (0.6)	10.30 (0.05)	32.6 (0.5)	2.10 (0.04)	···	···
SN 2002ef	4.7	···	···	13.11 (0.11)	206.7 (6.6)	0	···	···
SN 2002er	−4.6	18.73 (0.05)	127.6 (0.6)	11.58 (0.05)	25.0 (0.5)	5.11 (0.11)	···	···
SN 2002eu	−0.1	···	···	9.69 (0.07)	52.1 (3.2)	0	10.63 (0.11)	83.5 (1.8)
SN 2002fb	1.0	···	···	10.31 (0.05)	255.3 (2.1)	0	···	···
SN 2002ha	−0.9	17.16 (0.05)	72.3 (0.7)	10.33 (0.05)	39.1 (0.7)	1.85 (0.04)	···	···
SN 2002ha	4.9	···	···	11.81 (0.05)	157.2 (1.0)	0	10.80 (0.05)	15.6 (0.3)
SN 2002he	0.3	···	···	15.46 (0.05)	227.3 (0.5)	0	···	···
SN 2002he	3.2	···	···	14.71 (0.05)	218.1 (0.5)	0	···	···
SN 2002hu	−5.8	20.01 (0.05)	56.4 (0.5)	11.20 (0.06)	54.1 (0.6)	1.04 (0.01)	···	···
SN 2002hw	−6.3	···	···	13.73 (0.05)	172.1 (0.8)	0	···	···
SN 2003U	−2.6	···	···	10.35 (0.09)	80.9 (3.1)	0	10.43 (0.10)	89.4 (1.6)
SN 2003W	−5.1	23.01 (0.05)	158.7 (0.9)	···	···	···	···	···
SN 2003Y	−1.7	···	···	11.00 (0.06)	227.2 (3.1)	0	···	···
SN 2003cq	−0.2	18.70 (0.21)	107.6 (3.8)	11.38 (0.16)	37.2 (3.3)	2.89 (0.27)	···	···
SN 2003fa	−8.2	21.15 (0.10)	37.6 (2.7)	12.84 (0.63)	31.3 (3.1)	1.20 (0.15)	···	···
SN 2003gn	−5.4	24.65 (1.36)	81.8 (35.8)	16.93 (2.28)	93.1 (33.0)	0.88 (0.49)	···	···
SN 2003gt	−5.1	24.15 (0.17)	9.8 (1.8)	11.54 (0.05)	58.5 (0.9)	0.17 (0.03)	12.28 (0.05)	13.0 (0.6)
SN 2003he	2.7	17.77 (0.13)	92.8 (2.2)	10.46 (0.08)	30.8 (1.7)	3.01 (0.18)	···	···
SN 2003hs	−5.5	19.73 (0.17)	144.6 (5.8)	···	···	···	···	···
SN 2003kf	−7.5	23.49 (0.05)	73.2 (0.2)	13.17 (0.05)	66.1 (0.1)	1.11 (0.01)	12.20 (0.05)	4.8 (0.1)
SN 2004ey	−7.6	22.82 (0.05)	91.9 (0.4)	13.13 (0.05)	56.4 (0.4)	1.63 (0.01)	···	···
SN 2004fu	−2.7	20.31 (0.05)	149.7 (0.4)	12.31 (0.05)	32.4 (0.4)	4.62 (0.05)	···	···
SN 2005er	1.7	···	···	10.91 (0.08)	251.2 (4.6)	0	···	···
SN 2005eq	−3.0	21.85 (0.05)	27.0 (0.6)	11.53 (0.08)	57.3 (0.8)	0.47 (0.01)	10.40 (0.05)	12.7 (0.3)
SN 2005eu	−9.1	21.79 (0.05)	24.2 (0.4)	11.51 (0.05)	37.1 (0.5)	0.65 (0.01)	···	···
SN 2006bt	−5.3	19.16 (0.06)	52.1 (0.8)	11.45 (0.07)	38.1 (0.9)	1.37 (0.04)	···	···
SN 2006or	−2.8	16.33 (0.05)	140.0 (0.6)	···	···	···	···	···
SN 2006sr	2.7	···	···	11.98 (0.08)	111.4 (2.3)	0	11.75 (0.09)	43.0 (1.0)
SN 2007A	2.4	17.91 (0.05)	33.3 (0.6)	11.07 (0.05)	60.8 (0.7)	0.55 (0.01)	···	···
SN 2007le	−10.3	32.19 (0.05)	53.8 (1.3)	21.67 (0.09)	164.3 (1.5)	0.33 (0.01)	···	···
SN 2007le	−9.4	31.57 (0.05)	36.0 (0.8)	22.08 (0.06)	170.8 (1.0)	0.21 (0.01)	···	···
SN 2007on	−3.0	18.44 (0.05)	41.8 (0.3)	12.09 (0.05)	59.7 (0.4)	0.70 (0.01)	···	···
SN 2008Z	−2.3	20.98 (0.14)	34.7 (2.2)	12.23 (0.12)	58.2 (2.1)	0.60 (0.04)	···	···
SN 2008ar	2.8	22.51 (0.22)	127.6 (4.6)	13.99 (0.15)	34.2 (3.4)	3.73 (0.39)	···	···
SN 2008s1[c]	−6.4	18.96 (0.17)	11.7 (1.9)	11.92 (0.11)	51.2 (1.6)	0.23 (0.04)	···	···
SN 2008s1[c]	−4.4	18.71 (0.54)	20.6 (5.0)	11.23 (0.41)	56.9 (6.2)	0.36 (0.10)	···	···
SN 2008s1[c]	−3.4	18.38 (0.11)	14.7 (1.9)	11.90 (0.12)	62.5 (2.0)	0.23 (0.03)	···	···
SN 2008s1[c]	0.5	···	···	11.41 (0.15)	118.9 (5.4)	0	10.56 (0.14)	20.4 (1.8)

Continued on next page

Table A2 — Continued

SN Name	Phase (d)[a]	HVF v (10^3 km s^{-1})	HVF pEW (Å)	PVF v (10^3 km s^{-1})	PVF pEW (Å)	$R_{\rm CaHK}$[b]	Si II λ3858 v (10^3 km s^{-1})	Si II λ3858 pEW (Å)
SN 2008s1[c]	4.4	···	···	11.52 (0.06)	125.5 (2.3)	0	10.55 (0.06)	21.3 (0.9)
SN 2008dx	2.5	···	···	11.61 (0.21)	170.9 (9.7)	0	···	···
SN 2008ec	−0.2	···	···	11.43 (0.05)	131.6 (1.6)	0	11.06 (0.05)	39.0 (0.7)
SN 2009ig	−14.3	37.16 (0.05)	24.4 (1.2)	27.86 (0.13)	117.2 (1.3)	0.21 (0.01)	···	···
SN 2009ig	−10.9	30.22 (0.08)	57.0 (2.5)	19.89 (0.16)	161.3 (2.3)	0.35 (0.02)	···	···
SN 2009ig	−9.9	28.48 (0.07)	99.3 (2.6)	19.57 (0.21)	87.5 (2.3)	1.14 (0.04)	···	···
SN 2009ig	−9.4	26.63 (0.05)	169.1 (0.6)	13.96 (0.05)	27.1 (0.5)	6.25 (0.11)	···	···
SN 2009ig	−8.9	25.47 (0.05)	148.1 (0.4)	13.99 (0.05)	29.9 (0.3)	4.95 (0.05)	···	···
SN 2009ig	−8.4	25.48 (0.05)	164.8 (0.6)	13.08 (0.05)	22.9 (0.4)	7.21 (0.13)	···	···
SN 2009ig	−7.9	24.75 (0.05)	147.0 (0.3)	13.46 (0.05)	24.8 (0.2)	5.94 (0.05)	···	···
SN 2009ig	−6.9	24.25 (0.05)	130.1 (0.3)	13.54 (0.05)	30.9 (0.2)	4.22 (0.03)	···	···
SN 2009ig	−6.0	23.43 (0.05)	119.1 (0.2)	13.58 (0.05)	26.8 (0.2)	4.44 (0.03)	···	···
SN 2011by	−11.7	22.58 (0.67)	31.8 (4.4)	13.61 (0.19)	68.2 (2.3)	0.47 (0.07)	12.96 (0.05)	14.9 (2.3)
SN 2011by	−5.7	24.13 (0.15)	7.8 (0.6)	11.97 (0.05)	68.7 (0.3)	0.11 (0.01)	12.17 (0.05)	21.7 (0.4)
SN 2011by	−3.8	19.29 (0.05)	31.8 (0.3)	11.52 (0.05)	65.5 (0.4)	0.49 (0.01)	···	···
SN 2011by	0.2	17.28 (0.08)	44.9 (0.8)	10.56 (0.05)	52.5 (0.8)	0.86 (0.02)	···	···
SN 2011by	4.2	16.55 (0.06)	30.5 (0.6)	10.64 (0.05)	55.1 (0.7)	0.55 (0.01)	···	···
SN 2011fe	−16.0	31.16 (0.10)	24.9 (1.3)	21.70 (0.11)	123.0 (1.6)	0.20 (0.01)	···	···
SN 2011fe	−15.0	24.05 (0.49)	95.2 (5.9)	16.06 (0.29)	51.6 (6.5)	1.84 (0.26)	···	···
SN 2011fe	−13.0	20.92 (0.24)	118.2 (4.2)	13.17 (0.15)	29.6 (3.7)	3.99 (0.51)	···	···
SN 2011fe	−10.0	20.66 (0.05)	73.6 (0.2)	12.49 (0.05)	52.8 (0.2)	1.39 (0.01)	···	···
SN 2012cg	−11.8	23.79 (0.34)	76.6 (4.1)	14.85 (0.41)	48.4 (4.1)	1.58 (0.16)	···	···
SN 2012cg	−3.8	20.56 (0.05)	52.5 (0.3)	11.79 (0.05)	47.9 (0.4)	1.10 (0.01)	···	···
SN 2012fr	−6.7	24.89 (0.05)	167.5 (0.6)	11.95 (0.09)	12.9 (0.6)	13.04 (0.61)	···	···
SN 2012fr	−5.6	24.32 (0.05)	138.0 (0.6)	11.64 (0.05)	25.4 (0.4)	5.43 (0.09)	12.15 (0.05)	3.1 (0.1)
SN 2012fr	−4.7	23.84 (0.05)	141.2 (0.7)	11.59 (0.10)	26.0 (0.8)	5.44 (0.18)	···	···
SN 2012fr	−3.7	23.46 (0.05)	131.5 (0.7)	11.85 (0.09)	28.9 (0.9)	4.55 (0.14)	···	···
SN 2012fr	1.3	22.60 (0.06)	84.6 (1.1)	13.81 (0.11)	49.8 (1.3)	1.70 (0.05)	···	···
SN 2012fr	2.3	20.15 (0.10)	98.5 (2.1)	11.29 (0.07)	44.5 (1.4)	2.21 (0.08)	···	···
SN 2012fr	3.2	20.91 (0.05)	100.4 (0.8)	11.75 (0.05)	30.0 (1.1)	3.34 (0.12)	···	···
SN 2013cs	−8.9	21.49 (0.09)	125.5 (1.4)	13.74 (0.05)	35.7 (1.2)	3.52 (0.13)	···	···
SN 2013cs	−3.0	17.67 (0.06)	97.6 (1.0)	10.70 (0.05)	34.3 (0.9)	2.85 (0.08)	···	···

[a] Phases are in rest-frame days.

[b] $R_{\rm CaHK}$ is the ratio of the pEW of the HVF to the pEW of the PVF, as defined by Childress et al. (2014).

[c] Also known as SNF20080514-002.

Table A3: Si II λ6355 Fit Results

SN Name	Phase (d)[a]	HVF v (10^3 km s^{-1})	HVF pEW (Å)	PVF v (10^3 km s^{-1})	PVF pEW (Å)	$R_{\rm Si}$[b]
SN 1989M	2.5	···	···	12.33 (0.05)	132.9 (0.1)	0
SN 1989M	3.5	···	···	12.19 (0.05)	124.2 (0.1)	0
SN 1991T	−10.1	···	···	10.66 (0.06)	21.1 (0.3)	0
SN 1991T	−9.1	···	···	9.93 (0.09)	17.4 (0.4)	0
SN 1991bg	0.1	···	···	9.63 (0.05)	96.0 (0.6)	0
SN 1991bg	1.1	···	···	9.21 (0.05)	94.5 (0.9)	0
SN 1994D	−12.3	19.03 (0.05)	40.1 (0.9)	13.67 (0.05)	97.8 (0.6)	0.41 (0.01)
SN 1994D	−11.3	18.82 (0.06)	34.7 (1.5)	13.30 (0.08)	96.2 (0.5)	0.36 (0.02)
SN 1994D	−9.3	17.47 (0.10)	20.3 (0.7)	11.76 (0.05)	65.5 (0.6)	0.31 (0.01)
SN 1994D	−7.7	18.17 (0.06)	6.5 (0.2)	11.77 (0.05)	76.4 (0.6)	0.09 (0.01)
SN 1994D	−6.3	···	···	10.79 (0.05)	86.5 (0.2)	0
SN 1994D	−5.3	···	···	11.07 (0.05)	83.8 (0.2)	0
SN 1994D	−3.9	···	···	10.92 (0.05)	85.5 (0.1)	0
SN 1994D	−3.3	···	···	10.80 (0.05)	90.4 (0.1)	0
SN 1994S	1.1	···	···	10.40 (0.05)	85.6 (0.2)	0
SN 1995D	3.8	···	···	10.17 (0.05)	80.2 (0.1)	0
SN 1995E	−2.5	···	···	10.68 (0.05)	101.8 (0.1)	0
SN 1995ac	−6.3	···	···	10.16 (0.13)	20.0 (1.3)	0
SN 1997Y	1.3	···	···	10.51 (0.05)	110.6 (0.3)	0
SN 1997br	−4.8	···	···	10.77 (0.05)	23.0 (0.2)	0
SN 1997do	−5.7	···	···	13.96 (0.05)	110.6 (0.2)	0
SN 1998dk	−7.2	···	···	14.41 (0.05)	112.2 (0.2)	0
SN 1998dk	−0.5	···	···	12.38 (0.05)	108.0 (0.1)	0
SN 1998dm	−12.5	···	···	12.18 (0.05)	66.4 (0.1)	0
SN 1998dm	−5.6	···	···	10.86 (0.05)	66.2 (0.1)	0
SN 1998ef	−8.6	···	···	14.32 (0.05)	150.6 (0.3)	0
SN 1998es	0.3	···	···	10.24 (0.05)	59.5 (0.1)	0
SN 1999aa	−10.6	···	···	12.60 (0.07)	31.4 (0.5)	0
SN 1999aa	0.2	···	···	10.35 (0.05)	59.6 (0.2)	0
SN 1999ac	−3.7	···	···	11.19 (0.05)	76.7 (0.1)	0
SN 1999ac	−0.9	···	···	10.40 (0.05)	86.3 (0.2)	0
SN 1999cp	4.9	···	···	10.43 (0.05)	105.4 (0.1)	0
SN 1999da	−2.1	···	···	10.66 (0.05)	129.5 (0.2)	0
SN 1999dk	−6.6	···	···	14.55 (0.05)	134.8 (0.1)	0
SN 1999dq	−3.9	···	···	10.97 (0.05)	42.0 (0.2)	0
SN 1999dq	3.0	···	···	10.86 (0.05)	61.7 (0.1)	0
SN 1999gd	−1.1	···	···	10.42 (0.05)	116.5 (0.4)	0
SN 1999gh	4.1	···	···	10.58 (0.05)	164.5 (0.2)	0
SN 2000cp	2.9	···	···	11.00 (0.05)	145.1 (0.3)	0
SN 2000cw	4.8	···	···	9.91 (0.05)	111.8 (0.3)	0
SN 2000dg	−5.1	···	···	10.90 (0.05)	76.4 (0.2)	0
SN 2000dg	4.7	···	···	10.39 (0.05)	72.8 (0.3)	0
SN 2000dk	1.0	···	···	10.67 (0.05)	124.3 (0.1)	0
SN 2000dm	−1.6	···	···	11.08 (0.05)	106.9 (0.1)	0
SN 2000dn	−0.9	···	···	10.19 (0.05)	119.4 (0.4)	0
SN 2000dx	−9.3	···	···	15.11 (0.05)	151.2 (1.5)	0
SN 2000fa	−8.3	···	···	14.13 (0.05)	95.6 (0.6)	0
SN 2001az	−3.2	···	···	11.73 (0.05)	81.5 (0.6)	0
SN 2001ba	−4.6	···	···	12.77 (0.11)	144.2 (7.6)	0
SN 2001bf	1.2	···	···	11.75 (0.05)	130.0 (0.2)	0
SN 2001br	3.5	···	···	12.93 (0.05)	133.9 (1.3)	0
SN 2001br	3.5	···	···	12.56 (0.05)	152.5 (0.7)	0
SN 2001bp	0.5	···	···	10.86 (0.05)	75.4 (1.2)	0
SN 2001cp	1.4	···	···	10.61 (0.05)	81.2 (0.3)	0
SN 2001da	−1.1	···	···	11.35 (0.05)	121.4 (0.3)	0
SN 2001eh	−5.6	···	···	11.18 (0.05)	43.4 (0.7)	0
SN 2001eh	−4.5	···	···	11.05 (0.05)	42.2 (0.4)	0
SN 2001eh	3.3	···	···	10.84 (0.05)	61.1 (0.2)	0
SN 2001ep	2.8	···	···	10.16 (0.05)	120.9 (0.1)	0
SN 2001ex	−1.8	···	···	9.92 (0.05)	123.0 (0.6)	0
SN 2001fe	−1.0	···	···	11.07 (0.05)	73.2 (0.1)	0
SN 2002aw	2.1	···	···	10.21 (0.05)	99.9 (0.8)	0
SN 2002bf	3.0	18.48 (0.05)	38.5 (0.5)	13.68 (0.05)	133.4 (0.1)	0.29 (0.01)
SN 2002bo	−11.9	20.97 (0.07)	36.4 (2.3)	15.63 (0.11)	103.7 (0.2)	0.35 (0.02)

Continued on next page

Table A3 — Continued

SN Name	Phase (d)[a]	HVF v (10^3 km s^{-1})	HVF pEW (Å)	PVF v (10^3 km s^{-1})	PVF pEW (Å)	$R_{\rm Si}^{\rm b}$
SN 2002bo	−1.1	···	···	13.07 (0.05)	156.5 (0.5)	0
SN 2002cd	1.1	···	···	15.23 (0.05)	121.9 (0.1)	0
SN 2002cf	−0.8	···	···	10.22 (0.05)	117.6 (0.4)	0
SN 2002ck	3.6	···	···	10.31 (0.05)	76.1 (0.6)	0
SN 2002cr	−6.8	···	···	11.08 (0.05)	105.5 (0.3)	0
SN 2002cs	−7.8	19.17 (0.05)	22.5 (1.0)	14.91 (0.05)	104.4 (0.1)	0.22 (0.01)
SN 2002cu	−5.3	19.51 (0.05)	20.0 (0.8)	13.24 (0.05)	123.6 (0.1)	0.16 (0.01)
SN 2002de	−0.3	···	···	11.59 (0.05)	102.8 (1.3)	0
SN 2002dj	−8.0	···	···	15.59 (0.05)	150.2 (0.3)	0
SN 2002dk	−1.2	···	···	10.43 (0.05)	116.8 (0.5)	0
SN 2002eb	1.7	···	···	10.23 (0.05)	72.7 (0.2)	0
SN 2002ef	4.7	···	···	11.43 (0.05)	108.4 (0.5)	0
SN 2002er	−4.6	···	···	12.05 (0.05)	112.6 (0.1)	0
SN 2002eu	−0.1	···	···	11.02 (0.05)	128.2 (0.5)	0
SN 2002fb	1.0	···	···	10.57 (0.05)	101.9 (0.3)	0
SN 2002ha	−0.9	···	···	10.93 (0.05)	106.7 (0.1)	0
SN 2002ha	4.9	···	···	10.38 (0.05)	106.2 (0.2)	0
SN 2002he	−5.9	···	···	13.30 (0.05)	110.1 (0.4)	0
SN 2002he	−1.0	···	···	12.52 (0.05)	123.2 (0.3)	0
SN 2002he	0.3	···	···	12.36 (0.05)	126.5 (0.2)	0
SN 2002he	3.2	···	···	12.07 (0.05)	127.7 (0.3)	0
SN 2002hu	−5.8	···	···	10.46 (0.05)	58.1 (0.3)	0
SN 2002hw	−6.3	···	···	11.25 (0.05)	94.4 (0.3)	0
SN 2003U	−2.6	···	···	11.30 (0.05)	130.1 (0.4)	0
SN 2003W	−5.1	20.77 (0.05)	31.5 (2.3)	15.07 (0.13)	118.8 (0.1)	0.27 (0.02)
SN 2003Y	−1.7	···	···	9.86 (0.05)	99.4 (0.5)	0
SN 2003cq	−0.2	···	···	12.08 (0.05)	129.2 (0.8)	0
SN 2003fa	−8.2	···	···	11.73 (0.06)	42.4 (0.8)	0
SN 2003gn	−5.4	···	···	13.39 (0.05)	154.1 (1.2)	0
SN 2003gn	3.3	···	···	10.99 (0.06)	194.3 (3.9)	0
SN 2003gt	−5.1	···	···	11.39 (0.05)	75.4 (0.3)	0
SN 2003he	2.7	···	···	11.31 (0.05)	103.2 (0.3)	0
SN 2003hs	−5.5	···	···	13.55 (0.05)	160.3 (1.3)	0
SN 2003iv	1.8	···	···	10.56 (0.05)	112.6 (0.2)	0
SN 2003kf	−7.5	···	···	12.07 (0.05)	68.4 (0.1)	0
SN 2004as	−4.4	17.14 (0.05)	12.2 (0.7)	12.33 (0.05)	120.6 (0.1)	0.10 (0.01)
SN 2004bl	4.6	···	···	10.72 (0.05)	98.3 (0.4)	0
SN 2004br	3.5	···	···	11.03 (0.05)	43.1 (0.6)	0
SN 2004bv	−7.1	···	···	11.05 (0.05)	40.8 (0.3)	0
SN 2004bw	−10.0	···	···	13.46 (0.05)	116.7 (2.1)	0
SN 2004dt	−6.5	19.18 (0.05)	56.2 (1.1)	13.20 (0.05)	117.5 (0.3)	0.48 (0.01)
SN 2004dt	1.4	···	···	13.54 (0.05)	182.5 (0.3)	0
SN 2004ef	−5.5	18.45 (0.05)	18.6 (0.8)	13.05 (0.05)	117.0 (3.7)	0.16 (0.01)
SN 2004eo	−5.6	···	···	11.07 (0.05)	105.4 (0.3)	0
SN 2004ey	−7.6	···	···	11.81 (0.05)	80.0 (0.1)	0
SN 2004fu	−2.7	···	···	12.90 (0.05)	133.5 (0.1)	0
SN 2004fu	2.4	···	···	11.98 (0.05)	137.4 (0.1)	0
SN 2004fz	−5.2	···	···	10.44 (0.05)	91.4 (0.2)	0
SN 2004gs	0.4	···	···	10.43 (0.05)	131.3 (0.3)	0
SN 2004gu	−4.7	···	···	10.89 (0.17)	31.4 (1.6)	0
SN 2005M	−1.4	···	···	10.67 (0.06)	70.6 (1.3)	0
SN 2005W	0.6	···	···	10.60 (0.05)	115.6 (0.3)	0
SN 2005ag	0.5	···	···	11.37 (0.05)	91.0 (1.8)	0
SN 2005am	4.5	···	···	11.15 (0.05)	116.7 (0.1)	0
SN 2005ao	−1.3	···	···	11.55 (0.05)	77.4 (0.5)	0
SN 2005ao	0.5	···	···	11.46 (0.05)	76.4 (0.4)	0
SN 2005bc	1.6	···	···	10.70 (0.05)	115.5 (0.2)	0
SN 2005bl	−5.6	···	···	10.69 (0.10)	54.5 (3.5)	0
SN 2005cf	−10.9	18.79 (0.05)	53.1 (0.6)	12.47 (0.05)	88.8 (0.1)	0.60 (0.01)
SN 2005cf	−2.1	···	···	10.23 (0.05)	84.3 (0.1)	0
SN 2005cf	−1.2	···	···	10.11 (0.05)	86.0 (0.1)	0
SN 2005cg	−10.1	20.83 (0.23)	21.2 (2.3)	13.51 (0.22)	59.3 (2.0)	0.36 (0.04)
SN 2005cg	−9.1	19.53 (0.09)	22.5 (0.8)	12.77 (0.06)	48.4 (0.2)	0.46 (0.02)
SN 2005cg	−4.3	···	···	12.11 (0.05)	67.2 (0.3)	0
SN 2005cg	−0.4	···	···	11.56 (0.05)	75.2 (0.3)	0

Continued on next page

Table A3 — Continued

SN Name	Phase (d)[a]	HVF v (10^3 km s^{-1})	HVF pEW (Å)	PVF v (10^3 km s^{-1})	PVF pEW (Å)	$\mathcal{R}_{\rm Si}$[b]
SN 2005cg	4.5	···	···	11.33 (0.05)	80.7 (0.3)	0
SN 2005de	−0.8	···	···	10.23 (0.05)	102.2 (0.4)	0
SN 2005dv	−0.6	···	···	12.55 (0.05)	153.7 (0.6)	0
SN 2005el	−6.7	···	···	11.33 (0.05)	67.3 (0.2)	0
SN 2005el	1.2	···	···	10.46 (0.05)	89.9 (0.2)	0
SN 2005er	−0.3	···	···	8.74 (0.05)	98.2 (0.3)	0
SN 2005er	1.7	···	···	9.35 (0.05)	65.9 (0.3)	0
SN 2005eq	−6.0	···	···	10.30 (0.09)	61.8 (1.7)	0
SN 2005eq	−3.0	···	···	10.20 (0.05)	44.3 (0.1)	0
SN 2005eq	0.7	···	···	10.09 (0.05)	53.3 (0.2)	0
SN 2005eu	−10.1	···	···	11.48 (0.05)	38.6 (0.2)	0
SN 2005eu	−9.1	···	···	11.26 (0.05)	36.3 (0.3)	0
SN 2005eu	−5.5	···	···	11.27 (0.05)	50.2 (0.6)	0
SN 2005hj	−5.2	···	···	10.35 (0.10)	29.6 (1.4)	0
SN 2005hj	−4.3	···	···	10.69 (0.06)	26.9 (0.9)	0
SN 2005hj	0.5	···	···	10.55 (0.05)	44.6 (0.6)	0
SN 2005hj	2.4	···	···	10.62 (0.05)	42.3 (0.7)	0
SN 2005hj	3.3	···	···	10.62 (0.05)	51.0 (0.5)	0
SN 2005iq	−5.9	···	···	11.60 (0.05)	91.9 (0.2)	0
SN 2005ki	1.6	···	···	11.03 (0.05)	106.7 (0.1)	0
SN 2005lz	0.6	···	···	10.11 (0.05)	112.5 (0.3)	0
SN 2005ms	−1.9	···	···	11.84 (0.05)	120.8 (0.8)	0
SN 2005na	0.0	···	···	10.55 (0.05)	72.2 (0.4)	0
SN 2005na	1.0	···	···	10.30 (0.05)	70.5 (0.6)	0
SN 2006D	3.7	···	···	10.42 (0.05)	99.3 (0.1)	0
SN 2006N	−1.9	···	···	11.39 (0.05)	99.2 (0.2)	0
SN 2006N	−0.9	···	···	11.30 (0.05)	111.6 (0.2)	0
SN 2006S	−3.9	···	···	11.08 (0.05)	48.6 (1.0)	0
SN 2006S	3.0	···	···	10.71 (0.05)	73.1 (0.5)	0
SN 2006X	−11.2	23.07 (0.05)	45.3 (1.0)	17.37 (0.05)	128.0 (16.3)	0.35 (0.01)
SN 2006X	−10.2	22.89 (0.05)	42.2 (1.0)	17.17 (0.05)	137.3 (0.6)	0.31 (0.01)
SN 2006X	−9.2	22.41 (0.05)	48.9 (1.2)	16.52 (0.05)	137.2 (30.5)	0.36 (0.01)
SN 2006X	−8.2	22.15 (0.05)	44.7 (0.7)	16.35 (0.05)	143.8 (3.9)	0.31 (0.01)
SN 2006X	−7.2	21.55 (0.05)	50.8 (0.6)	15.77 (0.05)	135.4 (4.5)	0.37 (0.01)
SN 2006X	−6.2	21.43 (0.05)	39.6 (0.6)	15.88 (0.05)	151.4 (0.8)	0.26 (0.01)
SN 2006X	−5.2	21.01 (0.05)	39.6 (0.7)	15.52 (0.05)	152.6 (10.4)	0.26 (0.01)
SN 2006X	−0.2	19.67 (0.05)	26.2 (0.8)	14.80 (0.05)	155.5 (9.5)	0.17 (0.01)
SN 2006X	0.8	19.29 (0.05)	22.3 (0.7)	14.59 (0.05)	158.6 (0.6)	0.14 (0.01)
SN 2006X	1.8	18.97 (0.05)	17.9 (0.5)	14.53 (0.05)	156.2 (2.3)	0.11 (0.01)
SN 2006X	2.8	···	···	14.57 (0.05)	179.4 (0.2)	0
SN 2006X	3.2	···	···	14.74 (0.05)	188.7 (0.1)	0
SN 2006ax	−10.1	···	···	12.25 (0.05)	87.4 (0.4)	0
SN 2006bt	−5.3	···	···	12.12 (0.05)	113.6 (0.3)	0
SN 2006bt	−4.5	···	···	11.88 (0.05)	111.7 (0.4)	0
SN 2006bt	2.3	···	···	10.51 (0.05)	131.8 (0.3)	0
SN 2006bu	4.2	···	···	11.18 (0.05)	81.8 (0.7)	0
SN 2006bz	−2.4	···	···	10.85 (0.05)	101.9 (0.8)	0
SN 2006cj	3.4	···	···	10.93 (0.05)	71.7 (0.7)	0
SN 2006cm	−1.2	···	···	11.15 (0.05)	48.3 (0.3)	0
SN 2006cp	−5.3	···	···	14.41 (0.05)	164.0 (0.3)	0
SN 2006cq	2.0	···	···	10.16 (0.05)	93.7 (0.8)	0
SN 2006cs	2.3	···	···	10.73 (0.05)	91.6 (0.5)	0
SN 2006cz	1.1	···	···	11.86 (0.05)	57.6 (0.4)	0
SN 2006dm	−7.9	···	···	12.25 (0.05)	103.0 (0.9)	0
SN 2006ef	3.2	···	···	11.81 (0.05)	140.1 (0.1)	0
SN 2006gr	−8.7	···	···	16.35 (0.05)	81.4 (0.6)	0
SN 2006ej	−3.7	···	···	12.40 (0.05)	114.9 (0.2)	0
SN 2006em	4.2	···	···	8.23 (0.05)	79.1 (0.3)	0
SN 2006et	3.3	···	···	9.91 (0.05)	73.4 (0.2)	0
SN 2006gj	4.7	···	···	9.91 (0.05)	123.0 (0.5)	0
SN 2006gt	3.1	···	···	9.83 (0.05)	120.2 (0.8)	0
SN 2006ke	2.4	···	···	9.10 (0.05)	66.1 (0.4)	0
SN 2006kf	−9.0	···	···	13.31 (0.05)	129.1 (0.2)	0
SN 2006kf	−3.1	···	···	11.32 (0.05)	115.2 (0.1)	0
SN 2006le	−8.7	20.03 (0.05)	19.6 (0.2)	13.05 (0.05)	64.3 (0.2)	0.31 (0.01)

Continued on next page

Table A3 — Continued

SN Name	Phase (d)[a]	HVF v (10^3 km s^{-1})	HVF pEW (Å)	PVF v (10^3 km s^{-1})	PVF pEW (Å)	$R_{\rm Si}$[b]
SN 2006lf	−6.3	···	···	11.72 (0.05)	95.6 (0.1)	0
SN 2006or	−2.8	···	···	11.34 (0.05)	112.8 (0.3)	0
SN 2006os	−0.9	···	···	12.20 (0.05)	131.5 (0.5)	0
SN 2006qo	−11.1	···	···	12.24 (0.10)	21.0 (0.8)	0
SN 2006sr	−2.3	···	···	12.47 (0.05)	111.2 (0.2)	0
SN 2006sr	2.7	···	···	11.73 (0.05)	116.0 (0.2)	0
SN 2007A	2.4	···	···	10.60 (0.05)	89.3 (0.1)	0
SN 2007F	−9.4	···	···	12.14 (0.05)	64.3 (0.3)	0
SN 2007F	3.2	···	···	10.60 (0.05)	86.7 (0.2)	0
SN 2007N	0.4	···	···	10.33 (0.05)	90.4 (0.2)	0
SN 2007O	−0.3	···	···	10.00 (0.05)	75.2 (0.2)	0
SN 2007S	−6.0	···	···	11.07 (0.05)	41.9 (0.4)	0
SN 2007af	−9.8	···	···	12.28 (0.05)	99.3 (0.2)	0
SN 2007af	−1.3	···	···	10.62 (0.05)	110.1 (0.1)	0
SN 2007af	0.2	···	···	10.56 (0.05)	108.4 (0.3)	0
SN 2007af	2.8	···	···	10.23 (0.05)	116.8 (0.1)	0
SN 2007af	3.8	···	···	10.08 (0.05)	111.2 (0.1)	0
SN 2007al	3.4	···	···	8.73 (0.05)	73.4 (0.5)	0
SN 2007ba	2.1	···	···	9.63 (0.05)	111.0 (0.7)	0
SN 2007bc	0.6	···	···	9.85 (0.05)	101.2 (0.2)	0
SN 2007bd	−5.8	···	···	13.36 (0.05)	108.7 (0.9)	0
SN 2007bm	−7.8	···	···	11.22 (0.05)	87.9 (0.2)	0
SN 2007bz	1.7	···	···	11.70 (0.05)	69.9 (0.4)	0
SN 2007ca	−11.1	···	···	12.44 (0.05)	54.9 (0.6)	0
SN 2007ci	−6.6	···	···	12.26 (0.05)	117.0 (0.5)	0
SN 2007ci	−1.7	···	···	11.83 (0.05)	122.7 (0.3)	0
SN 2007co	−4.1	···	···	12.50 (0.05)	124.1 (0.3)	0
SN 2007co	−0.6	···	···	11.73 (0.05)	114.4 (0.5)	0
SN 2007co	0.9	···	···	11.51 (0.05)	121.6 (0.2)	0
SN 2007cq	−5.8	···	···	10.48 (0.05)	40.2 (0.5)	0
SN 2007fb	2.0	···	···	10.80 (0.05)	117.3 (0.3)	0
SN 2007fr	−5.8	···	···	11.48 (0.05)	113.4 (0.8)	0
SN 2007fr	−1.3	···	···	10.74 (0.05)	118.2 (0.8)	0
SN 2007gi	−7.3	22.18 (0.05)	33.8 (0.3)	16.79 (0.05)	147.9 (1.4)	0.23 (0.01)
SN 2007gi	−0.4	20.05 (0.05)	32.9 (0.4)	14.87 (0.05)	151.6 (0.8)	0.22 (0.01)
SN 2007gk	−1.7	···	···	13.66 (0.05)	171.4 (0.2)	0
SN 2007hj	−1.2	···	···	11.71 (0.05)	149.3 (0.2)	0
SN 2007le	−10.3	21.47 (0.05)	33.6 (0.7)	15.00 (0.05)	138.8 (1.1)	0.24 (0.01)
SN 2007le	−9.4	21.38 (0.05)	21.3 (0.3)	14.52 (0.05)	113.1 (1.1)	0.19 (0.01)
SN 2007s1[c]	−1.2	···	···	11.37 (0.05)	125.1 (0.3)	0
SN 2007on	−3.0	···	···	11.46 (0.05)	117.2 (0.1)	0
SN 2007on	−3.0	···	···	11.52 (0.05)	119.8 (0.1)	0
SN 2007qe	−6.5	···	···	15.18 (0.05)	142.5 (0.3)	0
SN 2008Z	−2.3	···	···	11.46 (0.05)	55.8 (0.2)	0
SN 2008ar	−8.9	18.48 (0.11)	27.9 (1.6)	12.17 (0.09)	84.4 (0.2)	0.33 (0.02)
SN 2008ar	2.8	···	···	10.34 (0.05)	92.0 (0.8)	0
SN 2008bt	−1.1	···	···	9.75 (0.05)	97.6 (1.1)	0
SN 2008cl	4.2	···	···	10.95 (0.05)	108.9 (1.8)	0
SN 2008s1[d]	−6.4	···	···	11.03 (0.05)	69.1 (0.3)	0
SN 2008s1[d]	−4.4	···	···	10.86 (0.05)	71.9 (0.9)	0
SN 2008s1[d]	−3.4	···	···	10.76 (0.05)	82.1 (0.5)	0
SN 2008s1[d]	0.5	···	···	10.56 (0.05)	96.1 (0.5)	0
SN 2008s1[d]	4.4	···	···	10.39 (0.05)	96.0 (0.2)	0
SN 2008dx	2.5	···	···	8.85 (0.05)	90.8 (0.8)	0
SN 2008ec	−0.2	···	···	10.75 (0.05)	119.4 (0.2)	0
SN 2008ei	3.3	18.29 (0.05)	22.5 (0.9)	13.83 (0.05)	159.3 (0.2)	0.14 (0.01)
SN 2008s5[e]	1.3	···	···	9.13 (0.05)	53.6 (0.3)	0
SN 2008hs	−7.9	···	···	11.97 (0.05)	109.5 (0.4)	0
SN 2008hs	−6.3	···	···	11.55 (0.05)	112.4 (0.4)	0
SN 2008hv	−9.2	18.82 (0.08)	35.6 (1.2)	12.79 (0.07)	74.8 (0.7)	0.48 (0.02)
SN 2009ad	−3.4	···	···	10.79 (0.05)	61.0 (0.2)	0
SN 2009an	−5.8	···	···	13.98 (0.05)	149.2 (0.2)	0
SN 2009an	−3.8	···	···	13.01 (0.05)	140.2 (0.2)	0
SN 2009an	−2.9	···	···	12.68 (0.05)	137.2 (0.3)	0

Continued on next page

Table A3 — Continued

SN Name	Phase (d)[a]	HVF v (10^3 km s^{-1})	HVF pEW (Å)	PVF v (10^3 km s^{-1})	PVF pEW (Å)	$\mathcal{R}_{\rm Si}$[b]
SN 2009fx	−2.2	···	···	10.11 (0.05)	40.7 (0.7)	0
SN 2009ig	−14.4	25.10 (0.05)	59.1 (1.5)	19.06 (0.08)	97.5 (0.4)	0.61 (0.02)
SN 2009ig	−14.3	25.08 (0.05)	61.0 (1.0)	19.06 (0.06)	102.3 (1.1)	0.60 (0.01)
SN 2009ig	−14.2	25.21 (0.05)	43.3 (1.6)	19.66 (0.09)	122.6 (0.6)	0.35 (0.01)
SN 2009ig	−13.9	24.08 (0.05)	72.4 (0.9)	17.63 (0.05)	76.5 (1.2)	0.95 (0.02)
SN 2009ig	−13.3	24.33 (0.05)	45.6 (0.4)	18.13 (0.05)	110.1 (1.0)	0.41 (0.01)
SN 2009ig	−12.4	23.88 (0.05)	30.4 (0.5)	17.61 (0.05)	104.4 (0.5)	0.29 (0.01)
SN 2009ig	−12.3	24.02 (0.05)	28.9 (0.9)	17.57 (0.06)	108.6 (0.2)	0.27 (0.01)
SN 2009ig	−11.4	23.62 (0.05)	21.3 (0.2)	16.72 (0.05)	95.9 (0.2)	0.22 (0.01)
SN 2009ig	−11.3	23.55 (0.05)	19.4 (0.2)	16.60 (0.05)	96.9 (0.1)	0.20 (0.01)
SN 2009ig	−10.9	23.14 (0.05)	14.4 (0.3)	15.80 (0.05)	86.4 (0.7)	0.17 (0.01)
SN 2009ig	−10.3	23.13 (0.05)	13.3 (0.3)	15.76 (0.05)	77.0 (0.1)	0.17 (0.01)
SN 2009ig	−9.9	22.96 (0.05)	10.4 (0.3)	15.08 (0.05)	82.7 (0.7)	0.13 (0.01)
SN 2009ig	−9.4	22.90 (0.05)	9.8 (0.1)	14.96 (0.05)	80.8 (1.5)	0.12 (0.01)
SN 2009ig	−8.9	22.70 (0.05)	7.8 (0.3)	14.56 (0.05)	79.9 (0.4)	0.10 (0.01)
SN 2009ig	−8.4	22.40 (0.05)	4.4 (0.2)	14.89 (0.05)	87.3 (3.4)	0.05 (0.01)
SN 2009ig	−7.9	···	···	14.46 (0.05)	80.9 (0.2)	0
SN 2009ig	−6.9	···	···	14.30 (0.05)	77.6 (0.2)	0
SN 2009ig	−6.9	···	···	14.21 (0.05)	75.9 (0.2)	0
SN 2009ig	−6.0	···	···	13.87 (0.05)	78.6 (0.1)	0
SN 2009ig	−6.0	···	···	13.83 (0.05)	73.0 (0.1)	0
SN 2009ig	−4.0	···	···	13.56 (0.05)	77.7 (0.2)	0
SN 2009ig	−3.0	···	···	13.60 (0.05)	77.7 (0.2)	0
SN 2009ig	−2.0	···	···	13.65 (0.05)	80.7 (0.2)	0
SN 2009ig	−1.0	···	···	13.66 (0.05)	81.6 (0.2)	0
SN 2009ig	3.4	···	···	13.59 (0.05)	84.2 (0.2)	0
SN 2009ig	4.3	···	···	13.73 (0.05)	81.5 (0.3)	0
SN 2009no	2.1	···	···	10.03 (0.05)	63.5 (0.3)	0
SN 2009nq	−3.1	···	···	10.19 (0.05)	88.7 (0.1)	0
SN 2010Y	−7.2	···	···	11.03 (0.05)	90.1 (0.4)	0
SN 2010Y	−3.2	···	···	10.54 (0.05)	104.8 (0.2)	0
PTF 10bjs	−9.8	···	···	14.02 (0.06)	40.4 (1.1)	0
PTF 10bjs	−8.6	···	···	14.09 (0.06)	38.3 (1.0)	0
PTF 10bjs	−7.4	···	···	14.02 (0.05)	40.0 (0.5)	0
PTF 10bjs	−6.6	···	···	13.96 (0.05)	46.4 (0.6)	0
PTF 10bjs	−5.5	···	···	14.03 (0.05)	44.7 (0.8)	0
PTF 10bjs	−1.8	···	···	13.79 (0.05)	55.6 (0.3)	0
PTF 10bjs	0.2	···	···	13.79 (0.05)	60.3 (0.3)	0
SN 2010ai	−10.5	···	···	13.60 (0.05)	94.1 (0.8)	0
SN 2010ai	−8.6	···	···	12.44 (0.05)	89.6 (0.3)	0
SN 2010ai	−3.7	···	···	11.34 (0.05)	99.8 (0.2)	0
SN 2010ai	−0.8	···	···	11.08 (0.05)	104.0 (0.2)	0
PTF 10fps	0.0	···	···	9.93 (0.05)	105.8 (0.4)	0
PTF 10fps	0.9	···	···	9.90 (0.05)	103.6 (0.6)	0
PTF 10fps	3.9	···	···	9.56 (0.05)	105.9 (0.6)	0
SN 2010dm	−6.5	17.73 (0.11)	3.6 (0.5)	11.78 (0.07)	35.9 (0.6)	0.10 (0.01)
PTF 10icb	−9.8	···	···	12.00 (0.05)	62.7 (0.3)	0
SN 2010ex	1.1	···	···	10.89 (0.05)	80.3 (0.3)	0
PTF 10qjl	−3.0	···	···	11.01 (0.05)	59.9 (0.5)	0
SN 2010ii	−6.1	···	···	14.16 (0.05)	108.5 (0.3)	0
SN 2010ii	−0.5	···	···	12.24 (0.05)	105.7 (0.2)	0
SN 2010it	−9.5	···	···	15.10 (0.05)	131.8 (0.4)	0
SN 2010it	−8.5	···	···	14.29 (0.05)	105.0 (0.3)	0
SN 2010it	−6.6	···	···	13.45 (0.05)	89.8 (0.4)	0
SN 2010it	−2.6	···	···	12.20 (0.05)	80.2 (0.3)	0
SN 2010it	−0.6	···	···	12.13 (0.05)	107.4 (0.4)	0
SN 2010it	3.3	···	···	11.55 (0.05)	100.7 (0.3)	0
PTF 10ygu	−3.7	20.73 (0.14)	43.8 (3.4)	14.43 (0.20)	87.7 (2.7)	0.50 (0.04)
SN 2010iw	−4.9	17.16 (0.07)	4.4 (0.2)	10.50 (0.05)	37.6 (0.2)	0.12 (0.01)
SN 2010iw	−3.0	···	···	10.39 (0.05)	44.3 (0.4)	0
SN 2010iw	−0.1	···	···	10.36 (0.05)	53.3 (0.3)	0
SN 2010iw	3.9	···	···	10.22 (0.05)	63.3 (0.2)	0
SN 2010kg	−9.9	21.98 (0.05)	56.6 (1.8)	16.68 (0.09)	96.2 (0.7)	0.59 (0.02)
SN 2010kg	−9.0	21.84 (0.05)	30.4 (1.6)	17.05 (0.09)	126.4 (3.1)	0.24 (0.01)
SN 2010kg	−8.0	20.95 (0.05)	48.4 (1.2)	15.70 (0.06)	103.8 (2.0)	0.47 (0.01)

Continued on next page

Table A3 — Continued

SN Name	Phase (d)[a]	HVF v (10^3 km s^{-1})	HVF pEW (Å)	PVF v (10^3 km s^{-1})	PVF pEW (Å)	$R_{\rm Si}$[b]
SN 2010kg	−6.0	20.52 (0.05)	33.1 (0.9)	15.32 (0.05)	120.3 (4.1)	0.28 (0.01)
SN 2010kg	−5.0	19.81 (0.05)	43.4 (1.0)	14.30 (0.05)	107.1 (21.3)	0.40 (0.01)
SN 2010kg	−4.1	19.77 (0.05)	36.8 (0.6)	14.22 (0.05)	114.2 (17.6)	0.32 (0.01)
SN 2010kg	−3.1	19.64 (0.05)	32.7 (0.7)	14.09 (0.05)	118.2 (24.5)	0.28 (0.01)
SN 2010kg	−1.1	19.17 (0.05)	28.2 (0.4)	13.58 (0.05)	122.2 (0.9)	0.23 (0.01)
SN 2010kg	−0.1	19.17 (0.05)	28.6 (0.4)	13.51 (0.05)	122.8 (3.1)	0.23 (0.01)
SN 2010kg	0.9	18.72 (0.05)	28.1 (0.8)	13.08 (0.05)	128.2 (5.4)	0.22 (0.01)
SN 2010kg	2.8	18.45 (0.05)	30.7 (0.4)	12.71 (0.05)	124.8 (91.4)	0.25 (0.01)
SN 2010kg	4.8	18.16 (0.05)	32.4 (0.5)	12.49 (0.05)	123.1 (1.5)	0.26 (0.01)
SN 2011ao	−7.5	17.52 (0.11)	38.8 (1.4)	11.71 (0.14)	41.4 (4.2)	0.94 (0.05)
SN 2011ao	−6.7	17.35 (0.09)	32.9 (0.9)	11.37 (0.09)	40.2 (9.5)	0.82 (0.03)
SN 2011ao	−5.8	17.40 (0.07)	27.2 (0.6)	11.21 (0.06)	42.4 (1.2)	0.64 (0.02)
SN 2011ao	−4.8	17.19 (0.06)	22.1 (0.5)	10.88 (0.05)	45.0 (1.0)	0.49 (0.01)
SN 2011ao	−1.8	16.99 (0.05)	9.0 (0.2)	10.41 (0.05)	57.1 (1.0)	0.16 (0.01)
SN 2011ao	−0.8	16.68 (0.05)	6.2 (0.2)	10.28 (0.05)	60.2 (21.3)	0.10 (0.01)
SN 2011ao	0.2	17.35 (0.11)	4.4 (0.3)	10.34 (0.05)	66.4 (0.6)	0.07 (0.01)
SN 2011ao	1.2	···	···	10.36 (0.05)	70.2 (0.3)	0
SN 2011ao	2.2	···	···	10.16 (0.05)	72.2 (0.2)	0
SN 2011ao	3.2	···	···	10.02 (0.05)	73.9 (0.4)	0
SN 2011by	−11.7	···	···	11.95 (0.05)	75.3 (0.1)	0
SN 2011by	−9.8	···	···	11.42 (0.05)	68.0 (0.1)	0
SN 2011by	−5.7	···	···	10.81 (0.05)	70.6 (0.1)	0
SN 2011by	−3.8	···	···	10.55 (0.05)	78.2 (0.1)	0
SN 2011by	0.2	···	···	10.27 (0.05)	88.6 (0.1)	0
SN 2011by	0.3	···	···	10.29 (0.05)	90.3 (0.2)	0
SN 2011by	2.3	···	···	10.20 (0.05)	92.7 (0.2)	0
SN 2011by	4.2	···	···	10.02 (0.05)	93.6 (0.1)	0
SN 2011dm	−5.5	···	···	13.62 (0.05)	104.7 (0.1)	0
SN 2011ek	−6.0	···	···	13.75 (0.05)	145.2 (0.1)	0
SN 2011ek	−5.0	···	···	13.36 (0.05)	148.2 (0.1)	0
SN 2011ek	3.0	···	···	11.75 (0.05)	150.7 (0.1)	0
SN 2011fe	−16.0	20.16 (0.05)	22.7 (0.9)	15.53 (0.06)	69.1 (6.0)	0.33 (0.01)
SN 2011fe	−15.0	···	···	14.73 (0.05)	101.0 (0.4)	0
SN 2011fe	−15.0	···	···	15.20 (0.05)	103.8 (0.3)	0
SN 2011fe	−13.0	···	···	13.14 (0.05)	98.3 (0.2)	0
SN 2011fe	−12.0	···	···	13.01 (0.05)	107.5 (0.1)	0
SN 2011fe	−11.0	···	···	12.09 (0.05)	98.7 (0.2)	0
SN 2011fe	−10.0	···	···	11.77 (0.05)	96.9 (0.1)	0
SN 2011fe	−10.0	···	···	11.68 (0.05)	87.9 (0.2)	0
SN 2011fe	−9.0	···	···	11.23 (0.05)	85.7 (0.3)	0
SN 2011fe	−9.0	···	···	11.34 (0.05)	95.1 (0.1)	0
SN 2011fe	−7.0	···	···	11.21 (0.05)	85.0 (0.1)	0
SN 2011fe	−2.0	···	···	10.53 (0.05)	97.0 (0.1)	0
SN 2011fe	−1.0	···	···	10.58 (0.05)	98.7 (0.1)	0
SN 2011fe	2.0	···	···	10.44 (0.05)	103.2 (0.1)	0
SN 2011fe	3.0	···	···	10.26 (0.05)	103.1 (0.1)	0
SN 2011gy	−1.1	···	···	11.41 (0.05)	105.5 (0.1)	0
SN 2011hb	−5.8	17.77 (0.13)	23.8 (1.4)	11.90 (0.10)	61.7 (1.2)	0.39 (0.02)
SN 2011hb	−2.9	···	···	11.80 (0.05)	78.8 (0.4)	0
SN 2011hb	3.0	···	···	10.74 (0.05)	86.4 (0.4)	0
SN 2011ia	−3.0	···	···	10.68 (0.05)	63.2 (0.2)	0
SN 2012I	−1.0	···	···	10.95 (0.05)	102.1 (0.2)	0
SN 2012bh	0.0	···	···	10.36 (0.05)	85.5 (0.2)	0
SN 2012cg	−14.7	22.27 (0.14)	47.8 (1.9)	17.22 (0.19)	3.3 (5.1)	14.54 (4.88)
SN 2012cg	−13.8	22.07 (0.05)	15.9 (0.9)	17.05 (0.09)	61.5 (3.7)	0.26 (0.02)
SN 2012cg	−12.8	19.02 (0.13)	47.2 (1.8)	13.48 (0.13)	46.7 (4.8)	1.01 (0.06)
SN 2012cg	−11.8	18.92 (0.06)	32.2 (0.8)	13.21 (0.06)	59.5 (0.8)	0.54 (0.02)
SN 2012cg	−10.5	17.85 (0.17)	31.0 (1.6)	12.27 (0.11)	43.7 (8.7)	0.71 (0.04)
SN 2012cg	−9.6	18.07 (0.17)	15.3 (1.1)	12.21 (0.10)	45.2 (21.4)	0.34 (0.03)
SN 2012cg	−7.8	···	···	11.88 (0.05)	24.7 (0.2)	0
SN 2012cg	−6.8	···	···	11.34 (0.05)	50.4 (0.2)	0
SN 2012cg	−4.8	···	···	10.94 (0.05)	53.8 (0.1)	0
SN 2012cg	−3.8	···	···	10.89 (0.05)	51.9 (0.1)	0
SN 2012cg	−3.8	···	···	11.04 (0.05)	55.7 (0.2)	0
SN 2012cg	−0.5	···	···	10.58 (0.05)	63.2 (0.2)	0

Continued on next page

Table A3 — Continued

SN Name	Phase (d)[a]	HVF v (10^3 km s^{-1})	HVF pEW (Å)	PVF v (10^3 km s^{-1})	PVF pEW (Å)	$R_{\rm Si}$[b]
SN 2012da	−1.0	···	···	11.11 (0.05)	79.5 (0.2)	0
SN 2012fr	−14.4	23.61 (0.05)	159.8 (1.0)	···	···	···
SN 2012fr	−14.1	23.67 (0.05)	192.8 (0.1)	···	···	···
SN 2012fr	−12.6	22.43 (0.05)	124.6 (0.4)	14.00 (0.05)	26.0 (40.1)	4.79 (0.06)
SN 2012fr	−12.4	22.26 (0.05)	119.1 (0.4)	13.80 (0.05)	24.6 (0.1)	4.85 (0.07)
SN 2012fr	−11.4	21.91 (0.05)	94.3 (0.3)	13.22 (0.05)	26.7 (2.2)	3.53 (0.03)
SN 2012fr	−9.3	21.25 (0.05)	38.2 (0.3)	13.12 (0.05)	44.6 (0.2)	0.86 (0.01)
SN 2012fr	−8.4	21.13 (0.05)	32.0 (0.3)	12.92 (0.05)	45.3 (0.2)	0.71 (0.01)
SN 2012fr	−8.2	20.93 (0.05)	29.9 (0.2)	12.87 (0.05)	45.4 (0.3)	0.66 (0.01)
SN 2012fr	−7.6	20.58 (0.05)	24.1 (0.1)	12.46 (0.05)	47.9 (0.8)	0.50 (0.01)
SN 2012fr	−7.5	20.60 (0.05)	25.2 (0.2)	12.75 (0.05)	46.8 (0.6)	0.54 (0.01)
SN 2012fr	−6.7	20.38 (0.06)	17.2 (0.4)	12.64 (0.05)	52.8 (8.7)	0.33 (0.01)
SN 2012fr	−6.6	20.11 (0.05)	15.1 (0.1)	12.28 (0.05)	53.8 (4.5)	0.28 (0.01)
SN 2012fr	−6.4	20.50 (0.05)	17.9 (0.4)	12.70 (0.05)	53.2 (0.1)	0.34 (0.01)
SN 2012fr	−5.6	20.63 (0.05)	16.1 (0.2)	12.58 (0.05)	55.9 (11.7)	0.29 (0.01)
SN 2012fr	−4.7	19.69 (0.07)	9.8 (0.3)	12.49 (0.05)	56.9 (4.1)	0.17 (0.01)
SN 2012fr	−4.6	19.85 (0.05)	8.5 (0.1)	12.33 (0.05)	57.7 (3.2)	0.15 (0.01)
SN 2012fr	−3.7	19.00 (0.11)	7.7 (0.4)	12.40 (0.05)	57.9 (1.9)	0.13 (0.01)
SN 2012fr	−3.6	18.76 (0.05)	4.7 (0.1)	12.06 (0.05)	56.7 (1.0)	0.08 (0.01)
SN 2012fr	−2.5	···	···	12.41 (0.05)	64.0 (0.2)	0
SN 2012fr	−2.4	···	···	12.53 (0.05)	61.4 (0.2)	0
SN 2012fr	−1.4	···	···	12.48 (0.05)	59.7 (0.1)	0
SN 2012fr	−1.3	···	···	12.42 (0.05)	59.2 (0.1)	0
SN 2012fr	−0.3	···	···	12.42 (0.05)	60.8 (0.1)	0
SN 2012fr	0.4	···	···	12.15 (0.05)	63.4 (0.1)	0
SN 2012fr	0.7	···	···	12.51 (0.05)	62.3 (0.1)	0
SN 2012fr	1.3	···	···	12.48 (0.05)	63.6 (0.3)	0
SN 2012fr	1.7	···	···	12.36 (0.05)	61.1 (0.1)	0
SN 2012fr	2.3	···	···	12.29 (0.05)	61.1 (0.1)	0
SN 2012fr	3.2	···	···	12.52 (0.05)	64.9 (0.3)	0
SN 2012fr	4.5	···	···	12.48 (0.05)	62.1 (0.1)	0
SN 2013cs	−8.9	···	···	14.03 (0.05)	142.9 (0.2)	0
SN 2013cs	−3.0	···	···	12.81 (0.05)	146.3 (0.1)	0
SN 2013di	−1.6	···	···	11.46 (0.05)	85.6 (0.3)	0

[a]Phases are in rest-frame days.
[b]$R_{\rm Si}$ is the ratio of the pEW of the HVF to the pEW of the PVF, as defined by Childress et al. (2014).
[c]Also known as SNF20071021-000.
[d]Also known as SNF20080514-002.
[e]Also known as SNF20080909-030.

Table A4: CaIR3 Fit Results

SN Name	Phase (d)[a]	HVF v (10^3 km s^{-1})	HVF pEW (Å)	PVF v (10^3 km s^{-1})	PVF pEW (Å)	$R_{\rm CaIR3}$[b]
SN 1989M	2.5	···	···	13.33 (0.05)	197.1 (0.2)	0
SN 1989M	3.5	···	···	13.00 (0.05)	209.9 (0.2)	0
SN 1991bg	1.1	···	···	11.84 (0.05)	268.8 (1.2)	0
SN 1994D	−7.7	20.85 (0.05)	41.7 (0.2)	10.01 (0.05)	37.7 (0.8)	1.11 (0.02)
SN 1994D	−3.9	20.37 (0.05)	21.5 (0.2)	10.22 (0.05)	48.4 (1.9)	0.44 (0.02)
SN 1994D	−3.3	20.77 (0.05)	21.3 (0.2)	10.51 (0.05)	64.1 (2.2)	0.33 (0.01)
SN 1994S	1.1	18.12 (0.06)	31.3 (1.2)	10.14 (0.06)	109.1 (6.9)	0.29 (0.02)
SN 1995D	3.8	17.73 (0.05)	55.0 (0.3)	10.06 (0.05)	104.8 (2.0)	0.52 (0.01)
SN 1995E	−2.5	19.22 (0.05)	56.2 (0.3)	10.48 (0.05)	91.0 (1.3)	0.62 (0.01)
SN 1997Y	1.3	16.50 (0.13)	28.1 (2.0)	10.10 (0.10)	94.3 (10.5)	0.30 (0.04)
SN 1997do	−5.7	23.78 (0.05)	164.5 (0.3)	12.69 (0.05)	36.0 (0.6)	4.57 (0.07)
SN 1998dk	−7.2	25.15 (0.05)	155.6 (1.1)	14.12 (0.21)	94.2 (10.5)	1.65 (0.18)
SN 1998dk	−0.5	18.21 (0.05)	30.8 (0.5)	12.08 (0.05)	103.5 (2.8)	0.30 (0.01)
SN 1998dm	−12.5	21.63 (0.05)	97.8 (0.2)	11.46 (0.05)	51.7 (0.9)	1.89 (0.03)
SN 1998dm	−5.6	20.18 (0.05)	32.1 (0.2)	10.97 (0.05)	47.3 (0.7)	0.68 (0.01)
SN 1998ef	−8.6	21.51 (0.08)	147.2 (2.1)	12.62 (0.10)	79.9 (6.9)	1.84 (0.16)
SN 1998es	0.3	19.80 (0.05)	40.1 (0.2)	9.93 (0.05)	40.6 (0.9)	0.99 (0.02)
SN 1999aa	0.2	18.91 (0.05)	37.8 (0.4)	10.22 (0.05)	31.2 (1.7)	1.21 (0.07)
SN 1999ac	−0.9	17.71 (0.05)	106.2 (0.3)	9.62 (0.05)	58.6 (1.5)	1.81 (0.05)
SN 1999cp	4.9	···	···	10.61 (0.05)	184.7 (0.2)	0

Continued on next page

Table A4 — Continued

SN Name	Phase (d)[a]	HVF v (10^3 km s^{-1})	HVF pEW (Å)	PVF v (10^3 km s^{-1})	PVF pEW (Å)	$\bar{R}^{b}_{\rm CaIR3}$
SN 1999da	−2.1	···	···	14.48 (0.05)	377.7 (0.4)	0
SN 1999dk	−6.6	22.06 (0.05)	109.3 (0.3)	13.05 (0.05)	113.9 (2.0)	0.96 (0.02)
SN 1999dq	−3.9	23.01 (0.05)	15.6 (0.6)	11.71 (0.16)	25.1 (2.5)	0.62 (0.07)
SN 1999dq	3.0	19.76 (0.05)	57.7 (0.2)	10.61 (0.05)	49.4 (1.0)	1.17 (0.02)
SN 1999gd	−1.1	···	···	11.42 (0.05)	165.0 (1.0)	0
SN 1999gh	4.1	···	···	10.76 (0.05)	303.3 (0.6)	0
SN 2000cp	2.9	···	···	11.56 (0.05)	281.5 (2.0)	0
SN 2000cw	4.8	···	···	11.72 (0.05)	302.4 (1.4)	0
SN 2000dg	−5.1	21.68 (0.07)	24.7 (0.3)	10.47 (0.08)	69.7 (4.9)	0.35 (0.03)
SN 2000dg	4.7	···	···	10.65 (0.05)	106.3 (1.1)	0
SN 2000dk	1.0	···	···	11.90 (0.05)	249.3 (0.5)	0
SN 2000dm	−1.6	17.35 (0.05)	36.9 (0.7)	10.27 (0.05)	102.2 (3.3)	0.36 (0.01)
SN 2000dn	−5.6	18.21 (0.32)	49.7 (6.2)	9.53 (0.44)	90.6 (31.0)	0.55 (0.20)
SN 2000dn	−0.9	16.28 (0.07)	81.1 (2.5)	9.49 (0.08)	138.4 (8.5)	0.59 (0.04)
SN 2000dx	−9.3	23.35 (0.05)	367.1 (5.4)	···	···	···
SN 2000fa	−8.3	23.85 (0.05)	158.5 (0.7)	12.62 (0.07)	35.4 (2.4)	4.47 (0.30)
SN 2001az	−3.2	20.98 (0.08)	32.2 (1.2)	9.76 (0.13)	82.9 (8.7)	0.39 (0.04)
SN 2001bf	1.2	14.97 (0.05)	36.4 (0.4)	7.57 (0.05)	40.8 (1.7)	0.89 (0.04)
SN 2001br	3.5	···	···	12.88 (0.05)	239.6 (4.0)	0
SN 2001cp	1.4	18.20 (0.06)	43.0 (0.9)	10.62 (0.06)	84.5 (5.2)	0.51 (0.03)
SN 2001da	−1.1	19.90 (0.05)	113.5 (1.0)	10.89 (0.11)	138.2 (7.3)	0.82 (0.04)
SN 2001eh	−4.5	20.70 (0.05)	31.8 (1.0)	8.57 (0.12)	18.8 (3.0)	1.69 (0.28)
SN 2001eh	3.3	17.81 (0.05)	69.9 (0.7)	10.13 (0.05)	48.1 (1.9)	1.45 (0.06)
SN 2001ep	2.8	···	···	11.51 (0.05)	249.6 (0.3)	0
SN 2001ex	−1.8	···	···	11.21 (0.05)	335.0 (2.4)	0
SN 2001fe	−1.0	17.02 (0.08)	10.9 (0.6)	10.96 (0.06)	46.7 (4.1)	0.23 (0.02)
SN 2002aw	2.1	···	···	8.77 (0.09)	122.8 (3.0)	0
SN 2002bf	3.0	17.36 (0.05)	152.2 (0.5)	10.67 (0.05)	96.7 (2.1)	1.57 (0.03)
SN 2002bo	−11.9	24.88 (0.09)	246.7 (4.2)	16.01 (0.10)	123.9 (19.2)	1.99 (0.31)
SN 2002bo	−1.1	16.52 (0.05)	130.2 (1.5)	10.13 (0.09)	109.6 (4.9)	1.19 (0.05)
SN 2002cd	1.1	15.28 (0.05)	158.2 (0.3)	···	···	···
SN 2002cf	−0.8	···	···	12.18 (0.05)	275.9 (0.6)	0
SN 2002ck	3.6	17.01 (0.06)	50.6 (1.1)	10.26 (0.05)	96.5 (8.6)	0.52 (0.05)
SN 2002cr	−6.8	17.97 (0.05)	58.5 (0.8)	9.59 (0.07)	92.3 (3.5)	0.63 (0.03)
SN 2002cr	−5.8	16.67 (0.23)	44.8 (5.1)	8.62 (0.55)	76.5 (26.8)	0.59 (0.22)
SN 2002cr	−3.9	15.85 (0.36)	46.4 (6.3)	8.81 (0.38)	71.4 (24.0)	0.65 (0.24)
SN 2002cs	−7.8	21.12 (0.05)	31.8 (0.5)	14.08 (0.05)	79.8 (2.9)	0.40 (0.02)
SN 2002dj	−8.0	24.19 (0.05)	149.3 (0.9)	14.57 (0.09)	127.4 (6.3)	1.17 (0.06)
SN 2002dk	−1.2	19.50 (0.05)	101.4 (3.8)	12.61 (0.43)	264.4 (24.5)	0.38 (0.04)
SN 2002eb	1.7	19.58 (0.05)	56.1 (0.5)	9.49 (0.05)	55.5 (1.5)	1.01 (0.03)
SN 2002ef	4.7	···	···	11.94 (0.05)	192.8 (1.7)	0
SN 2002er	−4.6	20.07 (0.05)	105.7 (0.2)	11.32 (0.05)	118.8 (0.9)	0.89 (0.01)
SN 2002eu	−0.1	···	···	11.63 (0.05)	214.8 (1.2)	0
SN 2002fb	1.0	···	···	11.65 (0.05)	270.2 (0.7)	0
SN 2002ha	−0.9	17.17 (0.05)	49.4 (0.8)	10.28 (0.05)	94.6 (2.7)	0.52 (0.02)
SN 2002ha	4.9	···	···	10.99 (0.05)	236.7 (0.6)	0
SN 2002he	−5.9	20.77 (0.07)	30.7 (1.2)	12.43 (0.14)	105.5 (8.7)	0.29 (0.03)
SN 2002he	−1.0	18.40 (0.07)	28.0 (1.5)	11.77 (0.11)	126.0 (9.3)	0.22 (0.02)
SN 2002he	0.3	···	···	12.40 (0.05)	194.0 (0.6)	0
SN 2002he	3.2	···	···	12.02 (0.05)	226.6 (0.6)	0
SN 2002hu	−5.8	20.13 (0.05)	80.2 (0.7)	9.32 (0.06)	41.1 (2.2)	1.95 (0.11)
SN 2002hw	−6.3	···	···	12.64 (0.05)	175.6 (0.6)	0
SN 2003U	−2.6	···	···	12.39 (0.05)	192.2 (1.3)	0
SN 2003W	−7.0	21.87 (0.07)	202.8 (4.1)	···	···	···
SN 2003W	−6.0	20.57 (0.06)	178.6 (3.7)	···	···	···
SN 2003W	−5.1	20.15 (0.05)	257.0 (1.4)	···	···	···
SN 2003Y	−1.7	···	···	12.87 (0.05)	291.7 (1.0)	0
SN 2003cq	−0.2	18.53 (0.13)	51.9 (3.6)	10.71 (0.31)	124.2 (21.7)	0.42 (0.08)
SN 2003gn	−5.4	21.66 (0.05)	181.0 (3.1)	11.55 (0.19)	76.2 (11.6)	2.38 (0.36)
SN 2003gn	3.3	···	···	10.48 (0.16)	338.1 (16.0)	0
SN 2003gt	−5.1	22.23 (0.05)	26.4 (0.5)	11.02 (0.05)	57.0 (2.6)	0.46 (0.02)
SN 2003he	2.7	17.58 (0.06)	49.1 (1.9)	10.15 (0.14)	158.7 (13.0)	0.31 (0.03)
SN 2003hs	−5.5	16.12 (0.06)	307.6 (4.1)	···	···	···
SN 2003iv	1.8	···	···	10.47 (0.05)	213.4 (0.8)	0
SN 2003kf	−7.5	22.94 (0.05)	89.9 (0.1)	11.39 (0.05)	41.8 (0.6)	2.15 (0.03)

Continued on next page

Table A4 — Continued

SN Name	Phase (d)[a]	HVF v (10^3 km s^{-1})	HVF pEW (Å)	PVF v (10^3 km s^{-1})	PVF pEW (Å)	$R_{\rm CaIR3}$[b]
SN 2004as	−4.4	20.43 (0.05)	111.9 (2.1)	12.59 (0.17)	128.5 (11.6)	0.87 (0.08)
SN 2004bl	4.6	···	···	11.80 (0.05)	166.6 (1.7)	0
SN 2004bw	−7.1	21.35 (0.22)	115.0 (7.6)	11.79 (0.49)	65.4 (21.8)	1.76 (0.60)
SN 2004dt	−6.5	20.54 (0.05)	44.1 (0.6)	11.69 (0.08)	53.8 (3.7)	0.82 (0.06)
SN 2004dt	1.4	···	···	10.96 (0.05)	130.3 (1.1)	0
SN 2004ef	−5.5	22.24 (0.05)	101.7 (1.6)	11.95 (0.49)	99.2 (19.2)	1.03 (0.20)
SN 2004eo	−5.6	18.20 (0.05)	102.2 (0.7)	9.68 (0.05)	76.2 (1.9)	1.34 (0.03)
SN 2004ey	−7.6	21.93 (0.05)	90.1 (0.2)	10.91 (0.05)	46.3 (0.7)	1.95 (0.03)
SN 2004fu	−2.7	19.54 (0.05)	89.6 (0.5)	12.00 (0.05)	115.0 (2.3)	0.78 (0.02)
SN 2004fu	2.4	···	···	12.50 (0.05)	230.3 (0.2)	0
SN 2004fz	−5.2	18.59 (0.05)	36.7 (0.5)	10.39 (0.05)	75.6 (2.1)	0.49 (0.01)
SN 2004gs	0.4	···	···	11.43 (0.05)	249.1 (1.0)	0
SN 2005W	0.6	···	···	11.70 (0.05)	212.6 (0.7)	0
SN 2005am	4.5	···	···	11.41 (0.05)	223.2 (0.2)	0
SN 2005ao	−1.3	16.62 (0.16)	22.8 (2.9)	11.48 (0.13)	72.7 (12.5)	0.31 (0.07)
SN 2005ao	0.5	19.61 (0.10)	32.1 (1.9)	11.36 (0.14)	118.7 (14.4)	0.27 (0.04)
SN 2005bc	1.6	···	···	11.79 (0.05)	205.1 (0.4)	0
SN 2005cf	−10.9	25.12 (0.05)	216.5 (4.1)	16.01 (0.09)	189.9 (13.3)	1.14 (0.08)
SN 2005cf	−2.1	20.66 (0.05)	141.9 (0.3)	9.80 (0.05)	67.3 (1.6)	2.11 (0.05)
SN 2005cf	−1.2	20.13 (0.05)	125.3 (0.4)	9.92 (0.05)	62.6 (1.2)	2.00 (0.04)
SN 2005cg	−10.1	24.56 (0.18)	108.3 (17.9)	11.66 (5.94)	78.2 (0.1)	1.38 (1.94)
SN 2005cg	−9.1	23.46 (0.05)	109.8 (1.2)	10.63 (0.32)	32.5 (6.2)	3.38 (0.64)
SN 2005cg	−4.3	21.91 (0.05)	78.9 (0.9)	10.79 (0.21)	35.8 (5.1)	2.21 (0.32)
SN 2005cg	−0.4	20.45 (0.05)	65.3 (0.9)	11.03 (0.09)	49.6 (3.9)	1.32 (0.10)
SN 2005cg	4.5	19.20 (0.06)	59.5 (1.4)	11.02 (0.10)	95.6 (7.3)	0.62 (0.05)
SN 2005de	−0.8	17.97 (0.05)	65.9 (1.6)	10.16 (0.08)	113.7 (5.9)	0.58 (0.03)
SN 2005dv	−0.6	···	···	13.34 (0.05)	258.8 (1.3)	0
SN 2005el	−6.7	20.77 (0.05)	45.3 (0.3)	11.23 (0.06)	52.2 (2.0)	0.87 (0.03)
SN 2005el	1.2	17.77 (0.05)	36.5 (0.7)	10.11 (0.05)	93.2 (4.2)	0.39 (0.02)
SN 2005er	−0.3	···	···	13.42 (0.05)	396.9 (0.3)	0
SN 2005er	1.7	···	···	12.83 (0.05)	358.2 (0.4)	0
SN 2005eq	−3.0	20.58 (0.05)	37.5 (0.2)	9.31 (0.05)	13.3 (0.7)	2.82 (0.16)
SN 2005eq	0.7	19.24 (0.05)	46.5 (0.5)	9.53 (0.07)	34.2 (2.3)	1.36 (0.09)
SN 2005eu	−10.1	23.59 (0.05)	18.4 (0.2)	···	···	···
SN 2005hj	3.3	16.63 (0.31)	26.5 (3.0)	9.86 (0.39)	48.1 (18.5)	0.55 (0.22)
SN 2005iq	−5.9	19.54 (0.05)	63.5 (0.5)	10.78 (0.05)	80.6 (2.1)	0.79 (0.02)
SN 2005ki	1.6	18.36 (0.05)	23.0 (0.2)	10.65 (0.05)	72.5 (1.7)	0.32 (0.01)
SN 2005lz	0.6	···	···	10.42 (0.05)	159.5 (0.7)	0
SN 2005ms	−1.9	···	···	13.58 (0.05)	205.6 (3.1)	0
SN 2005na	0.0	19.20 (0.17)	16.2 (1.0)	10.04 (0.11)	45.6 (7.4)	0.36 (0.06)
SN 2005na	1.0	···	···	10.27 (0.11)	158.0 (4.1)	0
SN 2006D	3.7	···	···	12.20 (0.05)	207.9 (0.3)	0
SN 2006N	−1.9	···	···	11.89 (0.05)	85.4 (0.6)	0
SN 2006N	−0.9	···	···	11.74 (0.05)	153.0 (0.7)	0
SN 2006S	−3.9	20.05 (0.26)	96.6 (5.7)	9.37 (0.96)	49.2 (42.4)	1.96 (1.70)
SN 2006S	3.0	18.68 (0.05)	83.0 (1.1)	9.76 (0.08)	96.0 (6.7)	0.87 (0.06)
SN 2006X	−11.2	32.29 (0.05)	270.2 (1.6)	19.92 (0.07)	287.7 (9.9)	0.94 (0.03)
SN 2006X	−10.2	31.74 (0.05)	253.0 (2.5)	19.82 (0.11)	283.4 (14.4)	0.89 (0.05)
SN 2006X	−9.2	29.84 (0.05)	242.2 (2.1)	18.57 (0.10)	252.8 (12.7)	0.96 (0.05)
SN 2006X	−8.2	28.29 (0.05)	232.5 (2.1)	17.54 (0.10)	225.5 (13.0)	1.03 (0.06)
SN 2006X	−7.2	26.34 (0.05)	255.1 (1.5)	15.99 (0.05)	170.6 (7.7)	1.50 (0.07)
SN 2006X	−6.2	20.86 (0.05)	210.9 (1.0)	14.57 (0.18)	16.9 (1.9)	12.52 (1.43)
SN 2006X	−5.2	20.84 (0.50)	191.1 (22.6)	13.72 (0.92)	31.6 (40.2)	6.04 (7.72)
SN 2006X	−0.2	19.02 (0.05)	150.4 (1.6)	12.28 (0.09)	131.9 (8.1)	1.14 (0.07)
SN 2006X	0.8	18.71 (0.05)	149.6 (1.2)	11.95 (0.06)	141.9 (6.0)	1.05 (0.05)
SN 2006X	1.8	18.65 (0.05)	147.6 (0.9)	11.60 (0.06)	166.6 (5.3)	0.89 (0.03)
SN 2006X	2.8	18.50 (0.05)	152.9 (1.3)	11.17 (0.08)	179.8 (8.0)	0.85 (0.04)
SN 2006X	3.2	18.51 (0.05)	131.2 (0.4)	11.13 (0.05)	175.2 (1.9)	0.75 (0.01)
SN 2006ax	−10.1	20.11 (0.05)	112.5 (0.9)	11.31 (0.08)	79.0 (4.0)	1.42 (0.07)
SN 2006bt	−5.3	19.42 (0.05)	62.7 (3.7)	12.44 (0.45)	150.3 (18.0)	0.42 (0.06)
SN 2006bt	−4.5	17.97 (0.05)	58.4 (3.2)	12.17 (0.66)	151.5 (18.6)	0.39 (0.05)
SN 2006bt	2.3	17.02 (0.05)	122.8 (4.1)	9.20 (0.19)	141.4 (14.8)	0.87 (0.10)
SN 2006bu	4.2	···	···	13.64 (0.06)	206.5 (4.2)	0
SN 2006bz	−2.4	···	···	13.23 (0.05)	352.6 (2.2)	0
SN 2006cm	−1.2	···	···	11.08 (0.05)	41.1 (0.6)	0

Continued on next page

Table A4 — Continued

SN Name	Phase (d)[a]	HVF v (10^3 km s^{-1})	HVF pEW (Å)	PVF v (10^3 km s^{-1})	PVF pEW (Å)	$R^{b}_{\rm CaIR3}$
SN 2006cp	−5.3	21.07 (0.05)	123.4 (2.4)	12.47 (0.25)	151.0 (15.7)	0.82 (0.09)
SN 2006cq	2.0	19.33 (0.11)	77.6 (7.2)	11.36 (2.39)	168.8 (115.7)	0.46 (0.32)
SN 2006cs	2.3	···	···	12.06 (0.05)	232.2 (2.2)	0
SN 2006cz	1.1	18.38 (0.71)	52.5 (19.4)	10.46 (1.59)	54.3 (73.3)	0.97 (1.35)
SN 2006dm	−7.9	22.01 (0.14)	58.6 (5.7)	12.86 (1.28)	185.2 (64.9)	0.32 (0.12)
SN 2006ef	3.2	···	···	11.24 (0.05)	180.8 (0.4)	0
SN 2006gr	−8.7	23.53 (0.05)	150.1 (1.1)	···	···	···
SN 2006ej	−3.7	18.96 (0.05)	28.4 (0.7)	11.84 (0.09)	110.6 (5.0)	0.26 (0.01)
SN 2006em	4.2	···	···	12.48 (0.05)	291.4 (0.6)	0
SN 2006et	3.3	17.46 (0.05)	90.6 (0.6)	9.22 (0.05)	44.2 (2.7)	2.05 (0.13)
SN 2006gj	4.7	···	···	10.78 (0.05)	265.5 (1.1)	0
SN 2006gt	3.1	···	···	10.97 (0.05)	270.1 (2.4)	0
SN 2006ke	2.4	···	···	12.16 (0.05)	175.4 (1.0)	0
SN 2006kf	−9.0	19.49 (0.13)	79.7 (2.9)	11.58 (0.27)	67.7 (14.3)	1.18 (0.25)
SN 2006kf	−3.1	···	···	11.78 (0.05)	145.1 (0.5)	0
SN 2006le	−8.7	25.46 (0.05)	140.2 (0.6)	14.52 (0.09)	37.0 (2.4)	3.79 (0.24)
SN 2006lf	−6.3	18.47 (0.05)	59.1 (0.2)	10.77 (0.05)	67.5 (0.5)	0.87 (0.01)
SN 2006or	−2.8	···	···	12.03 (0.05)	207.0 (0.7)	0
SN 2006os	−0.9	18.49 (0.10)	70.2 (3.6)	10.80 (0.25)	115.8 (16.5)	0.61 (0.09)
SN 2006sr	−2.3	···	···	12.59 (0.05)	116.5 (0.6)	0
SN 2006sr	2.7	···	···	11.83 (0.05)	165.2 (0.6)	0
SN 2007A	2.4	17.02 (0.05)	32.9 (0.5)	8.94 (0.05)	78.1 (2.8)	0.42 (0.02)
SN 2007F	−9.4	24.20 (0.05)	110.2 (0.4)	11.14 (0.05)	43.9 (1.4)	2.51 (0.08)
SN 2007F	3.2	16.19 (0.05)	36.0 (1.0)	10.88 (0.05)	80.0 (4.5)	0.45 (0.03)
SN 2007N	0.4	19.73 (0.05)	234.2 (0.4)	10.93 (0.05)	172.5 (2.5)	1.36 (0.02)
SN 2007O	−0.3	19.17 (0.05)	86.9 (0.3)	9.30 (0.05)	41.4 (0.7)	2.10 (0.04)
SN 2007S	−6.0	19.83 (0.05)	42.7 (0.8)	10.33 (0.32)	15.5 (4.4)	2.75 (0.78)
SN 2007af	−9.8	20.52 (0.05)	128.3 (0.8)	11.59 (0.07)	85.4 (4.3)	1.50 (0.08)
SN 2007af	−1.3	17.86 (0.05)	42.7 (0.8)	10.77 (0.05)	137.2 (3.4)	0.31 (0.01)
SN 2007af	0.2	···	···	11.43 (0.05)	164.9 (1.0)	0
SN 2007af	2.8	···	···	10.87 (0.05)	232.0 (0.1)	0
SN 2007af	3.8	···	···	10.93 (0.05)	229.2 (0.3)	0
SN 2007al	3.4	···	···	12.05 (0.05)	291.2 (0.8)	0
SN 2007ba	2.1	···	···	11.77 (0.05)	324.2 (2.1)	0
SN 2007bc	0.6	···	···	10.96 (0.05)	158.1 (0.7)	0
SN 2007bd	−5.8	···	···	14.64 (0.06)	161.3 (2.4)	0
SN 2007bm	−7.8	19.30 (0.05)	61.8 (0.3)	10.29 (0.05)	70.6 (1.7)	0.88 (0.02)
SN 2007bz	1.7	···	···	12.31 (0.05)	94.3 (1.3)	0
SN 2007ca	−11.1	22.86 (0.05)	110.8 (1.1)	11.75 (0.35)	69.2 (12.1)	1.60 (0.28)
SN 2007ci	−6.6	17.38 (0.14)	114.4 (3.8)	11.12 (0.17)	69.9 (7.8)	1.64 (0.19)
SN 2007ci	−1.7	···	···	12.24 (0.05)	132.6 (0.9)	0
SN 2007co	−4.1	20.13 (0.05)	135.4 (1.0)	11.32 (0.09)	109.8 (5.0)	1.23 (0.06)
SN 2007co	−0.6	18.54 (0.05)	110.2 (1.6)	10.37 (0.12)	108.1 (6.6)	1.02 (0.06)
SN 2007co	0.9	18.05 (0.05)	101.0 (1.1)	10.75 (0.06)	133.3 (3.9)	0.76 (0.02)
SN 2007cq	−5.8	···	···	12.43 (0.05)	68.2 (1.0)	0
SN 2007fb	2.0	···	···	11.40 (0.05)	157.5 (0.6)	0
SN 2007fr	−5.8	···	···	13.08 (0.05)	203.8 (1.9)	0
SN 2007fr	−1.3	···	···	12.36 (0.05)	246.0 (2.2)	0
SN 2007gi	−7.3	20.44 (0.05)	287.6 (0.2)	···	···	···
SN 2007gi	−0.4	18.46 (0.05)	146.1 (0.4)	12.12 (0.05)	105.1 (1.4)	1.39 (0.02)
SN 2007gk	−1.7	19.82 (0.05)	96.7 (1.5)	12.01 (0.13)	199.0 (7.2)	0.49 (0.02)
SN 2007hj	−1.2	···	···	12.98 (0.05)	283.1 (0.4)	0
SN 2007le	−10.3	28.99 (0.05)	370.5 (3.2)	20.31 (0.05)	146.5 (12.9)	2.53 (0.22)
SN 2007le	−9.4	27.75 (0.05)	231.0 (15.0)	19.77 (0.43)	121.0 (25.2)	1.91 (0.42)
SN 2007s1[c]	−1.2	···	···	14.23 (0.05)	291.5 (1.3)	0
SN 2007on	−3.0	17.23 (0.05)	87.9 (1.6)	10.61 (0.07)	134.9 (5.7)	0.65 (0.03)
SN 2007qe	−8.2	29.17 (0.27)	279.3 (17.1)	17.32 (0.58)	107.1 (70.3)	2.61 (1.72)
SN 2007qe	−6.5	28.33 (0.05)	154.0 (6.0)	18.83 (0.35)	198.4 (25.5)	0.78 (0.10)
SN 2007qe	−2.5	25.21 (0.63)	117.0 (16.2)	14.04 (2.67)	115.3 (161.9)	1.01 (1.43)
SN 2008ar	−8.9	23.65 (0.05)	212.3 (1.9)	12.17 (0.11)	34.9 (3.6)	6.08 (0.63)
SN 2008ar	−5.6	22.20 (0.15)	146.5 (9.6)	11.35 (0.69)	32.7 (18.7)	4.48 (2.57)
SN 2008ar	1.5	17.98 (0.23)	70.0 (6.2)	9.68 (0.56)	70.5 (25.5)	0.99 (0.37)
SN 2008ar	2.8	18.07 (0.11)	65.9 (3.2)	8.84 (0.39)	108.8 (23.8)	0.61 (0.14)
SN 2008ar	4.3	15.81 (0.18)	67.7 (6.5)	8.49 (0.43)	107.5 (28.7)	0.63 (0.18)
SN 2008bt	−1.1	···	···	12.11 (0.05)	177.3 (1.9)	0

Continued on next page

Table A4 — Continued

SN Name	Phase (d)[a]	HVF v (10^3 km s^{-1})	HVF pEW (Å)	PVF v (10^3 km s^{-1})	PVF pEW (Å)	$R^{b}_{\rm CaIR3}$
SN 2008cl	4.2	···	···	10.50 (0.10)	251.2 (9.9)	0
SN 2008s1[d]	−6.4	21.61 (0.08)	19.5 (0.5)	11.05 (0.34)	90.2 (12.8)	0.22 (0.03)
SN 2008s1[d]	−4.4	22.82 (0.11)	40.6 (2.4)	10.51 (8.36)	176.2 (277.9)	0.23 (0.36)
SN 2008s1[d]	−3.4	22.86 (0.09)	46.1 (1.0)	11.39 (0.33)	78.9 (12.8)	0.58 (0.10)
SN 2008s1[d]	0.5	···	···	11.20 (0.05)	135.9 (1.6)	0
SN 2008s1[d]	4.4	···	···	11.00 (0.05)	191.3 (0.8)	0
SN 2008dx	2.5	···	···	11.45 (0.05)	275.9 (1.4)	0
SN 2008ec	−9.8	···	···	13.27 (0.06)	132.4 (3.4)	0
SN 2008ec	−8.9	···	···	12.70 (0.07)	117.3 (3.4)	0
SN 2008ec	−6.0	···	···	11.99 (0.10)	95.6 (4.3)	0
SN 2008ec	−0.2	···	···	11.05 (0.05)	141.0 (0.4)	0
SN 2008ec	1.0	···	···	10.88 (0.08)	127.1 (6.1)	0
SN 2008ei	3.3	19.00 (0.05)	64.8 (4.1)	13.52 (0.42)	217.7 (24.4)	0.30 (0.04)
SN 2008s5[e]	1.3	18.61 (0.05)	57.3 (0.5)	8.52 (0.05)	44.0 (2.0)	1.30 (0.06)
SN 2008hm	1.3	18.90 (0.11)	78.4 (3.5)	10.48 (0.30)	89.1 (15.7)	0.88 (0.16)
SN 2008hs	−8.9	···	···	13.33 (0.08)	174.0 (5.9)	0
SN 2008hs	−7.9	···	···	13.77 (0.05)	215.4 (0.8)	0
SN 2008hs	−6.3	···	···	12.79 (0.05)	182.3 (1.0)	0
SN 2008hv	−11.7	24.96 (0.52)	218.1 (35.1)	16.01 (1.02)	130.0 (134.1)	1.68 (1.75)
SN 2008hv	−9.2	25.27 (0.05)	78.1 (3.3)	13.79 (0.89)	97.4 (23.2)	0.80 (0.19)
SN 2008hv	−6.6	22.48 (0.15)	73.1 (5.3)	11.20 (0.57)	22.6 (13.7)	3.23 (1.97)
SN 2009F	−3.0	···	···	11.84 (0.09)	181.7 (8.0)	0
SN 2009ad	−3.4	19.87 (0.07)	22.2 (0.7)	9.12 (0.14)	38.7 (3.9)	0.57 (0.06)
SN 2009an	−5.8	22.83 (0.05)	123.3 (0.9)	12.19 (0.17)	98.9 (9.3)	1.25 (0.12)
SN 2009an	−3.8	20.83 (0.05)	83.0 (0.8)	11.49 (0.11)	103.3 (5.9)	0.80 (0.05)
SN 2009an	−2.9	19.39 (0.06)	75.8 (1.6)	11.33 (0.14)	112.7 (8.3)	0.67 (0.05)
SN 2009ig	−14.4	35.15 (0.05)	138.7 (2.7)	25.52 (0.30)	287.0 (19.5)	0.48 (0.03)
SN 2009ig	−13.9	32.82 (0.11)	157.5 (19.1)	24.63 (0.23)	198.1 (43.6)	0.79 (0.20)
SN 2009ig	−12.4	30.87 (0.10)	219.6 (16.9)	23.16 (0.52)	109.6 (26.7)	2.00 (0.51)
SN 2009ig	−11.4	29.13 (0.05)	213.5 (4.2)	18.32 (0.31)	66.1 (8.2)	3.23 (0.41)
SN 2009ig	−10.9	27.50 (0.05)	152.4 (1.9)	15.82 (0.13)	7.7 (3.0)	19.78 (7.57)
SN 2009ig	−9.4	26.35 (0.05)	130.7 (0.3)	13.63 (0.05)	33.2 (1.3)	3.94 (0.15)
SN 2009ig	−8.4	25.65 (0.05)	112.1 (0.8)	14.73 (0.05)	10.2 (0.9)	11.04 (0.99)
SN 2009ig	−6.9	24.05 (0.05)	69.4 (0.5)	13.46 (0.08)	33.5 (2.0)	2.07 (0.12)
SN 2009ig	−6.0	23.18 (0.05)	36.3 (0.2)	12.92 (0.08)	39.8 (2.0)	0.91 (0.05)
SN 2009ig	−4.0	21.99 (0.05)	22.6 (0.4)	12.72 (0.09)	52.6 (3.4)	0.43 (0.03)
SN 2009ig	−3.0	21.94 (0.05)	19.6 (0.5)	12.91 (0.09)	70.2 (5.1)	0.28 (0.02)
SN 2009ig	−2.0	21.65 (0.11)	19.5 (0.9)	13.52 (0.14)	78.2 (9.1)	0.25 (0.03)
SN 2009ig	−1.0	20.97 (0.05)	21.5 (0.5)	13.39 (0.07)	88.5 (4.5)	0.24 (0.01)
SN 2009ig	3.4	···	···	13.63 (0.05)	124.1 (0.9)	0
SN 2009ig	4.3	···	···	13.66 (0.05)	135.2 (0.7)	0
SN 2009no	2.1	···	···	9.10 (0.05)	97.9 (1.1)	0
SN 2009nq	−3.1	18.26 (0.05)	65.3 (0.6)	9.60 (0.05)	63.1 (1.8)	1.03 (0.03)
SN 2010Y	−7.2	18.03 (0.23)	65.3 (3.7)	10.54 (0.31)	99.3 (16.5)	0.66 (0.12)
SN 2010Y	−3.2	···	···	11.06 (0.05)	155.2 (0.6)	0
PTF 10bjs	−9.8	25.34 (0.08)	63.2 (2.1)	14.74 (0.66)	16.8 (9.5)	3.77 (2.14)
PTF 10bjs	−8.6	25.01 (0.07)	70.1 (2.2)	15.25 (0.47)	13.2 (6.7)	5.33 (2.70)
PTF 10bjs	−7.4	24.85 (0.06)	72.0 (1.9)	14.63 (0.28)	18.6 (5.2)	3.86 (1.09)
PTF 10bjs	−6.6	25.07 (0.06)	60.6 (1.2)	15.12 (0.32)	21.3 (5.5)	2.84 (0.73)
PTF 10bjs	−5.5	23.82 (0.06)	49.7 (1.3)	13.00 (0.27)	31.8 (6.3)	1.56 (0.31)
PTF 10bjs	−1.8	22.20 (0.07)	24.9 (0.7)	12.92 (0.14)	33.6 (3.2)	0.74 (0.07)
PTF 10bjs	0.2	20.84 (0.09)	20.9 (1.4)	12.08 (0.23)	42.3 (5.8)	0.49 (0.07)
SN 2010ai	−10.5	···	···	14.72 (0.05)	176.4 (3.0)	0
SN 2010ai	−8.6	···	···	13.62 (0.05)	150.8 (0.8)	0
SN 2010ai	−3.7	···	···	12.61 (0.05)	101.9 (0.6)	0
SN 2010ai	−0.8	···	···	11.60 (0.05)	150.8 (0.9)	0
PTF 10fps	0.0	17.27 (0.10)	60.1 (3.1)	9.10 (0.23)	121.4 (13.3)	0.49 (0.06)
PTF 10fps	0.9	17.67 (0.15)	45.5 (4.5)	9.68 (0.45)	126.9 (25.3)	0.36 (0.08)
PTF 10fps	3.9	···	···	10.51 (0.05)	189.2 (1.4)	0
SN 2010dm	−6.5	20.90 (0.05)	46.1 (1.5)	9.86 (0.33)	21.7 (5.4)	2.13 (0.53)
PTF 10icb	−9.8	19.72 (0.05)	61.3 (0.6)	10.47 (0.11)	47.1 (3.6)	1.30 (0.10)
SN 2010ex	1.1	18.53 (0.07)	39.4 (0.9)	10.29 (0.09)	77.6 (5.9)	0.51 (0.04)
PTF 10qjl	−3.0	20.95 (0.08)	42.7 (1.2)	10.66 (0.11)	33.9 (4.3)	1.26 (0.16)
SN 2010ii	−6.1	···	···	14.91 (0.05)	130.8 (1.1)	0

Continued on next page

Table A4 — Continued

SN Name	Phase (d)[a]	HVF v (10^3 km s^{-1})	HVF pEW (Å)	PVF v (10^3 km s^{-1})	PVF pEW (Å)	$R^{b}_{\rm CaIR3}$
SN 2010ii	−0.5	···	···	11.28 (0.05)	80.9 (1.0)	0
SN 2010it	−9.5	25.86 (0.05)	161.4 (0.6)	13.75 (0.17)	73.7 (6.1)	2.19 (0.18)
SN 2010it	−8.5	24.61 (0.05)	98.9 (0.5)	13.22 (0.11)	56.3 (3.6)	1.76 (0.11)
SN 2010it	−6.6	22.27 (0.05)	58.8 (0.8)	12.63 (0.28)	75.1 (10.4)	0.78 (0.11)
SN 2010it	−2.6	···	···	12.57 (0.05)	73.0 (1.5)	0
SN 2010it	−0.6	···	···	11.93 (0.05)	106.9 (0.6)	0
SN 2010it	3.3	···	···	11.15 (0.05)	101.4 (0.7)	0
PTF 10ygu	−3.7	21.21 (0.07)	90.4 (2.0)	13.72 (0.19)	47.9 (9.3)	1.89 (0.37)
SN 2010iw	−4.9	20.80 (0.05)	50.7 (0.5)	10.39 (0.16)	39.5 (3.8)	1.28 (0.12)
SN 2010iw	−3.0	20.13 (0.05)	37.6 (0.6)	8.99 (0.19)	17.9 (2.6)	2.10 (0.30)
SN 2010iw	−0.1	20.31 (0.05)	32.7 (0.6)	9.41 (0.14)	34.5 (4.4)	0.95 (0.12)
SN 2010iw	3.9	19.98 (0.05)	26.6 (0.5)	9.65 (0.05)	45.7 (2.9)	0.58 (0.04)
SN 2010kg	−9.9	37.20 (0.05)	130.5 (8.1)	24.64 (1.66)	358.3 (0.1)	0.36 (0.08)
SN 2010kg	−9.0	32.95 (0.07)	221.3 (4.5)	21.41 (0.22)	187.3 (23.0)	1.18 (0.15)
SN 2010kg	−8.0	29.20 (0.06)	288.8 (2.9)	17.54 (0.06)	102.5 (10.5)	2.82 (0.29)
SN 2010kg	−6.0	26.17 (0.28)	109.9 (18.8)	17.45 (0.83)	150.6 (69.0)	0.73 (0.36)
SN 2010kg	−5.0	21.89 (0.13)	112.1 (5.3)	14.14 (0.28)	94.4 (23.2)	1.19 (0.30)
SN 2010kg	−4.1	19.77 (0.05)	130.9 (1.0)	11.68 (0.06)	60.6 (3.3)	2.16 (0.12)
SN 2010kg	−3.1	19.94 (0.05)	101.3 (0.8)	12.40 (0.06)	97.0 (3.8)	1.04 (0.04)
SN 2010kg	−1.1	17.98 (0.05)	124.6 (0.5)	10.83 (0.05)	82.1 (2.4)	1.52 (0.05)
SN 2010kg	−0.1	18.03 (0.05)	120.6 (0.9)	10.55 (0.06)	99.0 (4.0)	1.22 (0.05)
SN 2010kg	0.9	17.61 (0.05)	102.9 (2.1)	10.84 (0.24)	121.3 (13.2)	0.85 (0.09)
SN 2010kg	2.8	16.90 (0.05)	123.8 (1.2)	9.91 (0.08)	106.3 (5.4)	1.16 (0.06)
SN 2010kg	4.8	16.90 (0.05)	127.8 (1.3)	9.00 (0.08)	130.0 (5.2)	0.98 (0.04)
SN 2011ao	−7.5	20.89 (0.05)	113.1 (0.5)	10.96 (0.05)	44.3 (1.6)	2.55 (0.09)
SN 2011ao	−6.7	21.49 (0.05)	80.4 (1.9)	12.88 (0.24)	59.3 (8.1)	1.36 (0.19)
SN 2011ao	−5.8	21.63 (0.05)	77.2 (2.0)	11.43 (0.74)	76.1 (20.6)	1.01 (0.28)
SN 2011ao	−4.8	20.62 (0.05)	80.2 (0.3)	10.96 (0.07)	37.6 (1.7)	2.13 (0.10)
SN 2011ao	−1.8	20.00 (0.05)	76.2 (0.4)	10.07 (0.05)	36.3 (1.4)	2.10 (0.08)
SN 2011ao	−0.8	19.58 (0.05)	79.1 (0.5)	10.59 (0.12)	44.0 (2.6)	1.80 (0.11)
SN 2011ao	0.2	19.85 (0.05)	72.9 (0.5)	9.95 (0.14)	42.1 (3.3)	1.73 (0.14)
SN 2011ao	1.2	19.53 (0.05)	78.5 (0.6)	9.74 (0.07)	43.4 (2.6)	1.81 (0.11)
SN 2011ao	2.2	18.94 (0.05)	74.3 (0.5)	9.55 (0.05)	47.0 (2.3)	1.58 (0.08)
SN 2011ao	3.2	18.56 (0.05)	88.1 (0.6)	9.23 (0.06)	54.3 (2.6)	1.62 (0.08)
SN 2011by	−11.7	19.65 (0.05)	94.6 (0.3)	11.39 (0.05)	58.4 (1.3)	1.62 (0.04)
SN 2011by	−9.8	19.41 (0.05)	50.1 (0.3)	10.64 (0.05)	64.0 (1.9)	0.78 (0.02)
SN 2011by	−5.7	19.30 (0.05)	34.7 (0.2)	9.55 (0.05)	50.5 (1.0)	0.69 (0.01)
SN 2011by	−3.8	20.08 (0.05)	26.1 (0.1)	10.02 (0.05)	70.3 (1.1)	0.37 (0.01)
SN 2011by	0.2	17.74 (0.05)	27.2 (0.3)	10.15 (0.05)	83.0 (2.5)	0.33 (0.01)
SN 2011by	0.3	17.28 (0.05)	29.9 (0.6)	10.31 (0.05)	99.2 (3.8)	0.30 (0.01)
SN 2011by	2.3	17.45 (0.05)	30.5 (0.9)	10.02 (0.07)	116.6 (6.6)	0.26 (0.02)
SN 2011by	4.2	17.26 (0.05)	36.3 (0.3)	10.17 (0.05)	133.4 (2.5)	0.27 (0.01)
SN 2011dm	−5.5	22.09 (0.05)	90.3 (0.2)	13.00 (0.05)	88.2 (1.0)	1.02 (0.01)
SN 2011ek	−6.0	···	···	14.54 (0.05)	218.1 (0.3)	0
SN 2011ek	−5.0	···	···	14.13 (0.05)	218.8 (0.3)	0
SN 2011ek	3.0	···	···	11.96 (0.05)	272.9 (0.6)	0
SN 2011fe	−17.0	28.26 (0.35)	197.5 (36.5)	15.92 (2.17)	327.3 (0.1)	0.60 (0.36)
SN 2011fe	−16.0	26.90 (0.05)	176.5 (2.2)	16.70 (0.15)	181.1 (14.7)	0.97 (0.08)
SN 2011fe	−15.0	24.35 (0.05)	122.5 (1.3)	14.93 (0.20)	225.6 (11.8)	0.54 (0.03)
SN 2011fe	−13.0	21.39 (0.05)	169.4 (0.7)	12.51 (0.05)	149.4 (4.7)	1.13 (0.04)
SN 2011fe	−12.0	20.97 (0.05)	107.4 (0.2)	12.23 (0.05)	193.1 (1.7)	0.56 (0.01)
SN 2011fe	−11.0	19.22 (0.05)	110.4 (0.5)	10.66 (0.06)	98.7 (3.3)	1.12 (0.04)
SN 2011fe	−10.0	19.48 (0.05)	77.0 (0.2)	10.35 (0.05)	96.5 (2.0)	0.80 (0.02)
SN 2011fe	−10.0	19.22 (0.05)	89.0 (0.1)	10.71 (0.05)	93.0 (0.4)	0.96 (0.01)
SN 2011fe	−9.0	19.16 (0.05)	57.2 (0.3)	10.46 (0.05)	76.7 (2.3)	0.75 (0.02)
SN 2011fe	−9.0	19.94 (0.05)	58.5 (0.2)	10.20 (0.05)	128.4 (2.0)	0.46 (0.01)
SN 2011fe	−7.0	20.24 (0.05)	40.8 (0.3)	10.91 (0.05)	63.3 (1.4)	0.64 (0.02)
SN 2011fe	−2.0	19.27 (0.05)	27.2 (0.1)	9.86 (0.05)	135.4 (1.4)	0.20 (0.01)
SN 2011fe	−1.0	18.73 (0.05)	28.6 (0.1)	9.76 (0.05)	137.2 (1.2)	0.21 (0.01)
SN 2011fe	2.0	16.33 (0.05)	38.1 (0.2)	9.55 (0.05)	141.3 (1.0)	0.27 (0.01)
SN 2011fe	3.0	15.98 (0.05)	41.7 (0.2)	9.54 (0.05)	148.6 (1.0)	0.28 (0.01)
SN 2011gy	−1.1	···	···	12.01 (0.05)	103.0 (0.5)	0
SN 2011hb	−5.8	22.86 (0.05)	83.7 (2.6)	12.14 (0.85)	75.0 (17.2)	1.12 (0.26)
SN 2011hb	−2.9	21.47 (0.05)	70.5 (0.4)	10.50 (0.08)	31.6 (2.1)	2.23 (0.15)
SN 2011hb	3.0	19.51 (0.05)	74.9 (1.7)	9.64 (0.17)	67.3 (7.2)	1.11 (0.12)

Continued on next page

Table A4 — Continued

SN Name	Phase (d)[a]	HVF v (10^3 km s^{-1})	HVF pEW (Å)	PVF v (10^3 km s^{-1})	PVF pEW (Å)	$R_{\rm CaIR3}$[b]
SN 2011ia	−3.0	···	···	9.99 (0.05)	65.5 (1.0)	0
SN 2012I	−1.0	···	···	11.87 (0.05)	152.4 (0.6)	0
SN 2012bh	0.0	19.71 (0.05)	25.6 (0.5)	9.46 (0.10)	68.9 (6.2)	0.37 (0.03)
SN 2012cg	−12.8	24.21 (0.05)	86.6 (2.4)	16.42 (0.19)	101.3 (9.0)	0.85 (0.08)
SN 2012cg	−11.8	22.30 (0.05)	140.1 (0.7)	13.67 (0.06)	76.6 (3.3)	1.83 (0.08)
SN 2012cg	−10.5	21.32 (0.05)	122.7 (0.9)	11.88 (0.08)	50.7 (4.2)	2.42 (0.20)
SN 2012cg	−9.6	21.11 (0.05)	88.4 (1.2)	11.88 (0.10)	42.6 (3.9)	2.07 (0.19)
SN 2012cg	−7.8	21.43 (0.05)	55.3 (0.3)	11.86 (0.05)	29.7 (1.2)	1.86 (0.08)
SN 2012cg	−3.8	21.11 (0.05)	56.7 (0.1)	10.40 (0.05)	26.5 (0.4)	2.14 (0.03)
SN 2012cg	−3.8	21.07 (0.05)	48.2 (0.4)	10.56 (0.10)	33.0 (2.6)	1.46 (0.12)
SN 2012cg	−0.5	20.28 (0.05)	39.4 (0.3)	10.44 (0.05)	43.2 (1.9)	0.91 (0.04)
SN 2012da	−1.0	18.56 (0.05)	75.8 (1.2)	9.16 (0.14)	54.6 (5.6)	1.39 (0.14)
SN 2012fr	−14.4	32.78 (0.05)	450.1 (2.7)	···	···	···
SN 2012fr	−12.4	30.67 (0.05)	395.0 (0.4)	···	···	···
SN 2012fr	−11.4	30.17 (0.05)	330.7 (0.3)	···	···	···
SN 2012fr	−9.3	27.24 (0.05)	135.8 (0.9)	···	···	···
SN 2012fr	−8.4	26.00 (0.05)	110.1 (0.3)	···	···	···
SN 2012fr	−8.2	25.80 (0.05)	97.4 (0.3)	···	···	···
SN 2012fr	−7.5	25.33 (0.05)	95.9 (0.3)	···	···	···
SN 2012fr	−6.7	25.17 (0.05)	96.1 (1.3)	12.72 (0.23)	5.9 (2.1)	16.37 (5.76)
SN 2012fr	−6.4	24.80 (0.05)	98.2 (1.1)	11.84 (0.17)	26.7 (3.1)	3.67 (0.43)
SN 2012fr	−5.6	24.46 (0.05)	100.3 (0.2)	11.42 (0.05)	12.8 (0.4)	7.84 (0.26)
SN 2012fr	−4.7	24.14 (0.05)	99.4 (0.3)	11.30 (0.05)	13.1 (0.7)	7.60 (0.38)
SN 2012fr	−3.7	23.87 (0.05)	84.3 (0.4)	11.26 (0.05)	35.6 (1.9)	2.37 (0.13)
SN 2012fr	−2.5	22.96 (0.05)	90.7 (0.4)	11.58 (0.05)	31.9 (1.0)	2.85 (0.09)
SN 2012fr	−2.4	23.33 (0.05)	105.7 (1.9)	11.44 (0.09)	32.0 (3.2)	3.30 (0.33)
SN 2012fr	−1.4	22.67 (0.05)	86.0 (0.2)	12.15 (0.05)	39.8 (1.1)	2.16 (0.06)
SN 2012fr	−1.3	22.32 (0.05)	80.9 (0.1)	12.13 (0.05)	35.6 (0.9)	2.27 (0.06)
SN 2012fr	−0.3	21.65 (0.05)	80.8 (0.2)	12.03 (0.05)	49.8 (0.7)	1.62 (0.02)
SN 2012fr	0.7	21.56 (0.05)	82.0 (0.3)	12.22 (0.05)	68.3 (1.3)	1.20 (0.02)
SN 2012fr	1.3	20.61 (0.05)	82.6 (0.5)	11.68 (0.05)	62.3 (2.9)	1.33 (0.06)
SN 2012fr	1.7	21.02 (0.05)	79.7 (0.3)	12.32 (0.05)	85.8 (2.0)	0.93 (0.02)
SN 2012fr	2.3	20.92 (0.05)	71.2 (0.2)	11.98 (0.05)	67.5 (1.2)	1.05 (0.02)
SN 2012fr	3.2	19.42 (0.05)	86.6 (0.5)	11.91 (0.05)	63.7 (2.1)	1.36 (0.04)
SN 2012fr	4.5	19.58 (0.05)	57.9 (0.9)	11.60 (0.05)	133.2 (4.3)	0.43 (0.02)
SN 2013cs	−8.9	21.39 (0.05)	61.4 (0.8)	13.69 (0.08)	99.0 (4.2)	0.62 (0.03)
SN 2013cs	−3.0	16.47 (0.05)	32.1 (0.7)	10.65 (0.39)	135.4 (8.2)	0.24 (0.02)
SN 2013di	−1.6	20.42 (0.05)	104.5 (0.5)	10.28 (0.06)	47.0 (2.1)	2.22 (0.10)

[a]Phases are in rest-frame days.

[b]$R_{\rm CaIR3}$ is the ratio of the pEW of the HVF to the pEW of the PVF, as defined by Childress et al. (2014).

[c]Also known as SNF20071021-000.

[d]Also known as SNF20080514-002.

[e]Also known as SNF20080909-030.